1-1-1996

Synergistic properties of poly(ethylene 2,6-naphthalate) fibers blended with novel thermotropic liquid crystalline copolyesters.

Verna Charlene Lo
University of Massachusetts Amherst

SYNERGISTIC PROPERTIES OF POLY(ETHYLENE 2,6-NAPHTHALATE) FIBERS BLENDED WITH NOVEL THERMOTROPIC LIQUID CRYSTALLINE COPOLYESTERS

A Dissertation Presented

by

VERNA CHARLENE LO

Submitted to the Graduate School of the
University of Massachusetts Amherst in partial fulfillment
of the requirements for the degree of

DOCTOR OF PHILOSOPHY

May 1996

Polymer Science and Engineering

SYNERGISTIC PROPERTIES OF POLY(ETHYLENE 2,6-NAPHTHALATE) FIBERS BLENDED WITH NOVEL THERMOTROPIC LIQUID CRYSTALLINE COPOLYESTERS

A Dissertation Presented

by

VERNA CHARLENE LO

Approved to style and content by:

Richard J. Farris, Chair

Simon W. Kantor, Member

Thomas L. Lardner, Member

Richard J. Farris, Department Head
Polymer Science and Engineering

ACKNOWLEDGMENTS

My sincerest gratitude goes to my advisor, Professor Richard Farris. He has taught me how to appreciate the richness of scientific challenges and has consistently helped me find the right tools to address such challenges. He fosters a unique brand of integrated thinking within his group that combines the best of practicality with experimental creativity. For me, he has cultivated the goals of self-learning along with the effective communication of new ideas. While these skills are indeed valuable in a scientific career, I believe that these are two of the most vital skills that any person can teach another.

Support for this project was kindly provided by Eastman Kodak, AkzoNobel and the Materials Research Science and Engineering Committee. I am particularly grateful to Dr. Jehuda Greener from Eastman Kodak who has often offered me good advice and feedback over the past years on matters related to this project.

I am also very grateful to the other professors who have graciously served as members of my dissertation committee, lending me their insights. Professor Simon Kantor has steadily shown me how to see challenges from a different view, often broadening interpretations. Professor Lardner guided a good deal of the analysis in this dissertation through very well-chosen questions posed along the way.

Within the Farris lab and the LCP group, I have worked most closely with Professor Jae-Kon Choi. Through his patience, diligence, and advice, he has helped me in many ways which I cannot even begin to list. It has been an honor to work with him and I am genuinely in his debt.

I consider myself very fortunate to have worked within such a high-caliber environment. There is probably not a single professor in the entire PSE department from whom I have not learned something outside of class, in direct one-on-one discussions. I remember especially fruitful

discussions with Prof. Porter, Prof. Hoagland, and Prof. Muthukumar on matters related to their respective areas of expertise.

The Farris group, past and present, are a diverse bunch. I have benefited from the wealth their experience, gaining from their diverse backgrounds as chemists, chemical and mechanical engineers, and (fellow) materials science engineers. I have enjoyed working (and sharing precious bench space in the old lab) with Scott Joslin, Reiner Giesa, Zoran Petrovic, Joan Vrtis, Cindy Athanasiou, Anthony Karandinos, Bob Fleming, Mario Perez, Kapil Sheth, Dave Macon, Shalabh Tandon, Meredith White, Mike Chen, Dao Atong, Naveen Agarwal, Mitsuhiro Sakuda, Mun-bok Lee, Meng Hsieh, Jennifer Stewart, and Gene Kim. I've learned from them and from the diversity of their cultures. Special thanks goes to Meredith who has been about a good a friend and office-mate as one could hope for.

Other friends who have really been great are Georgia Dris, Regina Valluzzi, Kleanthes Koniaris, and Scott Nitzsche. They are, and have always been, unquestionably thoughtful, generous, and clever. To Kleanthes, who has spent much time helping me with matters both large and small, I especially owe a good deal of my sanity as well. And to our friend Scott who left us too soon, your friends will never forget you.

Finally, my family has always been behind me at every step. They have always encouraged me and provided both the tangible and intangible support for me to learn and to grow in whichever direction drew me. My father was my earliest influence on the importance and potential of focused effort; he specialized in designing bridges and dams here and abroad for the U.S. Army Corps of Engineers. He showed me, most fundamentally, that curiosity -- which inevitably leads to discovery -- is always its own reward.

Thus in remembrance of my father 羅永觀.

ABSTRACT

SYNERGISTIC PROPERTIES OF POLY(ETHYLENE 2,6-NAPHTHALATE) FIBERS BLENDED WITH NOVEL THERMOTROPIC LIQUID CRYSTALLINE COPOLYESTERS

MAY 1996

VERNA CHARLENE LO, B.S.E., UNIVERSITY OF MICHIGAN

M.S., UNIVERSITY OF MASSACHUSETTS AMHERST

Ph.D. UNIVERSITY OF MASSACHUSETTS AMHERST

Directed by: Professor Richard J. Farris

This dissertation discusses the formulation, processing, and properties of blends of semi-flexible thermotropic liquid crystalline polymer (TLCP) copolyesters within a matrix of poly(ethylene 2,6-naphthalate) (PEN). The TLCPs, both main-chain flexible and side-chain flexible, are categorized into three main classes: segmented block, alternating, and random (statistical). The TLCPs and the matrix were characterized in terms of their thermal, mechanical, and rheological properties. Several new structure-property relationships for the pure PEN fiber are established with strong implications for further processing studies. Fibers containing between 0% to 20% by weight of TLCP were melt-extruded into monofilaments with initial diameters from 100 - 120 μm. As-spun fibers were subjected to a two-stage post-treatment processing to maximize their mechanical performance.

The TLCPs were found to serve several roles within the matrix when blended in concentrations from 0.25% to 20% by weight. Thermally, they were able to plasticize and nucleate crystallinity within the matrix. A semi-flexible phenylene-based TLCP was able to plasticize the matrix by lowering the glass transition temperature by as much as 14 degrees. A semi-flexible naphthalene-based TLCP, when blended in at 1% concentration, was able to nearly double the amount

of PEN re-crystallized from the melt (from 20% to 40% crystallinity). Mechanically, all hot-drawn 1% polyblends of main-chain flexible TLCP gave rise to Young's modulus values between 29- 31 GPa.

Thermal data and morphology data indicate that even ideal levels of *in-situ* reinforcement are insufficient to account for the observed mechanical property enhancements. Evidence from thermal studies shows clearly that the TLCPs can modify the matrix in which they are blended. Striking matrix modification effects are found to occur, unexpectedly, both in the presence and in the absence of the nematic texture within the polyblend upon TLCP addition. There is also a relationship between the amount of PEN re-crystallized from the melt of the polyblends to the final mechanical properties of the fibers. Both thermal and mechanical properties of the final fibers are highly process-dependent. To this end, instrumentation techniques for new processing methods were investigated and developed.

TABLE OF CONTENTS

LIST OF TABLES

LIST OF FIGURES

CHAPTER 1

INTRODUCTION

1.1 Background

High-performance polymeric fibers find end uses in many products, from the commonplace to the specialized. For example, in the form of braids and twists, high-performance fibers are used alone and in blends to make rope, cord, and radial tire ply reinforcement [Shima et al., 1971]. In the form of weaves and composites, high-performance fibers are used in items as varied as bullet-proof body armor and boat sails.

The definition of a high-performance fiber, however, often varies according to the industrial application of the material. For example, flame retardancy and solvent resistance are highly desirable for aircraft applications whereas thermal stability is important to textile manufacturers [Allen, 1983]. Optical clarity is important for certain optoelectronic applications such as in wave guides and gradient index optical cables [Ho, et al., 1995]. Every industry, however, usually desires fibers of high modulus and strength.

High-performance polymeric fiber are made both from neat (pure) resins and blends of resins with other additives to form a composite. Examples of neat resin fibers are Allied-Signal Spectra® made from neat poly(ethylene) (PE) and duPont Kevlar® made from neat poly(*p*-phenylene terephthalamide) (PPTA). For composite materials, the most common reinforcement agents are Kevlar®, fiberglass, and graphite (which is made from a polymer precursor). For conventional composites, the level of reinforcement increases with the level of additive with the largest additive volume available commercially for composite fibers at about 65% [Miller, 1985].

The work in this thesis focuses on the formation, processing, and the resulting properties of molecular level composites of poly(ethylene 2,6-naphthalate) (PEN) containing only 0.25% to 20% polymeric additive. Unlike fiberglass or graphite, the polymeric additives are not inherently stiff and rigid but are capable of undergoing a molecular ordering transition through which they become partially needle-like (nematic). This thesis focuses on answering how and why these additives affect the thermal and mechanical properties of the matrix material, PEN. PEN is a potentially high-performance engineering thermoplastic which has not been widely studied or used in fibers -- either commercially or for research-purposes. All of thermotropic liquid crystalline polymers (TLCPs) are copolyesters specially synthesized on-site for compatibilization with PEN. The chemical structure of the TLCPs contain moieties which, to varying degrees, resemble that of PEN.

1.2 Commercial Spinning Processes

One of the critical requirements for polymeric fiber forming processes is to use a polymer of a sufficiently high molecular weight such that it is above the entanglement molecular weight [Zimmerman, 1992]. The presence of an entangled network is necessary not only for the fiber spinning process, but also for subsequent post-treatment processes [Ward, 1994]. Post-treatment, the simultaneous heating and stretching of a fiber over a short period of time, has tremendous impact on the final modulus and strength of fibers. (For example, Young's modulus, a measure of the stiffness of PEN, can easily be increased by an order of magnitude through post-treatment.)

Melt-extruded polymeric fiber is formed through rapid cooling from the molten liquid state. As a result, melt-extrusion processes preclude the use and associated costs of solvents and solvent-extraction steps to form the final product. In industrial settings, melt-extruded fiber production occurs commonly in a two-step process (TSP). TSP is a batch process in which essentially

amorphous fibers are extruded in a first step and then subjected to post-treatment in a subsequent step after the fiber has solidified. In newer one step processes (OSP), the goal is to both form and orient the fiber in one step while it is still liquid. As a result, OSP spinning speeds must be much higher than those for TSP. Commercial OSP spinning speeds for PET fiber exceed 5000 m/min [Kawaguchi, 1985].

Whether the fiber is oriented in one step or two, several physical parameters scale characteristically with the level of orientation attained in the bulk. Changes in stress-induced crystallinity and optical birefringence are often used to gauge the degree of orientation of the finished fiber with respect to its as-spun counterpart. A common benchmark of orientation is, however, a dimensionless strain quantity known as the draw ratio. Denoted by λ, the draw ratio characterizes the amount of macroscale uniaxial stretching of a fiber and is frequently calculated as the ratio of the square of the diameter of as-spun fiber to that of fully drawn fiber. λ may also be calculated as the ratio of the linear density of as-spun fiber to that of fully post-treated fiber. The validity of these calculations rests on the assumption that the fiber volume is conserved as it is deformed in drawing steps. For all cases, $\lambda \equiv 1$ for as-spun (i.e., undrawn) fiber.

λ is not necessarily a continuous quantity. Over certain temperature ranges above the glass transition temperature (T_g) of a fiber-forming polymer, a singularity can appear in λ due to the physical phenomenon of necking in drawn polymers. Necking is a type of segmental reorientation that results mainly from chains unraveling and moving to counteract the applied stress. This phenomenon is seen in fiberlines of many polymers in which the diameter undergoes a spontaneous and highly localized attenuation -- typically over a few microns. Crystallization does not occur beyond the necking point and the time required for the completion of necking depends on the viscous forces applied to the filament during necking [Katayama and Yoon, 1985]. The polymer

ceases necking and necking-associated crystallization at a draw level known as the natural draw ratio [King, 1990]. In process studies, the natural draw ratio is a kinetic quantity.

One of the applications that utilize necking phenomenon is the cold-drawing post-treatment process, the first of two drawing steps . Usually done just above the Tg of the as-spun fiber-forming material, cold-drawing affects increased crystallinity along the fiber axis while minimizing the energy available for other types of molecular motion. The onset of necking is a useful processing indicator that continuous cold-drawing is being done optimally at steady-state at a given temperature [Carraher, 1994].

1.3 Laboratory Scale Spinning Processes

Laboratory spinning processes differ significantly from industrial processes.

The general diferential equation and solutions for threadline tension as a function of position, *F(x)* are given as

$$\frac{dF}{dx} = W\frac{dV}{dx} - \pi\sigma\frac{dR}{dx} - \rho g R^2 + 2\pi R p_{xr,s} \tag{1}$$

$$F(x) = F(0) + W(V - V_o) + \pi\sigma(R_o - R) - \pi\rho g\int_0^x R^2 dx' + 2\pi\int_0^x R p_{xr,s}\, dx' \tag{2}$$

$$F(x) = F_{rheol}(0) + F_{inertia} + F_{surface} - F_{gravity} + F_{drag} \tag{3}$$

where the quantities for equations (1) - (3) are defined as follows:

W = mass throughput per spinneret orifice
V = axial velocity of the filament at position x from the spinneret
V_o = extrusion velocity
R = radius of the filament at position x from the spinneret
R_o = radius of the orifice
σ = surface tension
ρ = polymer density
g = acceleration of gravity
$p_{xr,s}$ = air drag (shear stress) on the filament surface

As suggested in the previous section, one of the main differences between industrial and laboratory spinning processes is the disparity of spinning speeds. Laboratory extrusion processes seldom exceed a few hundred meters per minute whereas faster industrial spinning speeds can approach 10,000 m/min. An important distinction arises in the contributions to the total spinning line tension among these two regimes. Whereas the rheological drag component dominates the total spinning line tension at laboratory speeds, air drag and inertial forces dominate only at the very high speeds of industrial scale production [Ziabicki, 1985]. Because rheological drag is controlled by the extruded polymer's viscosity (a material property), the studies in this thesis allow, at least in a relative sense, comparisons of the inherent "spinnability" of the different materials. Except for slow spinning of very thick filaments from low-viscosity fluids, gravity and surface tension effects typically account for less than 1% of the total tension in other cases. Figure 1.1 illustrates the relative contributions of these effects based on calculations.

1.4 PEN and PET

The thermoplastic resin used for most of the studies in this thesis is poly(ethylene 2,6-naphthalate) (PEN). PEN is very similar to poly(ethylene terephthalate) (PET), one of several

commonly used engineering polyesters. As shown in Figure 1.2, the substitution of a naphthalene unit in PEN in place of the phenylene moiety found in the chain backbone of PET gives PEN a more rigid chain structure compared to PET. The enhanced chain rigidity of PEN offers better dimensional and thermal stability and higher mechanical stiffness over that of PET as reflected in higher T_g, melting point (T_m), and Young's modulus.

Though ICI Ltd. first reported the synthesis of PEN in 1948, it was not commercialized until 1973 when Teijin Ltd., Japan began marketing PEN film under the tradename Q-Film® [Ghanem and Porter, 1989]. In 1976, Teijin patented a process for spinning PEN fiber [Hamana et al., 1976].

The costs of producing the intermediates of PEN, however, far exceed those for PET -- the high price and limited availability of dimethyl-2,6-naphthalenedicarboxylate (DM-2,6-NDC) has historically prevented the general commercialization of PEN. Nonetheless, PEN has become a polyester resin of significantly growing industrial interest due to recent reports of chemical companies scaling up production of the DM-2,6-NDC precursor. Also, recent work reveals that PEN exhibits unique oxygen barrier properties and dielectric properties, with promising applications in packaging [Stewart et al., 1993] and microelectronics [Yen et al., 1993] [Feyder, 1992].

PEN fiber has not been commercialized in any country other than Japan. Recent fiber-related publications originating from central research laboratories of corporations with fully commercialized PET fiber and film technologies have served to further widen the general interest in this polyester [Stewart et al., 1993] [Huijts and De Vries, 1993] [Huijts and Peters, 1994] [Jager et al., 1995] [Germroth, 1995].

1.5 Project Goals

Many of the studies in this thesis may serve as a backdrop for subsequent scale-up attempts. The first aim of these studies is to define processing windows for high-performance melt-extruded fibers based on PEN. The route to forming high-performance fiber involves the addition of small amounts of specialty liquid crystalline polymers (LCPs) coupled with special processing techniques of the blend. The second aim is to determine how such additives and processing techniques can positively affect the mechanical properties of the resulting PEN fiber. Several aspects of these studies bear comparison with similar studies on poly(ethylene terephthalate) (PET) which determined that the presence of nematic TLCPs can modify the crystallization behavior of the PET matrix and does not act as mechanical reinforcement [Joslin, 1994].

1.6 Liquid Crystalline Polymers

Friedel [1922] was the first to categorize liquid crystals into three main classes: nematic, cholesteric, and smectic. For liquid crystals, there is a direction toward which the molecular orientations are biased, at least on a local scale. This direction is known as the director (**n**) of the texture and is a fundamental property of the liquid crystal.

The nematic liquid crystalline (LC) phase possesses long range orientational order but lacks long range positional order. The axes of the rod-like molecules are aligned, albeit imperfectly, with the director. The order parameter S quantifies the degree of alignment.

The cholesteric state is equivalent to a nematic state that twists periodically about an axis normal to the director. The physical arrangement is the same as a nematic state containing a twist

distortion except that the twisted formation found in the cholesteric state is inherently stable and occurs spontaneously with chiral mesogenic molecules.

Smectic LC phases separate into layers in which the ends of the LC molecules segregate into common planes. Several variations of smectic phases are distinguishable, depending on the tilt angle of **n**. Like the other LC states, the smectic state contains no long-range positional order. The lateral arrangement of smectic systems is also random: there is no correlation in the lateral positions of molecules between successive layers.

While a molecule is said to be mesogenic if it is capable of forming LC phases, the actual inducement of liquid crystallinity relies on a number of factors. Lyotropic LC phases contain solvent molecules in addition to mesogens. They are distinguished from thermotropic LC systems which consist solely of mesogenic molecules. The thermotropic LC phase exists only over certain temperature ranges.

A class of materials known as liquid crystalline polymers (LCPs) may be regarded as high molecular weight analogs of small molecule LCs. Given the proper processing conditions, the two types of LCPs -- lyotropic and thermotropic -- have been shown to exhibit distinctive ordering characteristics atypical of other polymers.

The TLCP mesophase exists at a temperature between the crystal melting point, T_m and the upper transition temperature $T_{lc\rightarrow i}$, above which the liquid crystalline phase isotropizes into a liquid melt. One of the consequences of polymerization (i.e., the linking of rigid mesogenic groups) is to raise both these transition temperatures. The challenge in TLCP synthesis is to create a molecule which degrades at a temperature above $T_{lc\rightarrow i}$. Otherwise, the mesophase is unstable and gradually diminishes due to chemical decomposition.

The uniaxial LCP nematic mesophase is simple to identify through its optical properties. For nematics, a texture of dark, flexible, thread-like lines appears both with and without the use of

crossed polars [de Gennes and Prost, 1993]. The thread-like components are a type of disclination defect and correspond to lines of singularity in the molecular alignment of the polymers. Such disclinations occur at discontinuities in the director field. Under crossed polars, typical Schlieren textures which Friedel described as *structures à noyaux* (noyaux meaning nuclei) appear. These brushlike textures appear to emanate from point sources and contain dark regions where one of the principal directions describing the local optical properties in the sample plane is parallel to either the polarizer or analyzer. When the crossed polars are rotated, the brushes appear to rotate rather like small propellers.

1.7 Molecular Architecture

One of the ways to control the stability and thermal range of the mesophase is through modification of the molecular architecture. Poly(*p*-phenylene) (PPP) is liquid crystalline and is formed through polymerization at *para* linkages of aromatic groups as shown in Figure 1.3.

Crystals of PPP, however, will not melt below their decomposition temperature. Chain modification of structures based on PPP commonly result in polymers which exhibit a liquid crystalline phase but retain a workable range of liquid crystallinity.

For example, linkages through ester moieties adjacent to the *para* aromatic positions form the basis of two commercial aromatic polyesters: Amoco Xydar® and Hoechst-Celanese Vectra®. Vectra® is a fully aromatic copolyester containing all *para* linkages whereas Xydar® contains other bent (kinked) rigid units distributed randomly in the backbone. Figures 1.4 and 1.5 show the chemical structure of these commercial TLCPs.

The role of "spacer" units is to frustrate chain packing and crystallinity while shifting the mesogenic range of the LC phase to effectively lower temperatures. Other molecular modifications

designed to control the working mesogenic range of aromatic copolyesters include the addition of flexible spacer units along the backbone or onto side chains in either random or segmented placements [Donald and Windle, 1992].

Aromatic polyesters are, in fact, the most important class of TLCPs developed for structural applications. They are typically found in heat-resistant belting and printed circuit board substrates. Fiber applications range from use in sporting equipment to towing and mooring lines. While the engineering performance of TLCPs surpass those of traditional resins in several key areas, the high cost of LCPs precludes their widespread replacement of traditional resins in commercial applications.

The cost of LCPs is up to three orders of magnitude greater than that of traditional engineering resins. For example, in 1995, poly(propylene) cost $0.35-$0.45 per pound and PET cost $0.80-$1.20 per pound. LCPs, in contrast, range between $12- $30 per pound but can exceed several hundred dollars per pound for specialty applications [Bonis, 1995].

1.8 Orientation under Flow

One of the models used to describe the flow of rigid-rod nematic systems is the Ericksen-Leslie-Parodi model [Leslie, 1966] which uses a macroscopic treatment of rod-like small molecules based on classical continuum mechanics. Doi and Edwards developed a molecular model to treat solutions of rod-like macromolecules. They also extended the molecular model for dilute solutions of rigid rods to concentrations above the critical value necessary for liquid crystallinity. While these theories do predict the onset of spontaneously-formed nematic states, the proper design of experiments to determine the parameters of these models poses as a major difficulty. The physical and thermodynamic non-ideality of actual systems comprised of polydisperse rod-like macromole-

cules make for complex results even for broadly-studied systems such poly(γ-benzyl-L-glutamate) (PBLG). The physical limitations of real systems have led to the development of phenomenological models to characterize the rheological behavior of main-chain polymers.

1.9 LCP Rheology

The rheology of liquid crystalline solutions differs from that of isotropic solutions in many respects. For nematic mesophases, the needle-like structure results in distinctive rheological behavior. Phenomenological models are useful to fit experimental rheological data for main-chain polymers. For certain LCPs, a log-log plot of viscosity versus shear rate reveals three distinct regions of rheological behavior as shown in Figure 1.6.

Regions I and III are shear-thinning whereas Region II shows a plateau viscosity insensitive to shear rate. Most of the data collected for storage and loss shear moduli span over Regions II and III. The structural models proposed for this behavior indicate that the alignment of the director with respect to the flow field goes from a state of random orientation (due to disclination points at zero shear rate) to increasing re-orientation in the direction of flow as illustrated in Figure 1.7.

The shear rate dependence of viscosity flow curve is not, however, accepted as the general flow behavior for LCPs by all who study the rheology of LCPs [Handlos and Baird, 1995]. The overall indications lead to the conclusion that no single explanation will suffice for all systems. The results likely depend critically upon sample history and microstructure [Donald and White, 1992].

1.10 Fiber Spinning

For thermotropic fibers, the aim is to obtain the highest possible degree of chain alignment along the fiber axis. Calundann et alii [1988] present data showing that the development of orientation within thermotropic fibers is very efficient and can approach nearly perfect axial alignment even at very modest extension ratios approximately equal to three. Commercial Vectran® fiber (based on fully aromatic Hoechst-Celanese Vectra® A) experiences approximately a 90:1 draw-down ratio when spun from the melt. The domains of orientation within a single oriented filament range from 5 μm for macrofibrillation to 0.05 μm for microfibrillation as shown in Figure 1.8.

The needle-like, nematic texture found in many TLCPs also aids polymer processing of conventional melt-processable resins by reducing the processing viscosity in the direction of the flow field. Recent work has shown that the addition of less than 5% of a thermotropic copolyester to PET depresses the melt viscosity of the TLCP blend up to 80% compared to that of the neat PET resin [Narayan-Sarathy et al., 1995] Achieving a depressed melt viscosity advantageously reduces the amount of energy required to process a given melt. In no other polymeric forming process are the benefits of an included nematic phase more intuitive and apparent than in the one-dimensional process of fiber extrusion.

Because the relaxation times of TLCPs exceed those of ordinary polymers, it is possible to preserve the nematic component in the solid state as a separate phase given the proper processing conditions [Lee et al., 1993]. The inducement of the nematic texture within a fiber-forming process for blends has been suggested to lead to *in-situ* reinforcement of the matrix [Kiss, 1987]. Over the past fifteen years, considerable research and industrial interest has focused on the effects of melt blending nematic TCLPs with widely used engineering thermoplastics and thermosets. Many researchers have attempted to exploit the physical properties of TLCPs by blending them with ther-

moplastics such as poly(carbonate) [Federico, 1989] [Lin et al., 1993] [Shi, 1994], PET [Kyotani et al., 1992] [Mehta and Deopura, 1993] [Heino, 1994] [Joslin et al., 1994], and thermosets such as cross-linked polyetheretherketone and polyphenylenesulfide [Baird and Sun, 1990]. The reason for this interest is to explore the reinforcement effects of a potentially stiff, needle-like phase induced within a matrix during processing.

In some cases, the TLCPs used for study are wholly nematogenic. In other cases, they contain non-mesogenic spacer segments interspersed with the nematogens, resulting in a semi-flexible TLCP. When the semi-flexible TLCPs used for polyblending studies contained spacers chemically similar to the matrix, the working model becomes that of a "molecular composite" [Hwang et al., 1983]. This is because the chemical similarity of the spacer groups with the matrix allow their potential homogenization on a segmental level. Because the spacer groups are chemically bonded to nematogens, any nematic phase that develops is, in theory, physically anchored to the matrix on a molecular level.

In practice, *in-situ* reinforcement poses two distinct advantages over traditional types of composite reinforcement agents such chopped glass or graphite whiskers. First, the presence of a rigid fibrous phase increases processing viscosity and inevitably causes (costly) frictional wear on processing equipment such as extruder screw flights, barrels, and die orifices. Second, the TLCP phase, which not only depresses processing viscosity during melt-extrusion, results in a structural reinforcement at a size scale much smaller than is possible with traditional hard additives [Macosko, 1995]. Properly formed aggregates of a polyblended TLCP phase are typically fractions of a micron in diameter compared to several microns for glass or graphite.

The formation of a "skin-core" morphology is one of the most visible morphological artifacts associated with LC and LC-blended fibers. Different aspect ratios of the included LC phase can arise between the skin and core regions of an extruded sample such that the superstructure of

fiber appears to segregate into concentric regions. The outer "skin" portion contains finely-elongated fibrils while the "core" portion is considerably less oriented and contains more coarsely-elongated fibrils if any. A postulate is that the outer skin layer, which advances slowly out of the die as it contacts the die surface, forms under elongational flow conditions because it must accelerate to the final mean velocity of the solidified product downstream. The inner (core), which advances more rapidly than the skin out of the die suffers deceleration as it approaches the final mean velocity and loses any orientation initially present in this region. Figure 1.9 depicts this velocity field gradient.

Nematic TLCPs, at temperatures above the crystal-to-nematic transition ($T_{k \rightarrow n}$), typically elongate readily and efficiently under a velocity field. The presence of a birefringent nematic state becomes evident using polarized light microscopy. The presence of elongated fibrils (however well-oriented), which lead to the formation of *in-situ* composites, does not guarantee mechanical property enhancement. Several of the studies presented within this thesis point to this conclusion. Further, in a significant number of the studies, the formation of *in-situ* composites, even when assumed to arise under the most ideal of conditions, are insufficient to account for the observed mechanical property enhancements. As a result, it is misleading to presume that *in-situ* reinforcement is the sole reason for mechanical property enhancements which do occur. Recent work by Joslin [1994] and Chang and Farris [1995] indicate that in addition to serving as a processing aid which can strengthen a polyester matrix, compatibilized thermotropic copolyesters also behave as nucleating agents which inherently modify the polyester matrix. The present results show systematic synergistic effects in the majority of blend systems with PEN, and evidence of the TLCP serving as a nucleating agent in ten out of ten investigations of TLCP systems with PEN.

1.11 Dissertation Overview

This thesis presents investigations of several novel blend systems of semi-rigid thermotropic liquid crystalline copolyesters and PEN. The aim is to determine the ability of these TLCPs to improve the performance of PEN. The limited availability of TLCPs for blending require the screening procedure developed for these TLCPs with PEN to focus on low loading levels of TLCP to achieve synergistic effects between additive and matrix. All blends contain between 80% to 99.75% PEN by weight.

Chapter 2 involves a detailed study of the PEN matrix in the absence of any additives. Here the aim is to determine how the various properties of PEN fiber matrix material evolve as a function of processing conditions and at levels of drawing. Studies involve thermal, mechanical, and wide-angle x-ray diffraction (WAXD) studies of PEN at several levels of draw. Chapter 2 also includes a comparative study of processing conditions for laboratory spun and treated PEN with an industrial pilot process for PEN production.

Chapter 3 focuses on the differences in chemical architecture and accompanying thermal properties of the pure components. This chapter introduces a nomenclature system which categorizes each TLCP into one of three classes based on structure. All discussions of individual TLCPs discussed in the remaining sections use this nomenclature system. Chapter 3 also presents estimated values for the rigid rod content and molecular weights (based on measurements of inherent viscosity) of each TLCP.

Chapter 4 discusses the mechanical properties of blends of pure TLCPs with PEN and compares these properties with theoretical predictions based on composite models which take the aspect ratio of the included phase into account. The most striking feature is that the Young's modulus is nearly identical for all 1% blends of main-chain flexible TLCPs (all of which contain

flexible ester methylene spacers). The magnitude of the enhancements seen at 1% addition challenges several widely-held presumptions associated with the model of *in-situ* reinforcement for TLCPs.

Chapter 5 examines the thermal properties of the blended systems and focuses on the effects of TLCP concentration on T_g, T_m, cold-crystallization temperature (T_{cc}), and ΔH_m . Many of the studies corroborate that the TLCPs serve as a nucleating agent for PEN, modifying the crystalline properties of the matrix. These effects become more profound with increasing TLCP content. The thermal history of the blends plays an important role in both the detection of certain crystalline transitions and in the final quality of melt-spun fiber.

Chapter 6 presents a description of a custom-constructed instrument for post-treatment of polymer monofilaments. This instrument uses a technique known as "time-of-flight" to estimate real-time stresses and draw ratios which arise in the fiberline through the course of post-treatment. These are the main parameters associated with fiber drawing processes.

Overall, the TLCPs seem to play an important role in nucleation and crystallization of the matrix, with mechanical property enhancements occurring at lower loading levels. The final section, Chapter 7, summarizes the main findings of this thesis and offers suggestions for future work. These suggestions focus on specific studies to clarify the roles of the nematic state and ester interchange reactions in affecting the mechanical and thermal properties of treated fiber polyblends. Finally a systematic study of processing conditions correlated with mechanical properties is suggested.

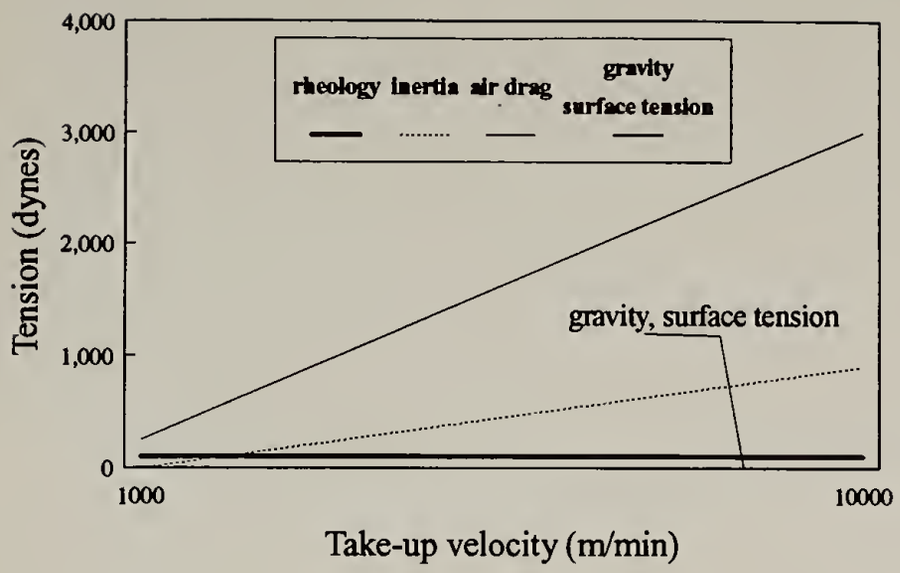

Figure 1.1. Maximum contributions to a polyester spinning line tension. Calculated tension vs. spinning speed for spinneret radius R_o=125 μm, filament radius R_L=9.25 μm (constant), in stationary cooling air.

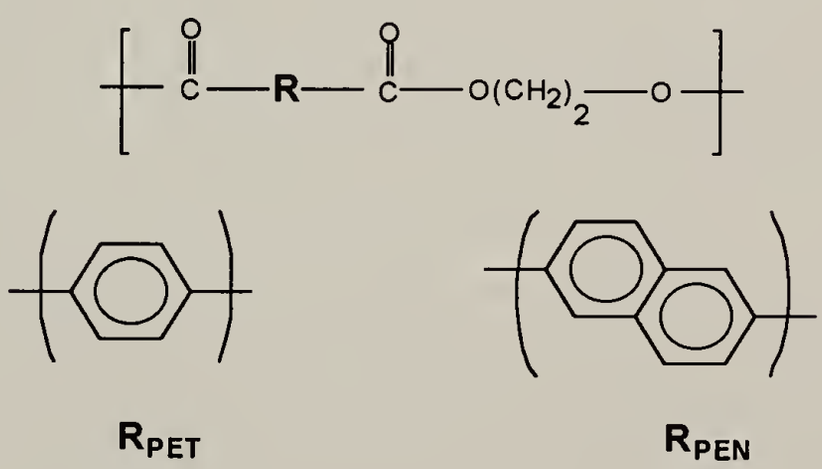

Figure 1.2. The similar structures of PEN and PET.

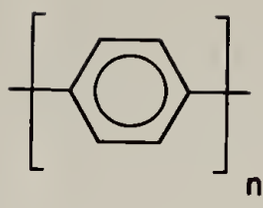

Figure 1.3. Repeat unit of PPP.

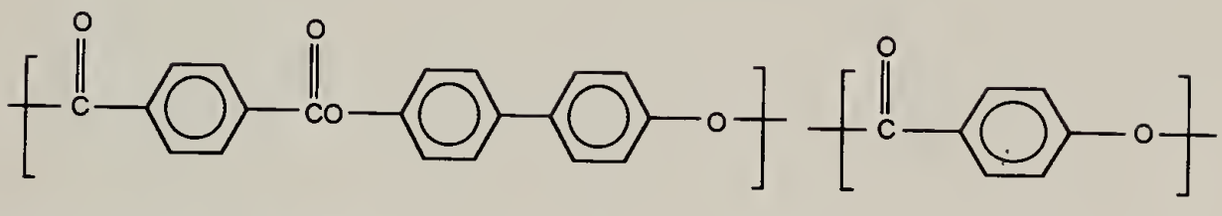

Figure 1.4. Amoco Xydar®.

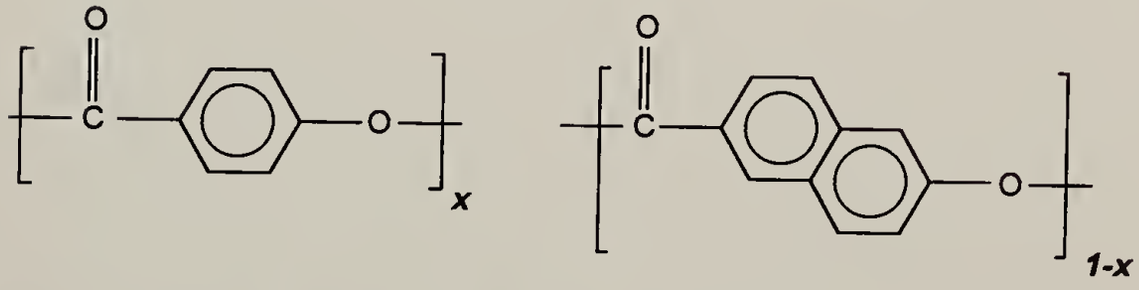

Figure 1.5. Hoechst-Celanese Vectra® A.

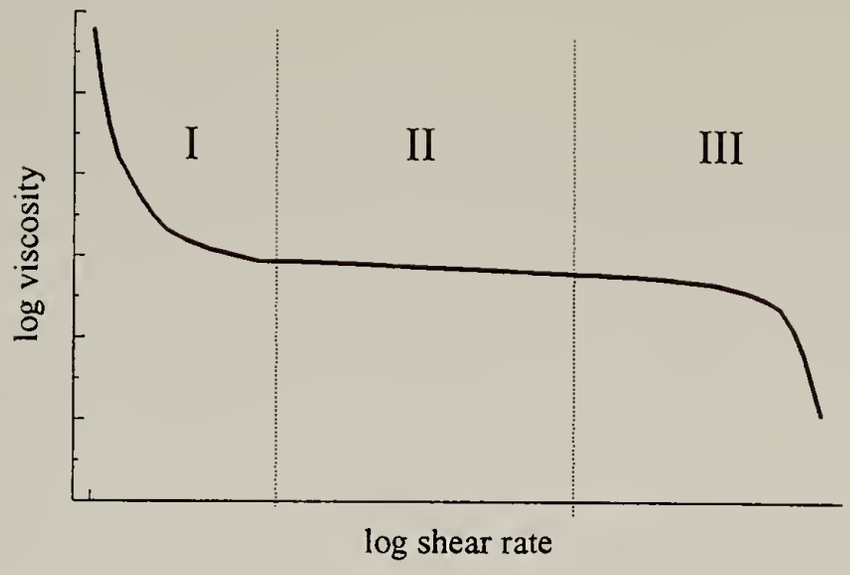

Figure 1.6. Rate dependence of viscosity.

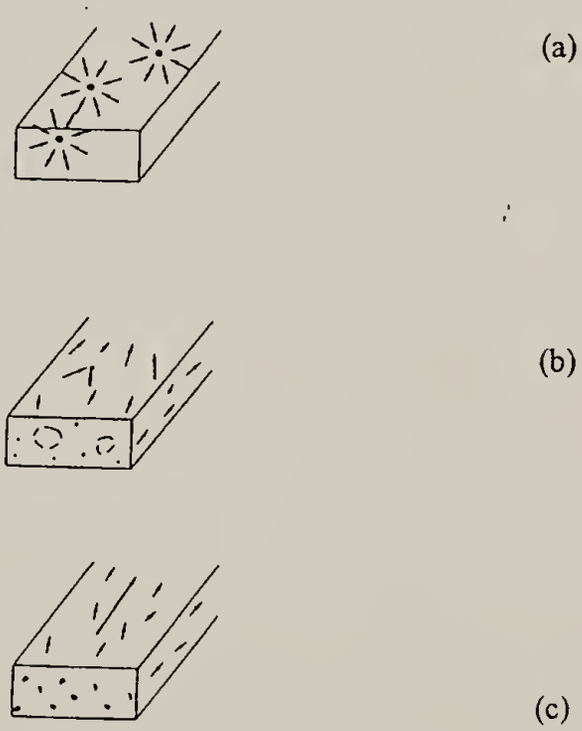

Figure 1.7. Three structural models proposed for an LCP under an applied stress field. (a) initial state in which directors point randomly; (b) development of continuous phase; (c) development of oriented phase.

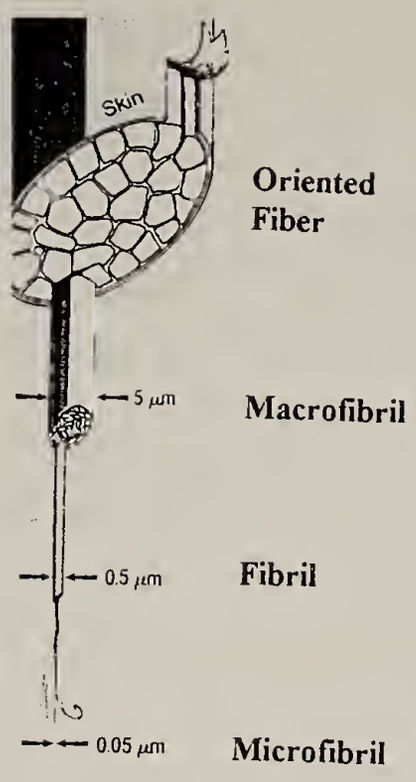

Figure 1.8. Vectran® fiber structural model.

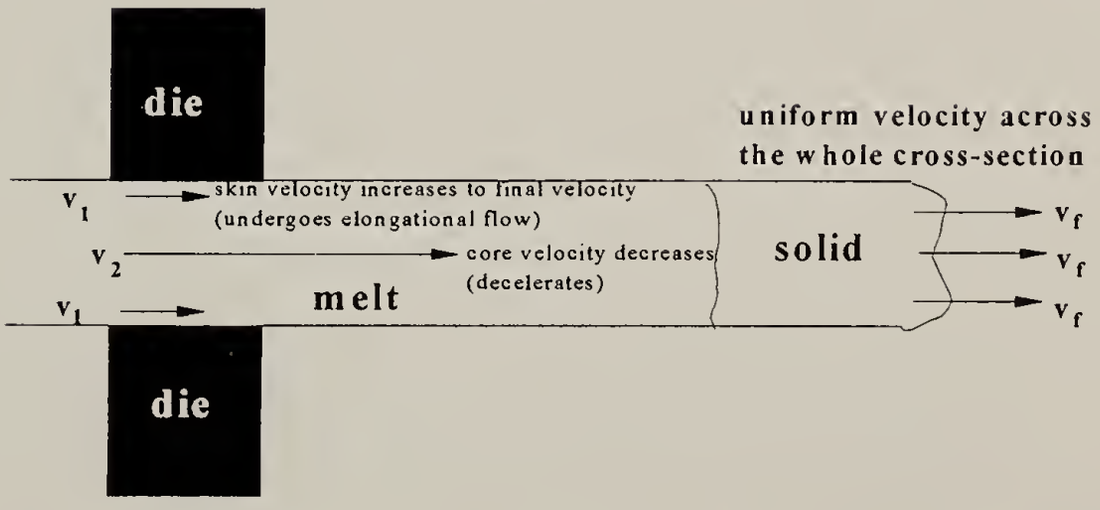

Figure 1.9. Shear velocity gradient at an extrusion die leading to skin-core morphology.

CHAPTER 2

STUDIES ON NEAT POLY(ETHYLENE 2,6-NAPHTHALATE)

2.1 Introduction

The chemical differences between PEN and PET manifest as significant differences in their physical properties. For example, PEN is more thermally stable than PET. For typical thermal transitions such as those shown in Figure 2.1 for (unoriented) PEN, the transition temperatures are systematically higher than those of PET. The substitution of a stiffer naphthalene moiety in PEN over that of phenylene in PET also results in higher values for certain mechanical properties [Huijts and Peters, 1994].

Because PET has been studied much more widely than PEN, comparatively fewer publications exist for PEN fibers than for PET.

This chapter describes and compares PEN fiber processing techniques for spinning monofilaments. This chapter also presents characterization studies of PEN fiber at different levels of solid-state drawing, in the absence of additives. Several of the structure/property studies are the first of their kind on PEN fiber.

2.2 Materials and Procedure

Eastman Kodak provided the PEN matrix material referenced by "KAN 440056" with batch designation "ER 7313." The material arrived in pellet form in two separate shipments and received no further purification prior to use. Table 2.1 provides details of the as-received materi-

als. (The two batches of PEN ultimately exhibited different thermal properties in the as-received form.)

The general procedure to transform bulk material into a useful and workable fiber form consists of three steps: pre-treatment, melt-extrusion, and post-treatment. The following studies concern only the PEN matrix material. The aim is to expose the matrix material to similar conditions that will be used in subsequent PEN-dominated blends.

2.2.1 Fiber Formation

The following descriptions of PEN fiber formation and processing were developed after several trials. The physical quality of melt-spun PEN, unlike PET, depends strongly on processing parameters in preliminary, intermediate, and final stages of processing. For example, experiments of spinning PET and PEN show that PEN is more sensitive to moisture.

The goal is to extrude a high-quality fiber that exits the die continuously as a transparent (or mostly translucent) stream, free of unmelted particles. Quality is gauged by how well the fiber is anticipated to behave under post-treatment. Previous melt-spinning experiments on PET on the same equipment reveal that only high-quality as-spun fiber lends itself to further post-treatment steps. Fiber quality is related to ease of post-treatment because fiber failure mechanisms are chiefly defect-driven. If the concentration of defects is not kept low, subsequent post-treatment results in fiber breakage rather than fiber strengthening.

While only high-quality fiber was actually used in subsequent studies, all varieties of fiber quality were encountered while developing the processing conditions for PEN. The worst possible result is the complete cessation of flow -- in which powdered polymer enters as a feed but nothing exits as an extrudate. In these situations, it is usually the case that unmelted polymer has accumu-

lated along the feed screw and blocked the flow passage. When flow is blocked, it is usually necessary to remove the feed source and dissemble the system for cleaning before re-building spinning operations. Table 2.2 serves as a brief troubleshooting guide that describes the symptoms, the probable cause, and the suggested solutions for the most common problems that arise when melt-spinning PEN.

2.2.1.1 Step 1: Pre-Treatment

The purpose of the following pre-treatment steps is to keep the PEN free of moisture and to subject it to the same homogenization steps as its counterpart in TLCP blends. These steps are very similar to previous steps taken with PET and its blends [Joslin, 1994]. The effects of residual moisture content in high temperature experiments for these polyester systems are of concern [Greener, 1994] [Kantor, 1995]. Researchers report similar levels of activation energy for hygroscopic weight increase for both PET and PEN films [Ouchi et al., 1992].

The pre-treatment procedure begins with drying the PEN pellets for 48 hours at 90°C. These conditions are important. These conditions were determined through three months of processing experiments concerning how to transform powdered PEN into a monofilament. Kodak provided information suggesting a drying temperature of 150°C, but this temperature seemed too close to the cold-crystallization temperature of PEN. Their suggested drying temperature could increase the level of crystallinity through cold-crystallization -- presenting a potential problem. Thus, drying trials were done at temperatures between 24 - 48 hours at 70° - 150°C in conjunction with spinning experiments. Generally, the higher the drying temperature and the longer the drying time, the more degraded and yellowed the PEN fiber stream appears during melt-extrusion. (For blends dried for 24 hours at 150° C, spinning at 305°C resulted in the appearance of unmelted particles in

the fiber stream. Spinning at 310°C resulted in a yellowed fiber stream containing bubbles. For blends dried for 24 hours at 70°C, spinning at 305°C resulted in the evolution of bubbles and vapors followed by the near-cessation of flow [with PEN exiting more as discrete "blobs" than as a stream]. Spinning at temperatures near 300° resulted in mostly bubble-ridden fiber. Heat is necessary when in drying PEN under vacuum. For blends dried 24 hours at room temperature, spinning at 290°C resulted in vapors evolved from a steadily flowing stream of yellowed, bubble-ridden fiber.)

The next step is to use a Carver laboratory press to compression mold the dried pellets under N_2 for 1 minute at 270°C between two stainless steel plates lined with sheets of duPont Kapton® polyimide film. The molded "cakes" are quenched quickly also under an N_2 atmosphere. (A new grade of low concentration zinc-impregnated polyimide film seemed to give better lift-off results than ordinary high-performance Kapton®.) The final thickness of the PEN melt-pressed cakes is approximately 2 mm. The effect of higher temperatures used in the initial pressing step significantly reduces the molecular weight of the sample. Table 2.3 details the effects of pre-treatment only on the molecular weight, determined by gel permeation chromatography (GPC) and inherent viscosity in a 40:60 (v/v) solution of 1,1,2,2- tetrachloroethane/*p*-chlorophenol at 26°C.

The third step is to break up and grind the melt-pressed cake into powder having a particulate size less than 1000 μm. An analytical mill with cooling water circulation to prevent sample heating and a wire sieve with a 1000 μm mesh are useful for these purposes. Figure 2.2 shows an example of a compression-molded cake and ground powder.

The final step prior to melt-extrusion is to redry the powder under vacuum for 48 hours at 90°C. Note that transporting vacuum-dried materials requires the use of a desiccator with minimal exposure of the materials to air in general.

2.2.1.2 Step 2: Melt-Extrusion

Melt-extrusion experiments are done using a ¼ inch diameter single screw extruder (shown in Figure 2.3) made by Randcastle Corporation having a 1575 μm diameter circular die orifice. This device has multiple temperature controls for different zones along the extruder barrel. The powder charge from pre-treatment steps enters the extruder (shown in Figure 2.3) through a hopper funnel fitted with a glass funnel feeding in N_2 purge gas at 8 psi.

An independent control for the screw speed in revolution per minutes (rpm) effectively determines the residence time of the molten charge as it flows down the barrel. The final quality of fiber product is very sensitive to the values of die zone temperature and screw speed.

Melt-extrusion of PEN was done at 290°C, which is just above the temperature corresponding to the end of the melting endotherm in DSC scans. All temperature set-points were 290°C. This temperature is 10 degrees higher than where Kodak processes their PEN and 13 to 30 degrees lower than those suggested by an analytical expression shown as a claim in a United States patent for spinning naphthalate fibers assigned to Teijin Ltd. [Hamana et al., 1973]. In practice, the studies herein reveal that die temperatures lower than 290°C resulted in unmelted particles in the stream. Temperatures 300°C or higher for neat PEN led to inconsistent extrudate flow, often containing clear signs of degradation.

The specific protocol used to pre-treat the charge for melt-extrusion is important. Only PEN prepared following protocol "B," again referring to Table 2.1, was used. PEN pre-treated in accordance with both protocols "B" and "C" resulted in a workable product, suitable for analysis. The use of protocol "B," however, resulted in comparatively less molecular weight reduction. PEN pre-treated in accordance with protocol "A," which received no compression-molding prior to extrusion, resulted in completely unusable product. In the case of protocol "A," the as-spun fiber

contained many bubbles when spun at a variety of spinning conditions. The conclusion is that using high molecular PEN containing relatively higher levels of moisture cause degradation that is detrimental to fiber quality.

The screw speed for extrusion was constant at 55 rpm, corresponding to a mass flow rate of just under 3 g/min. The molten polymer has 2-3 minutes residence time within the extruder barrel. Higher temperatures and longer residence times promote the likelihood of excessive transesterification and other degradative reactions [Stewart et al., 1993]. [Backson et al, 1995].

A take-up device winds the extruded fiber at approximately 75 m/min after it solidifies in ambient air after exiting the die orifice. Based on diameter measurements of as-spun fiber, the resulting spin-draw ratio (i.e. from the molten state) is approximately 300 for neat PEN and between 250 to 400 for PEN blends.

To clean the extruder before and after each melt-spinning experiment, flaked poly(propylene) (PP) obtained from Himont was used to flush the extruder barrel until the pure PP exits as a transparent extrudate.

2.2.1.3 Step 3: Post-Treatment

Post-treatment (also known as drawing) effectively transforms as-spun fiber into high-performance fiber by orienting the polymer chains within the fiber. Drawing for fiber-forming semi-crystalline polymers generally occurs through a two-stage process. Drawing, in both the "cold-" and subsequent "hot-drawing" steps, is critical for attaining high Young's modulus enhancement needed in fiber applications [Grulke, 1994]. As depicted in Figure 2.4, the only operational difference between cold- and hot-drawing steps is the temperature of the heated zone. While the generic process may appear simple, drawing has tremendous impact on the final mechanical

properties of the fiber and serves as a basic technique for polymer strengthening through re-crystallization [Pakhomov et al., 1993] [Zaitsev and Varyukhin, 1993].

Conventionally for polyesters, there are two stages of drawing. While the two stages are both done at temperatures T such that $T_g < T < T_m$, these stages of drawing are different in nature and obey different physical laws. Cold-drawing, which is usually done just above the T_g, can allow for a solid phase chain-folded to extended-chain transition within a neck region. Necking is the result of segmental orientation which occurs as polymer chains unravel locally and move to counteract the applied stress [Carraher, 1994]. Hot-drawing, constrained to temperatures above that of cold-drawing yet below T_m, allows plastic deformation of a newly built fibrillar structure from a natural up to an ultimate draw ratio. Both processes rely on elevated temperatures to lower the criterion for yielding and to allow for the mobility of polymer within a molecular network of chains [Egorov and Zhizghenkov, 1993] [Ward, 1994]. Generally, higher draw ratios result in higher Young's moduli such that maximizing the draw ratio is desirable in almost all cases [Bekhet et al., 1993] [Shaw and Gilbert, 1994].

In these studies with PEN, as-spun fiber feeds in at a rate between 0.7m/min to 1 m/min. Cold-drawing took place continuously at temperatures between 140°C to 145°C. Cold-drawing reached a limit at λ=5.9. Hot-drawing proceeded at 215°C, resulting in a final draw ratio of λ=12.5 for the most highly drawn specimens.

2.2.2. Mechanical Testing

Fiber specimens of 50 mm gage length were mounted onto paper tabs with an adhesive to facilitate specimen handling and testing alignment [Allen, 1983]. Fiber diameters were averaged over a minimum of five measurements per specimen using an Olympus microscope equipped with a

calibrated scale accurate to ± 0.5 μm. Tensile tests were performed using an Instron 5564 tensile tester programmed with a cross-head speed of 5 mm/min, giving a strain rate of 10% min^{-1}. The tester unit is linked to a personal computer running Instron Series IX software which sampled tensile data at 56 Hz for initial modulus measurements. The Young's modulus was determined from the best linear fit through the initial (elastic) region of the stress-strain beginning from the origin. Instrument compliance, done in accordance with ASTM Standard D3379-75 for the Instron 5564 using a series of Kevlar 149 fiber, is 0.12 mm/N. For these studies, this means that the apparent modulus is negligibly (0.01% to 0.015%) lower than the true modulus. Other tensile properties measured were ultimate strain and stress. Each tensile property was averaged over twelve tests performed at ambient conditions in the laboratory. Data for tests exhibiting slip or grip failure were omitted for modulus or ultimate property measurements, respectively.

The above methods are the same as those used to determine the tensile properties of PET fiber from previous work.

Though not employed here, other methods reported in literature to quantify the mechanical properties of PEN include microhardness tests and tensile testing using changes in crystalline *d*-spacing for strain measurements [Nakamae, et al., 1993] [Rueda et al., 1994].

2.2.3 Wide-Angle X-ray Diffraction (WAXD)

WAXD experiments were done on fiber samples using a Ni-filtered CuK_α source at 1.514Å collimated to 0.20 mm. To achieve an equivalent effective scattering volume for each fiber sample, monofilaments were densely wound in parallel around a punched grid sample holder such that each sample had an effective diameter of 1000 μm.

Samples were placed in an evacuated Statton camera chamber. The films were situated 53 cm away from a beam operating at 30 mA and 40 kV. Total exposure time was 5 hours for each sample.

2.3 Results and Discussion

The following details the results of mechanical, scattering, and thermal characterization for a series of neat PEN, post-treated to different extents.

2.3.1 Effects of Draw Ratio

The highest draw ratio (λ=12.1) obtained in this work with PEN surpasses previously-reported maximum draw ratios for PEN by over a factor of two [Ghanem and Porter, 1989].

A cold-drawn sample has seen temperatures near its T_g only. A hot-drawn sample has necessarily been drawn twice (the first of which the cold-drawing). Figure 2.5, a plot of Young's modulus as a function of post-treatment draw ratio, shows the effects of draw on the stiffness of the fibers. The change in Young's modulus rises sharply approaching the limit of cold-drawing at λ=5.9. Samples at this limit and below have been cold-drawn at 150°C. Samples above this limit have been subsequently hot-drawn at 215°C. Significant structural changes evolve as a function of draw ratio and temperature. To illustrate this, Figure 2.6 shows a series of WAXD patterns on the same draw ratio series of PEN. These panels reveal that the sample is essentially unoriented at low $\lambda < 3.0$. There is, however, a significant change in the observed structure within a relatively narrow range of draw: between $4.4 < \lambda < 5.9$, the structure changes from that of weakly-oriented to that of a highly-developed triclinic crystal structure [Mencik, 1967] [Buchner et al., 1988]. The

Young's modulus increases more than four-fold over this range. As a possible insight for the changes occurring during cold-drawing described above, existing WAXD work on initially-unoriented PEN films drawn uniaxially at 150°C evidence crystal lattice distortion followed by "double orientation" in which the naphthalene rings in the main chain become preferentially aligned parallel to the local film surface [Murakami et al., 1995].

Hot drawing to $\lambda > 5.9$ serves to enhance the existing triclinic crystal structure. Figure 2.7 shows a plot of modulus as a function of both draw ratio and the apparent heat of melting (ΔH_m), which is related to the level of crystallinity [Cheng and Wunderlich, 1988] [Cheng et al., 1988] [Buchner et al., 1989] and the amount of stored strain in the sample for drawn fibers. The stiffness increases as a function of both parameters.

Figure 2.8 shows the ultimate properties as a function of draw ratio. Ultimate properties are related to failure mechanisms which are primarily defect-driven. As a result, the standard deviations for the ultimate properties are characteristically higher than those for Young's modulus (about 20% as opposed to under 5% respectively) but the trends of higher strength and lower elongation with increasing draw are both clear.

2.3.2 PEN Comparisons

The following sub-section presents a comparative study of processing conditions for PEN from this thesis and those found in a recent publication from AkzoNobel [Jager et al., 1995], most likely to become one the first corporations outside of Japan to commercialize a fiber form of PEN. The second section provides a brief comparison between PEN and PET fiber formed on-site.

2.3.2.1 Comparison of PEN Processing Conditions

Figure 2.9 shows a comparison between Young's modulus for neat PEN achieved through processes discussed in preceding sections and those for a pilot process reported by Akzo. The result is that PEN fiber made here on-site is comparable or higher in stiffness than that made by Akzo. (The common benchmark is Diolen® 1125T, a commercial form of high-speed spun PET yarn made by Akzo.)

While the final Young's modulus of all three types of PEN fiber is virtually the same, a comparison of the processing conditions used to fabricate the fiber products reveals several differences. Table 2.4 is a summary of the steps to melt-spin PEN at both sites. "Akzo PEN4000", made through a one-step process as discussed in the previous chapter is the analogous naphthalate-based polyester to Diolen®. "Akzo PEN700b" is a relatively lower-speed spun which requires separate post-treatment steps. It is clear that one may form high-performance PEN fiber using far simpler and less aggressive conditions than those used in the industrial pilot process.

2.3.2.2 Comparison to PET

As shown in Figure 2.10, the yield properties of as-spun PEN and PET are nearly identical (yielding at approximately 3% strain at 50 MPa). The elastic tensile properties of neat PEN also compare favorably to those of PET. The Young's modulus of fully post-treated PEN, however, is much higher than that of PET. The biggest difference in processing conditions is that of cold-drawing. PET, whose T_g is 82° as measured by differential scanning calorimetry (DSC), is easily cold-drawn at 85°C. PEN, whose T_g is 119°C, was cold-drawn in these studies at 145°C. This

temperature is significantly higher than the glass transition and slightly lower than the temperature used to cold-draw subsequent blends.

2.4 Conclusions

This chapter described how to melt-spin PEN into a useful fiber form. One of the first observations is that the thermal history of the initial material determines the quality of the extruded fiber, and even the extent to which product is obtainable. The quality of the extruded fiber is especially sensitive to the total exposure time to the high temperatures of the die zone.

The mechanical properties of the PEN fiber depend strongly on the level of post-treatment. The morphological superstructure changes radically as a function of draw. The amount of draw attained during cold-drawing plays a large role in the final mechanical performance. The cold-drawing temperature generally dictates the maximum level of draw possible. In these cases, cold-drawing is done at a temperature well above the glass transition. Necking, a type of yield transition, is not observed during cold-drawing because the material is cold-drawn as a rubber. While these results are in accord with other preliminary published results on PEN fiber [Huijts and DeVries, 1993] [Jager et al., 1995], it differs from reports on PEN film which discuss PEN necking behavior at 145°C [Cakmak et al., 1990].

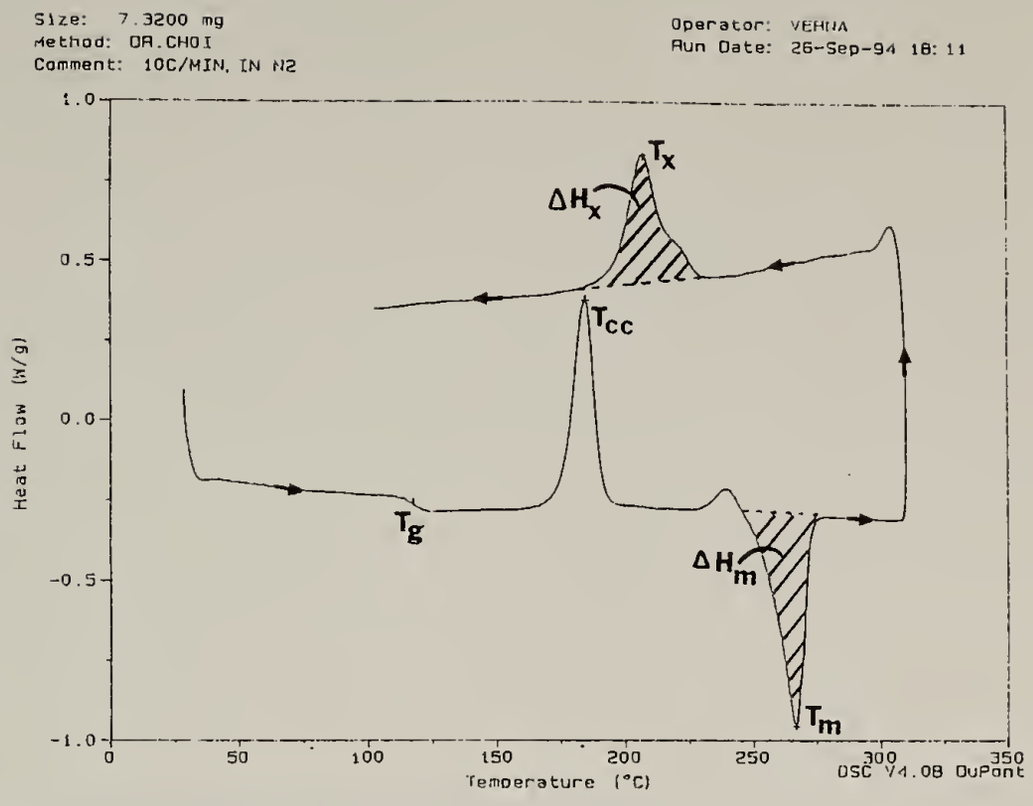

Figure 2.1. DSC scan of thermal transitions for unoriented PEN.

Figure 2.2. Melt-pressed and ground PEN.

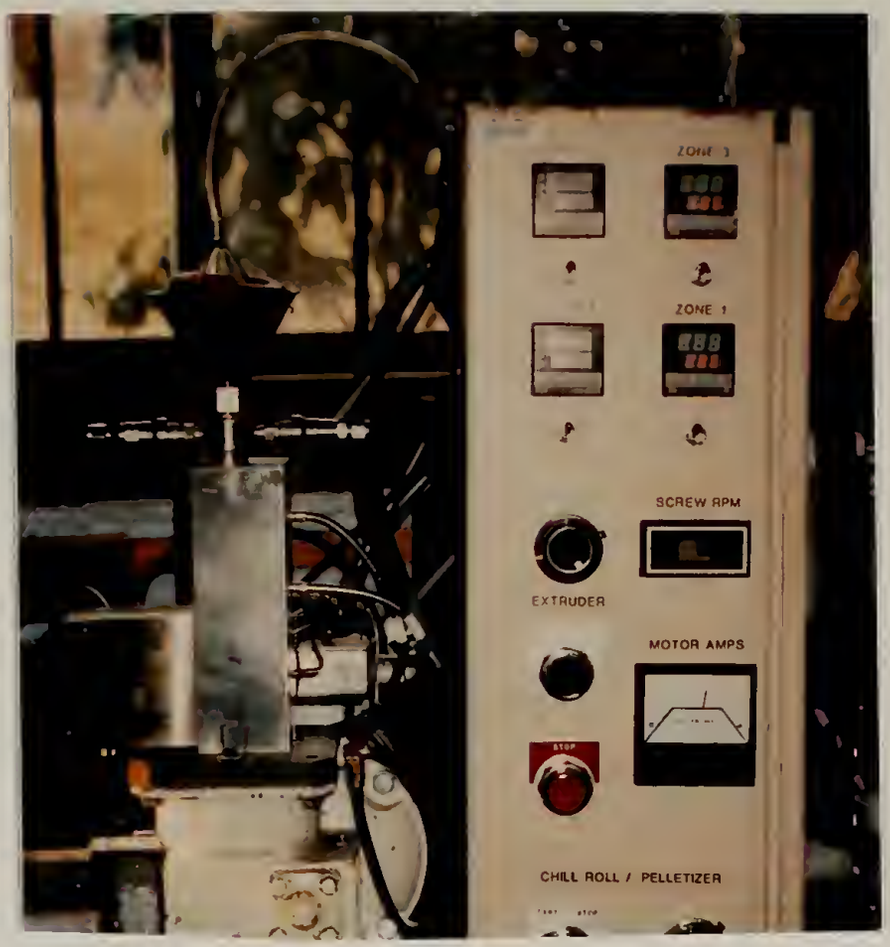

Figure 2.3. The Randcastle Microtruder, a single screw extruder for melt-spinning operations.

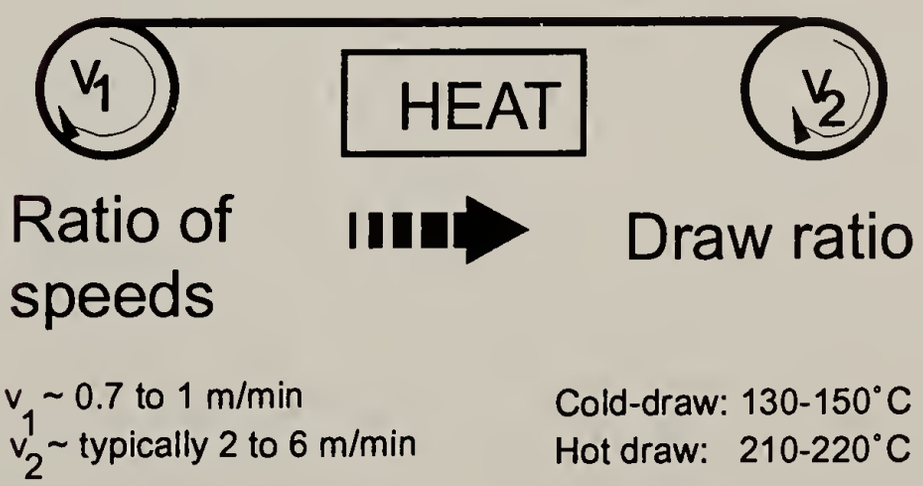

Figure 2.4. A generic depiction of the post-treatment process.

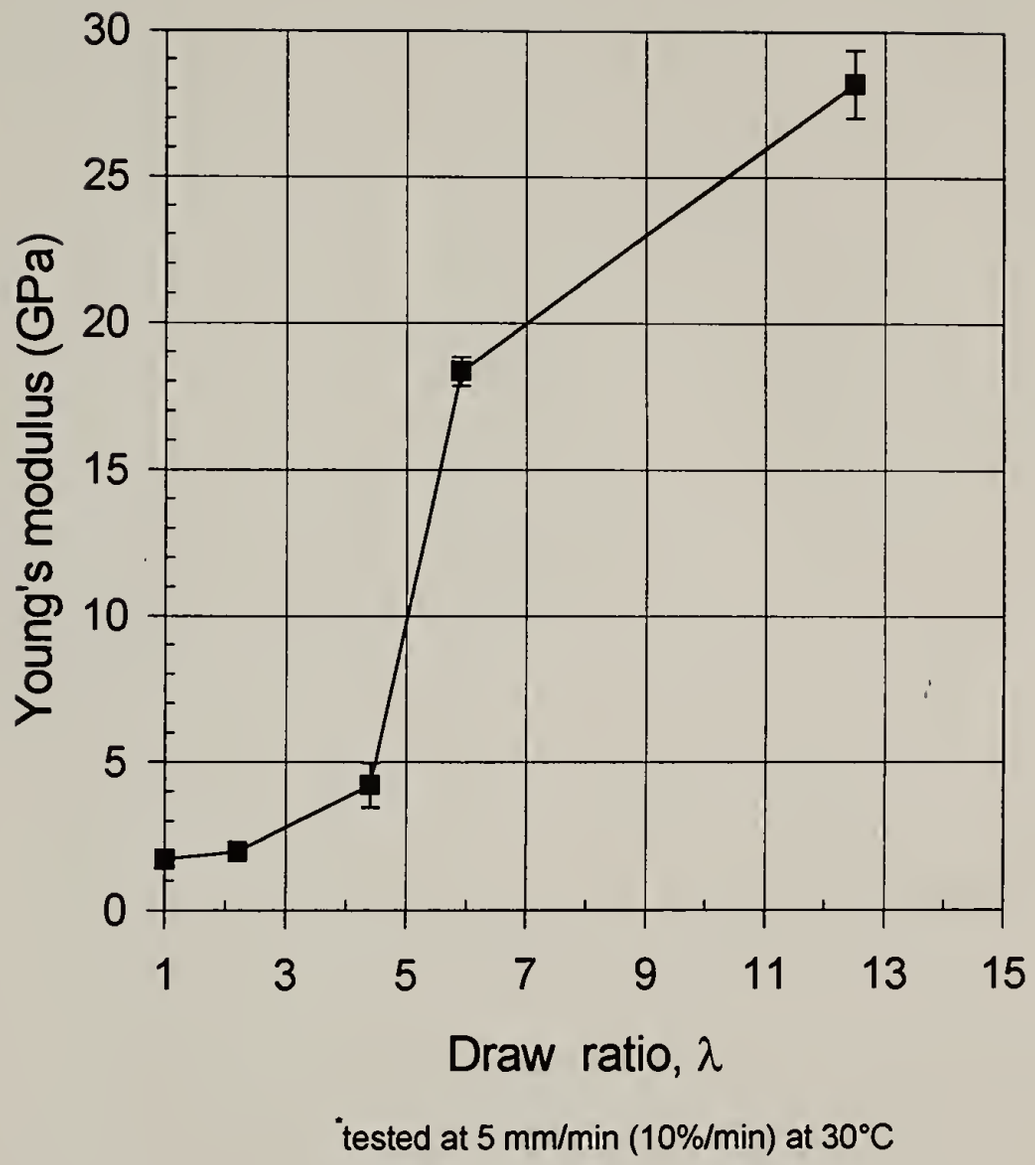

Figure 2.5. The effect of draw ratio on the Young's modulus of PEN monofilaments.

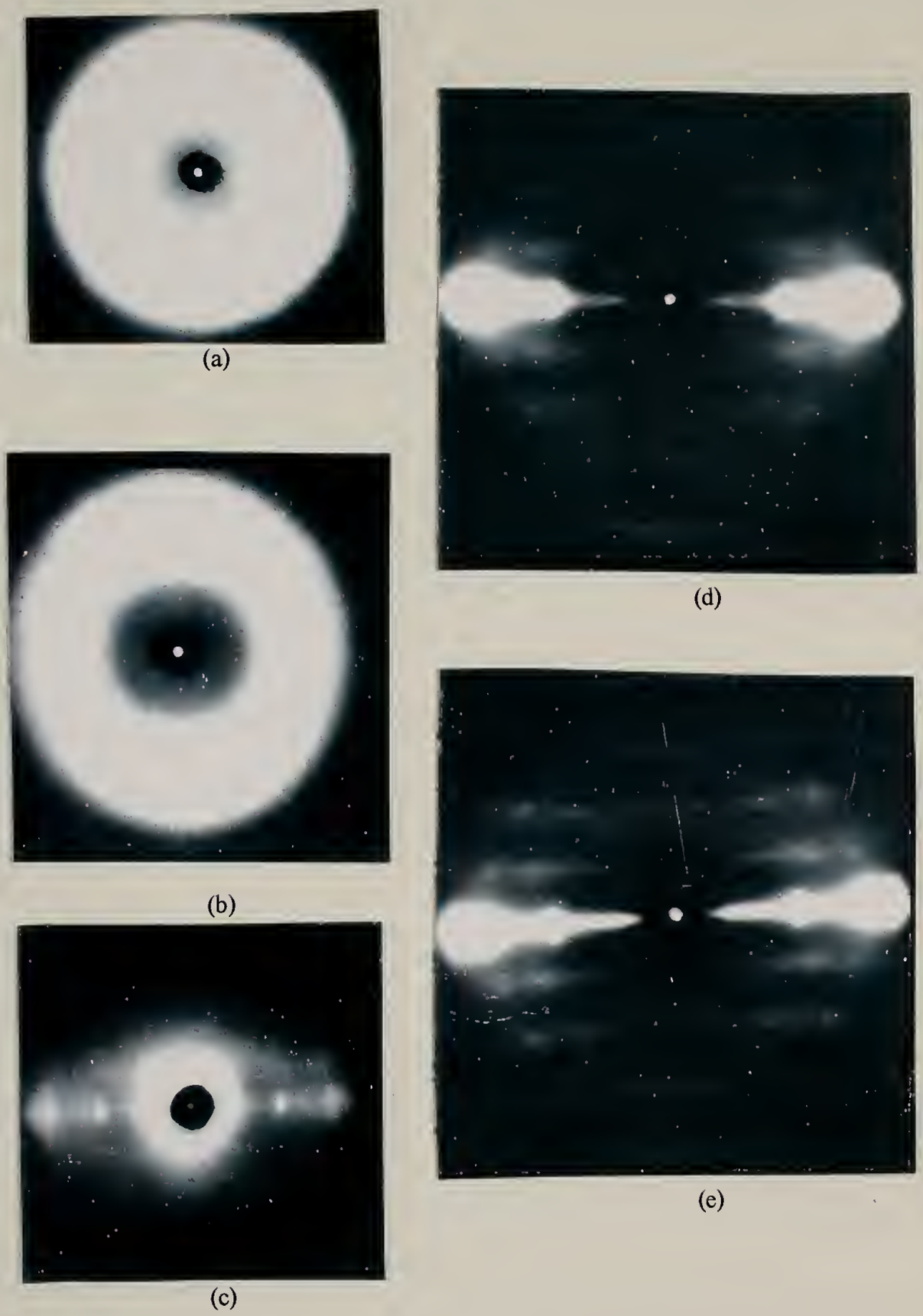

Figure 2.6. WAXD patterns for a series of drawn PEN monofilaments. (a) $\lambda \equiv 1.0$; (b) $\lambda = 2.2$; (c) $\lambda = 4.4$; (d) $\lambda = 5.9$; (e) $\lambda = 12.5$.

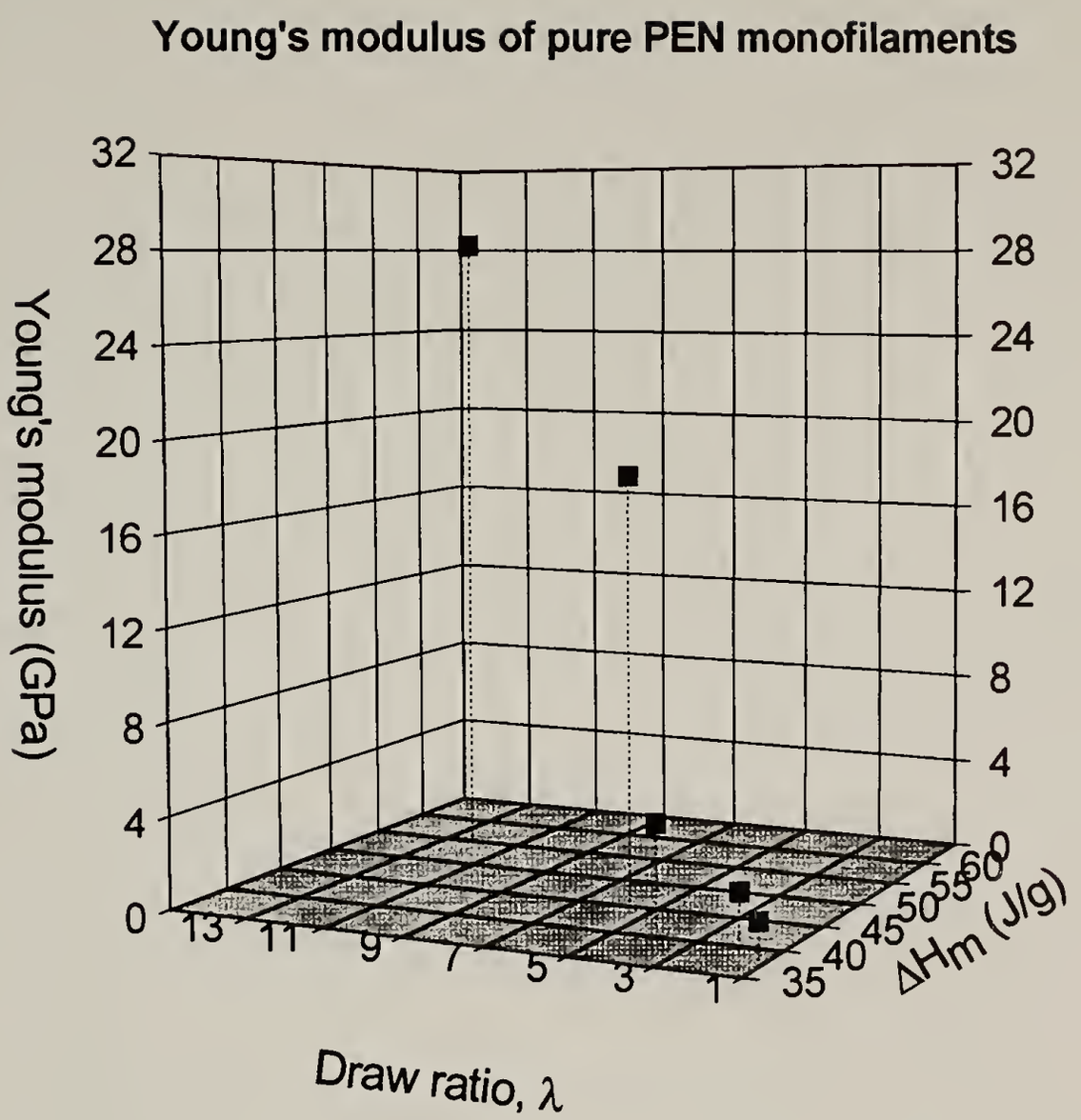

Figure 2.7. Young's modulus as a function of draw ratio and the apparent heat of melting for PEN monofilaments.

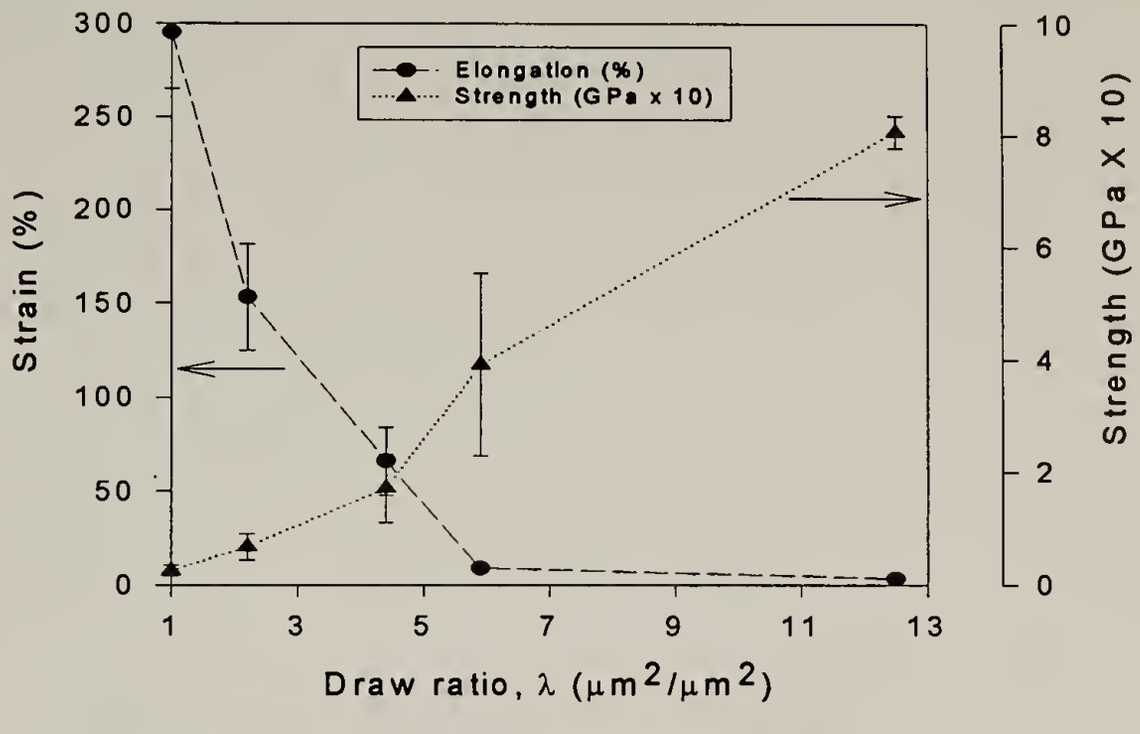

Figure 2.8. Ultimate properties of a PEN monofilament draw ratio series.

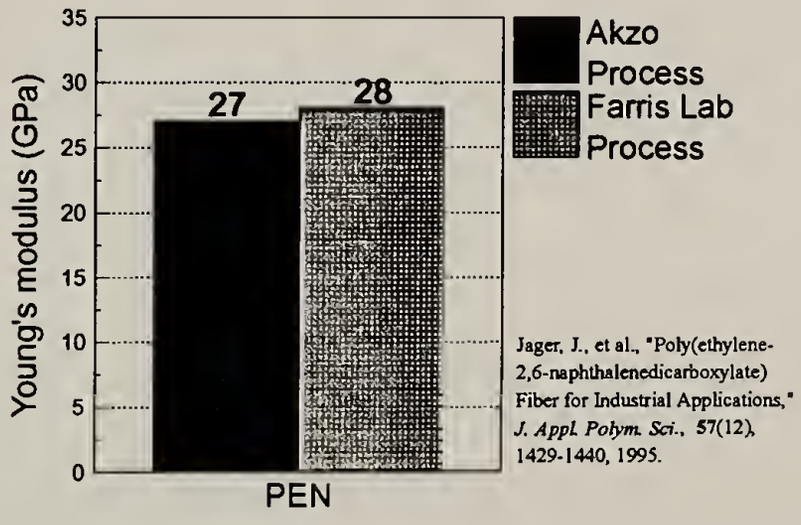

Figure 2.9. Comparison of mechanical properties achieved for PEN fibers.

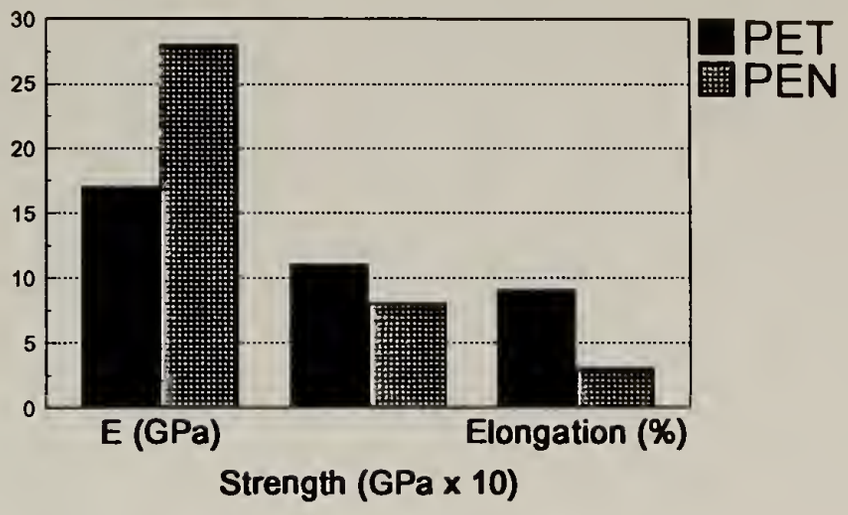

Figure 2.10. Mechanical properties of drawn PET and PEN fiber.

Table 2.1 PEN characterization data provided by Eastman Kodak.

Property	Value
As-received form	pellet
η_{inh} (dl/g)	0.69
Melt viscosity (P) (g cm^{-1} s^{-1})	7500 (at 305 °C)
T_g (°C)	120
T_m (°C)	266

Table 2.2. The symptoms, causes, and solutions of frequently encountered problems during the melt-spinning of PEN.

Symptoms	Probable cause	Suggested solution
Complete cessation of flow	Unmelted particles stuck to feed screw (most likely in Zone 1)	Quickly raise Zone 1-3 temperatures. If polymer does not flow out within 4-5 minutes, (1) spoon or vacuum out the feed (2) slow the screw speed to zero (3) reset target temperatures to just above Tg of material (4)momentarily shut off and remove feed cooling lines to quickly dissemble and remove external housing (5) re-attach feed cooling lines immediately (6) run cooling water faster to speed cooling process (7) carefully remove the die as soon as it is cool enough to handle with insulated gloves. It is only possible to easily remove the die while the material inside is semi-molten. The die has comparatively large thermal mass; other zones will cool much more quickly if the die is removed. (8) once temperatures of Zones 1-3 are near Tg, shut off all cooling water and remove cooling lines (9) quickly disassemble the extruder housing (10) clean out bore and screw. Note where along the bore/screw material got stuck (11) re-assemble and reset targets
Unmelted particles in the stream Translucent stream (i.e. not transparent)	Insufficient exposure of feed to high temperatures	Lower the screw speed Raise target temperatures If problem persists, try cleaning out the extruder. Note: pre-treatment conditions may have crystallized the material
Bubbles in the stream	degradation due to heat or impurities	Raise the screw speed Lower target temperatures if maximum screw speed still results in bubbles Note: impurities such as water many have remained in spite of pre-treatment conditions
Degraded particles or discolored appearance of polymer stream	degradation due to heat or impurities	Raise the screw speed Lower target temperatures if maximum screw speed still results in bubbles. Note: impurities such as water many have remained in spite of pre-treatment conditions

Table 2.3. Pre-treatment effects on the molecular weight of PEN.

	A Ground only	B 1 minute @ 270°C	C 1 minute @ 280°C
η^*_{inh} (dl/g)	0.69	0.67	0.57
M_n	16,000	14,000	12,950
M_w	42,400	35,600	33,250
M_z	65,150	54,250	51,250
PDI	2.6	2.5	2.6

*in (40/60) (v/v) 1,1,2,2-tetrachloroethane/*p*-chlorophenol at 26°C

Table 2.4 Comparison of PEN melt-processing conditions.

	Laboratory PEN	AKZO PEN700b	AKZO PEN4000
Spinning temperature (°C)	290	310	310
Spinning speed (m/min)	60	700	4000
Exit chamber temperature (°C)	N/A	354	N/A
Pre- cold drawing temperature (°C)	N/A	115-120	N/A
Cold-drawing temperature (°C)	140-145	130-140	N/A
Hot-drawing temperature (°C) / medium	215 / air	260 / hot steam	260 / hot steam
Hot-drawing exposure time	9 seconds	10 - 15 seconds	10 - 15 seconds
Finish	N/A	0.5 wt% oils and anti-stats	0.5 wt% oils and anti-stats
Final draw ratio	12.5	6.2	1.3
Final Young's modulus (GPa)	28	27	27

CHAPTER 3

PROPERTIES OF THE PURE TLCPS

3.1 Introduction

The polarizabilities of the rigid components incorporated in LCPs are highly anisotropic. As a result, LCPs have the ability to de-polarize and retard light, forming a topologically stable ensemble of defects known as a texture [De'Nève et al., 1995]. The nematic texture, observable through polarized light microscopy (PLM), resembles that of a colored marble surface. Their anisotropic nature also allows LCPs to scatter white light differently. When viewed without crossed polars, a nematic melt appears turbid and gives rise to stir-opalescence [Li et al., 1994].

While the optical characteristics of nematic LCPs are similar, their thermal and rheological properties in general depend strongly on their thermal histories [Han et al., 1994] [Han and Kim, 1995]. Some of these properties facilitate their role in compatibilized blends with thermoplastic polymers. (The term "miscible blend" implies a single phase structure, whereas a "compatibilized blend" refers to a polyphasic structure with interaction at phase boundaries [Jaffe et al., 1994]).

Ten thermotropic aromatic copolyesters recently synthesized by members of Prof. Lenz and Prof. Kantor's research group at the University of Massachusetts Department of Polymer Science and Engineering were designed for compatibilization and *in situ* fiber-forming studies with PEN. Each of these TLCPs contains main-chain mesogenic units which result in nematic textures over certain working temperature ranges. The total amount of each pure TLCP available for all characterization and subsequent blending procedures typically ranged between 7 - 10 grams.

Chemically, these TLCPs are very similar to one another and, to varying degrees, very similar to the PEN matrix itself. While these similarities are favorable in promoting compatibility with the matrix, they also manifest as similarities in other properties such as thermal transitions (associated with glass transition and melting behavior for example), and solvation by common organic solvents. As a result, it is difficult to distinguish the matrix from the TLCP in common characterization techniques. Also, the similarities in their chemical structures make for similarities in electron density -- precluding the successful application of various scattering and electron microscopy techniques to distinguish the two components.

The chemical similarity of these TLCPs also permits an added degree of chemical compatibilization with the matrix through transesterification reactions between ester groups on adjacent chains at temperatures approaching their melting points [Economy and Goranov, 1995] [Jo et al., 1995] [Su and Wei, 1995]. The result is randomization of otherwise blocky or homogeneous polymers [Backson et al., 1995]. In 1973, Lenz and Go coined the term "crystalline induced reorganization" to describe such reactions.

From a molecular structural standpoint, there are two broad types of LCPs: those with mesogenic units in the main-chain, and those with mesogenic units in a side-chain [Pucciariello and Carfagna, 1994]. While all of the LCPs discussed in this chapter are main-chain mesogenic and intended for blend compatibilization work with PEN, their specific architectures differ in a subtle, but systematic, manner. Each TLCP falls into one of three main classes discussed below. For ease of referencing, TLCP designations consist of a letter representing its class and a subscripted number representing its position within the class. TLCPs that are very similar chemically differ only by one iteration of the subscripted number. For example, for class X designated below, X_3 is more chemically similar to X_4 than it is to X_1.

3.2 Class X: Segmented Diad/Triad Copolyesters

These block copolyesters contain both mesogenic and non-mesogenic spacer units and Figure 3.1 shows their general structure. The mesogens, Diad4 and Triad-*m* are based on terephthaloyl (4-oxybenzoyl) (Diad) units with terephthaloyl bis (4-oxybenzoyl) (TR) or 2,6 naphthaloyl bis(4-oxybenzoyl) (TRN) units as shown in Figure 3.2. These diad and triad mesogens are so-named because of the presence of two or three aromatic moieties linked at *para* positions within the repeat units. The repeat unit of these copolyesters also contains spacer units, denoted by **Q** in Figure 3.1, between mesogenic units. Table 3.1 shows the variation of methylene spacers within Triad-*m* units and spacer type **Q** between mesogens. The placement of these spacers are designed to lower $T_{n\rightarrow i}$ while promoting compatibility with PEN. This class of copolyester is very similar and in some cases the same as those previously synthesized at the University of Massachusetts for blends with PET [Ignatious et al., 1994].

Figure 3.3 shows a series of polarized light micrographs of quenched blends of X_3 with PEN. Pure PEN, shown in Figure 3.3(a) is isotropic. The other micrographs, also taken at 200X, illustrate that the intensity of de-polarized light increases with TLCP content.

3.3 Class Y: Alternating Copolyesters

Figure 3.4 shows the basic architecture of a copolymer consisting of alternating A and B units and also the structures of the A and B units. Of the two structures, only component A is mesogenic. The systematic variation of $\mathbf{R_A}$ and $\mathbf{R_B}$ (shown in Table 3.2) is used to study the effect of increasing naphthalene content towards augmenting the physical compatibility of the non-mesogenic units with the matrix.

3.4 Class Z: Random Copolyesters

Two distinct types of random (statistical) copolymers were used for blending studies.

Figure 3.5 illustrates the general structure of the first type. These components within the repeat unit are present in a molar ratio of 2:1 as indicated. Only the less predominant component is mesogenic. Table 3.3 shows the variation of S from phenylene to naphthalene.

The second type of statistical copolymer differs not only from the first class, but also from all of the TLCPs mentioned thus far. Lenz et al. first reported the synthesis of "comb-like" polymers in the early 80's. These are rigid polymers with flexible side chains [Majnusz et al., 1983] [Dicke and Lenz, 1983]. While flexible spacers present in either a main or side chain serve similar purposes for melting point lowering of the molecule, side-chain flexible TLCPs tend to have greater solubility in organic solvents. The side chains act as a solvent that is bound to the main chain [Lee and Lee, 1994]. The implications are important for the majority of TLCP forming processes which exploit the properties of the nematic structure as a processing aid.

Polymer Z_3 is a random thermotropic copolyester incorporating hydroquinone flexible spacer units in a pendent side chain [Deak, 1995]. It is very similar to a related random thermotropic copolyester used in blend studies with PET [Joslin, 1994]. Figure 3.6 shows that Z_3 differs from its analog only in a higher molar ratio of mesogen to flexible spacer content. Both Z_3 and its existing analog are closely related to another butoxy hydroquinone side-chain flexible copolyester also recently synthesized within the Lenz research group [Narayan-Sarathy, 1995]. Rheological studies proved that this third copolyester reduced the processing viscosity of PET by nearly an order of magnitude at just 2.5% inclusion [Narayan-Sarathy et al., 1995].

3.5 Characterization Procedures

Each of the pure materials received viscometric and thermal characterization. The sections below explain the techniques and calculations based on this information.

3.5.1 Inherent Viscosity

Inherent viscosities were determined in solutions of 60:40 (v/v) *p*-chlorophenol/1,1,2,2-tetrachloroethane at 26°C (0.5 g/dl). Viscosity values were obtained for all cases where the polymer became soluble in the solvent. Molecular weight was estimated based on viscosity values, handbook values for a and ν for the Mark-Houwink equation (for a similar polyester in solvent system), and the known molecular weight of PEN from GPC measurements. Molecular weight estimates are provided for approximate comparison only. To arrive at more exact comparisons, one should only weigh the measured inherent viscosities against each other and not use the Mark-Houwink estimates based on these viscosities.

3.5.2 Mesogen Content

Estimates for the weight percentage of mesogen within each TLCP were calculated similarly to previous work [Joslin, 1994]. These values account only for the rigid portions within each molecule, thus omitting methylene flexible spacers within mesogenic sequences from the calculation. To the extent that the chemical structure of commercial Vectra® A is fully aromatic, these values indicate the fraction of each thermotropic copolyester that is similar in chemical nature to Vectra® A.

3.5.3 Thermal Characterization

Thermal transitions for each TLCPs were detected using DuPont DSC 2910 equipment at a heating rate of 10°C/min under a stream of N_2. DSC transitions were highly dependent on the thermal history of the sample, and thus all samples were studied with identical thermal histories.

Samples were (1) heated from 30° to 330°C, (2) quenched in liquid N_2, and (3) re-heated to 330°C. The reported temperatures correspond to those at transition peaks during second heating. There is generally not much difference between 1st and 2nd heating scans for the pure TLCPs. The same transitions during cooling can, however, result in differences for peak temperatures as shown for example in Figure 3.7 for polymer X_4. For each DSC curve shown in Figure 3.7, the lower temperature corresponds to the melting (or fusing) of BN segments. The melting points of butylene naphthalate (BN) segments (seen at 240°C and 237°C) depend on the molecular weight: Yoon and coworkers reported the melting endothem of pure poly(butylene naphthalate) (PBN) homopolymer at 247°C. Also for each DSC curve in Figure 3.7, the higher temperature endotherm corresponds to the crystal-to-nematic transition.

All subsequently reported thermal data for the pure TLCPs were recorded during 2nd heating scans at 10°C/min. The temperature and enthalpy changes were calibrated using an indium standard.

Optical textures of the melts were noted using an Olympus polarizing light microscope equipped with a digitally-controlled Linkham hot stage. Relative displacement of the top of two cover glasses sandwiching the molten TLCP easily resulted in the shearing and alignment of nematic Schlieren textures.

To characterize thermal stability, the temperature corresponding to 5% weight loss due to heating is measured by a thermogravimetric analyzer, DuPont TGA 2950 at 10°C/min under a stream of N_2.

3.6 Results and Discussion

Table 3.4 provides details about properties of the pure materials and a note about the origin of each material. For detailed information regarding the synthesis and characterization of each TLCP, appropriate references by Jo and coworkers [1995], Deak [1995], and Choi and coworkers [1996] should be consulted. This table also lists designations for Class X copolyesters according to TR-*m*(n:o:p) or TRN-*m*(n:o:p) nomenclature where (n:o:p) denotes the molar ratio of Diad4 : Triad-*m* : PBT (or PBN) sequences in the block copolymer.

3.6.1 TLCP Results

Most of the polymers were soluble and contain approximately 50% by weight mesogenic units except for the random TLCPs. All of the TLCPs exhibited a nematic Schlieren (marble-like) texture and gave rise to stir-opalescence. (Of all the systems, polymer X_3 showed the weakest stir-opalescence.)

The T_g of TLCPs is notably phase-dependent. Studies by Zachmann and coworkers on thermotropic copolyesters and terpolyesters of PET, PEN, and PHB reveal that the T_g of the co-polyesters captured in the LC phase is about 30°C lower than that in the isotropic phase. Perhaps as a result, the lack of a well-defined T_g is a common characteristic of TLCPs [Sarlin and Tormala, 1991] [Minkova et al., 1992]. For all of the TLCPs discussed in this chapter, the glass-to-

rubber transition was unobservable in DSC studies. Studies of T_g using dynamic mechanical methods and deuteron nuclear magnetic resonance are more effective [Zachmann et al., 1992] [Zachmann et al., 1993] [Spies and Zachmann, 1994].

It is common for TLCPs to exhibit multiple melting endotherms corresponding to different phenomena. Figure 3.8 shows additional examples of 2nd heating DSC scans for naphthalene-substituted alternating TLCPs Y_2 and Y_3. The crystal-to-nematic transition shifts to a lower temperature with increasing naphthalene content (present in both the mesogenic and non-mesogenic units) for Y_3. Unlike the other classes of TLCPs, those in class Y displayed endotherms corresponding to isotropization (clearing) prior to degradation [Choi et al., 1996]. In particular, Y_1 copolymer underwent isotropic transition at the lowest temperatures (under 290°C) on first and second heating. Its thermal behavior during DSC scans is shown in Figure 3.9.

All of the TLCPs except Y_3 were used in subsequent blend studies with PEN. Other researchers also recently synthesized a TLCP closely-related to polymer Y_3 as part of a series of naphthalene-based thermotropic copolyesters [Liu and Lee, 1995]. Their reported analog of Y_3 exhibited extreme difficulty recrystallizing from the melt state, with its degree of supercooling exceeding 150°C.

For all of the TLCPs discussed, the temperature at which 5% total weight loss ($T_d^{5\%}$) under N_2 occurs is about 50°C higher than those used in subsequent melt-spinning operations of blended TLCPs also done under a protective N_2 atmosphere. Thus, the thermal stability of the TLCPs at temperatures appropriate for melt-spinning is adequate.

For all classes of main-chain flexible polymer, the substitution of naphthalene for phenylene units adds to the thermal stability of the chain, as indicated by marked increases in $T_d^{5\%}$. Substitution of naphthalene from phenylene moieties in the segmented diad/triads also slows the

crystallization rate from the melt by lowering the supercooling values from 29° to 41°C [Choi et al., 1996].

3.6.2 Comparisons with TLCPs used with PET

The TR-4 type copolymers used both in this work with PEN (and in other studies with PET) contain two types of mesogenic units, Triad and Diad, within the repeat unit. The Diad units are shorter than the Triad units and thus melt at a lower temperature. For the segmented copolymers synthesized for blending with PEN, the lower melting diad units resulted in a small degree of biphasic texture visible at 250°C, below that formally assigned to $T_{k\rightarrow n}$.

The thermal transitions of chemically identical TR-4(2:4:7) copolymer X_2 and X_3 appear insensitive to changes in molecular weight. The molecular weight of X_3 is 38,000 g/mole, whereas the molecular weight of X_2 is near 16,000 g/mole. As shown in Table 3.4, the temperatures corresponding to the melting of PBT domains and crystal-to-nematic transition vary only by 3 degrees for X_2 and X_3.

The same type of TR-4(2:4:7) copolymer used in studies with PET showed similar DSC endotherm temperatures, but a biphasic state attributed to partial melting of diad units becomes initially visible at much lower temperatures near 202°C.

Another fundamental difference in TLCP thermal behavior occurs between side-chain flexible Z_3, an 80/20 (ehq/hq) random copolymer and a 60/40 (ehq/hq) random copolymer analog used in PET studies. The 60/40 random copolymer used in PET studies exhibited a PBT melting endotherm and a liquid crystal-to-liquid crystal (lc→lc) transition, going from a dense nematic texture to a loose nematic texture at 267°C. There was no such lc→lc transition seen for Z_3 co-

polymer; the singular $T_{k\rightarrow n}$ transition for Z_3 occurs at 293°C. No lc→lc transitions observed for any type of TLCPs used in PEN blend studies.

3.7 Conclusions

This chapter presented descriptions of several new thermotropic copolyesters. These copolyesters are similar to the A9XX series of Vectra®, the only series of Vectra® commercially available in fiber form. Vectra® A is a fully aromatic copolyester and suffers from limited tractability and solubility. In spite of its limited processability and the high cost of the constituent HNA monomer, Vectra® remains the most widely used of all thermotropic copolyesters for structural purposes.

These copolyesters differ from Vectra® A, most significantly, by the incorporation of flexible spacers in both the main chain and in side (pendent) groups. These spacers make the copolyesters more tractable and soluble under less aggressive conditions. These properties become important during melt-processing.

Over the past several decades, many others have also attempted to synthesize designed TLCPs through new chemistry such as discussed in this chapter. Thus, the development of new chemistry serves as one route to attaining new materials with tailored mechanical and processing characteristics. Blending, as an alternative route, also lends to property tailoring and allows for seemingly infinite possibilities. The real attractiveness of blending, however, rests in the lower costs and faster development times compared with techniques for new chemistry. The next chapter explores blend of the novel TLCPs with PEN, a relatively new polyester resin considered for commercial purposes.

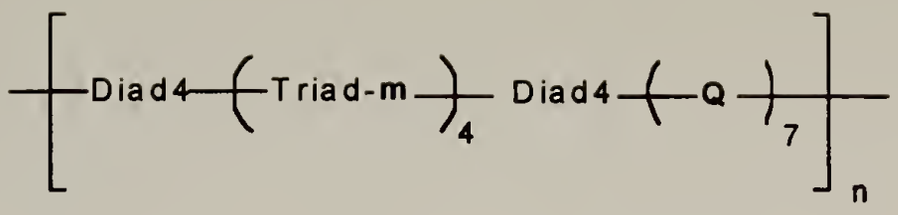

Figure 3.1. General structure of the segmented block copolymers for Class X copolyesters.

Diad 4:

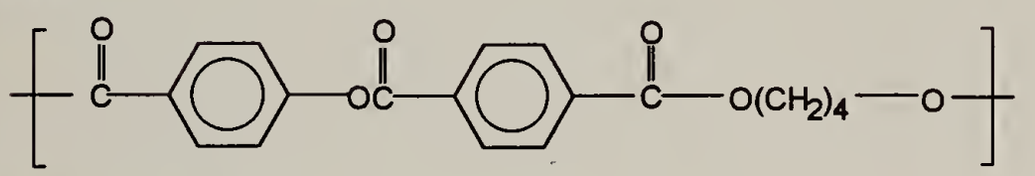

Triad-*m* (TR-*m*):

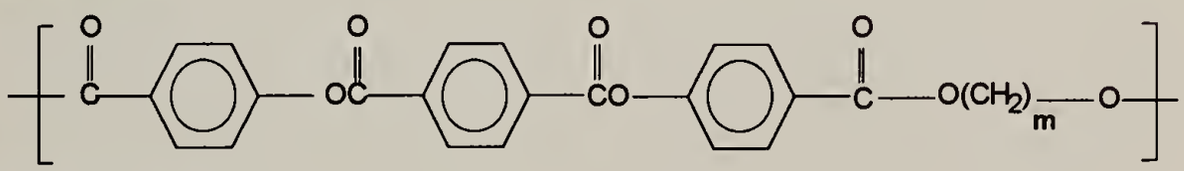

TriadN-*m* (TRN-*m*):

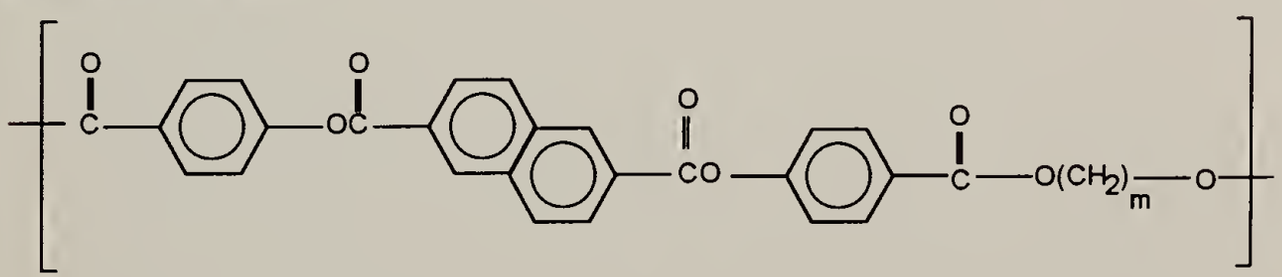

Figure 3.2. Diad4, Triad-*m*, and TriadN-*m* units for Class X copolyesters.

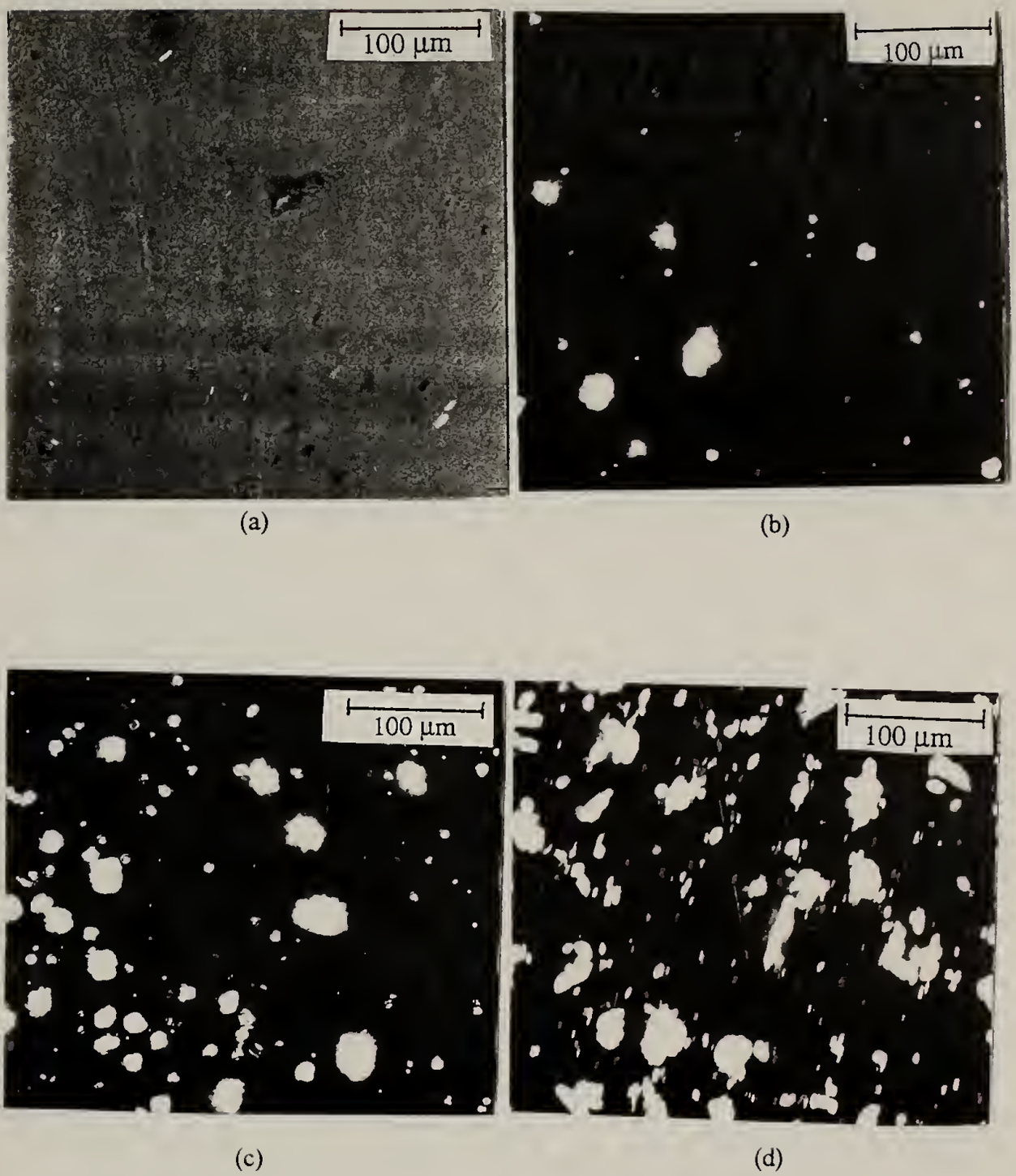

Figure 3.3 A series of polarized light micrographs of quenched blends of X_3 with PEN. (a) Featureless texture of neat PEN quenched from the melt at 300°C; (b) Biphasic texture of 5% X_3 quenched from the melt at 300°C; (c) Increased birefringent intensity seen for 10% X_3 blend quenched from the melt at 300°C; (d) Largest relative birefringent intensity seen for 20% X_3 blend quenched from the melt at 300°C.

A:

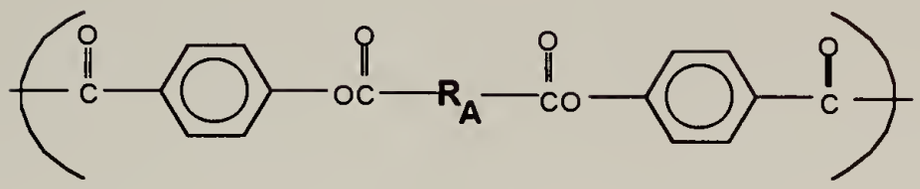

B:

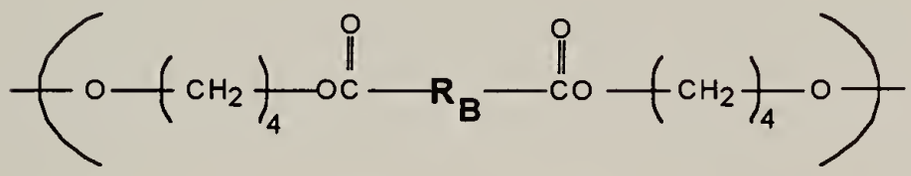

Figure 3.4. General structure of the alternating copolymers for Class Y copolyesters.

First type of random copolymer:

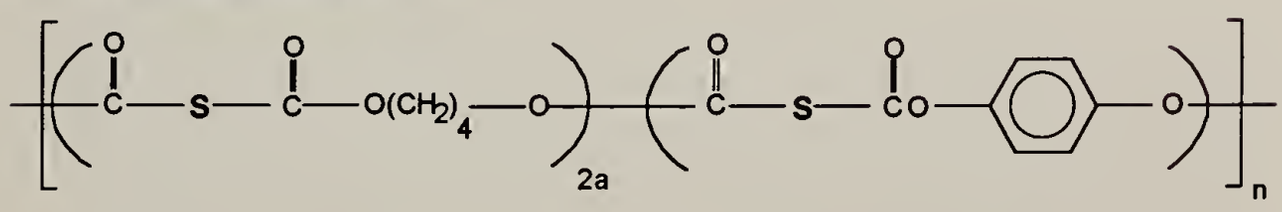

Figure 3.5. Structure of the first type of random (statistical) copolymer for Class Z copolyesters.

Side-chain flexible random copolymer:

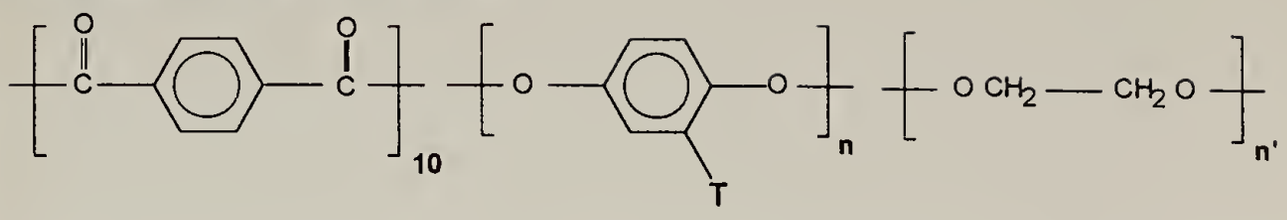

	T	Name of T substituent	n	n'
Polymer Z3	$O(C_2H_5)$	ethoxy hydroquinone	8	2
Existing analog to Z3	$O(C_2H_5)$	ethoxy hydroquinone	6	4

Figure 3.6. Structure of the second type of random (statistical) copolymer and its existing analog used in blend studies with PET. These TLCPs are side-chain flexible.

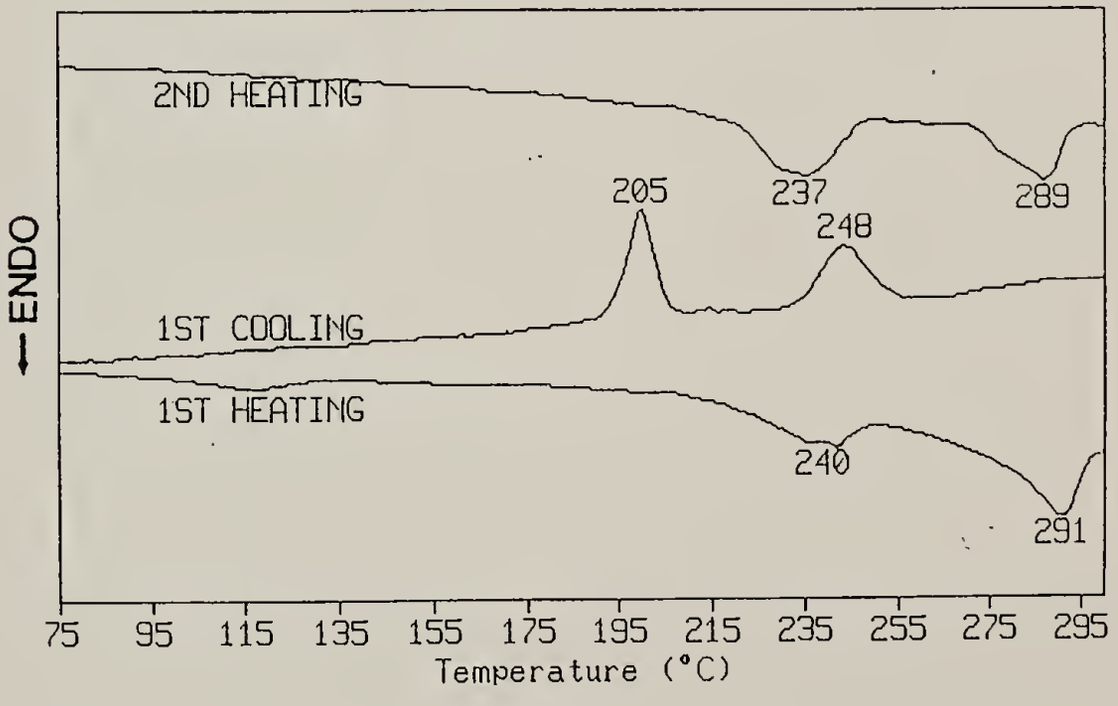

Figure 3.7. Examples of first and second heats (and first cooling) for X_4 copolymer.

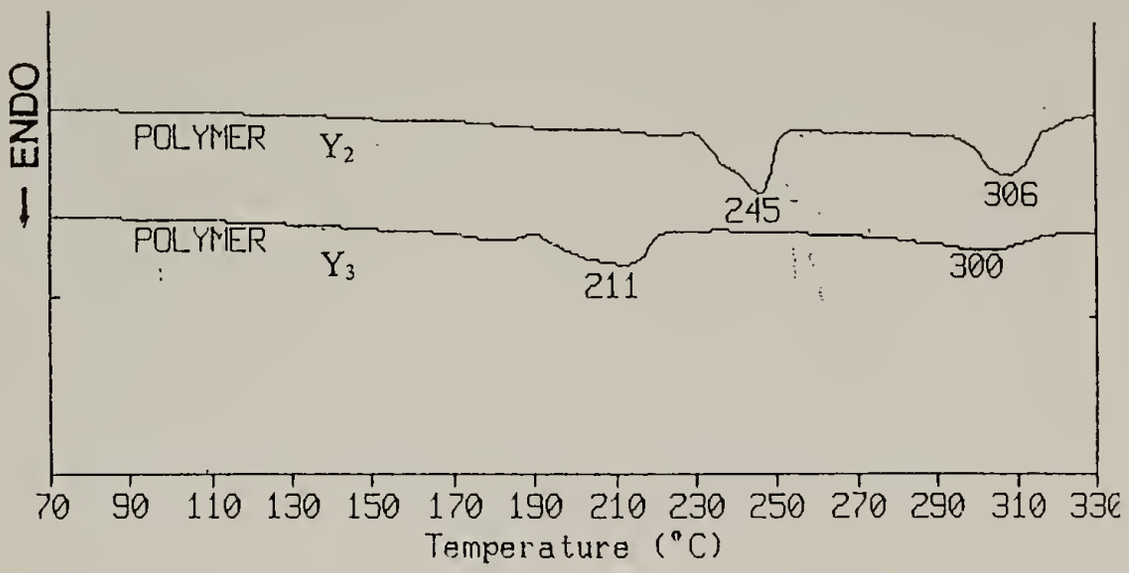

Figure 3.8. Examples of second heats for Y_2 and Y_3 TLCPs which isotropize prior to degrading.

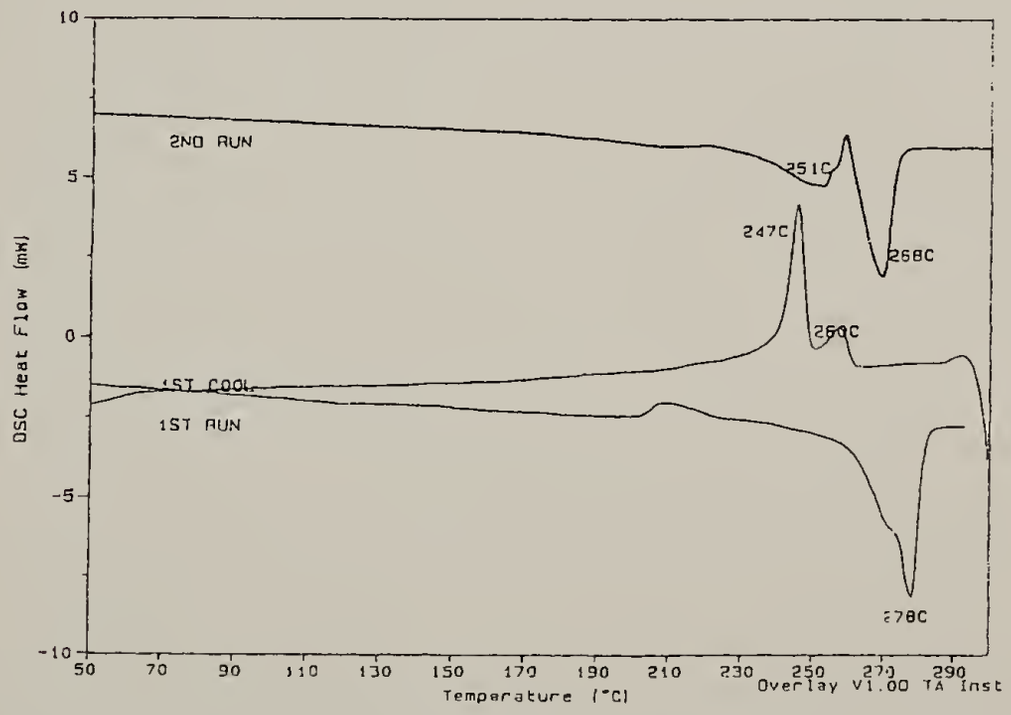

Figure 3.9. Examples of first and second heats (and first cooling) for Y_1 copolymer. This TLCP isotropizes at relatively low temperatures below 290°C.

Table 3.1 Variation of substituent parameters for Class X segmented block copolyesters.

	η_{inh} (dl/g)	m	Q
Polymer X_1 TR-2(2:4:7)	insol.	2	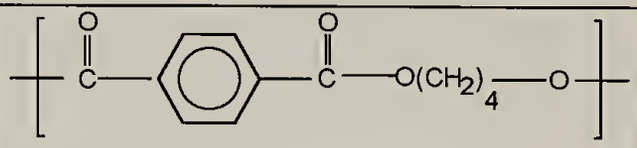
Polymer X_2 TR-4(2:4:7)	0.72	4	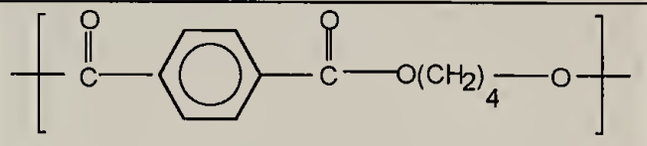
Polymer X_3 TR-4(2:4:7)	1.30	4	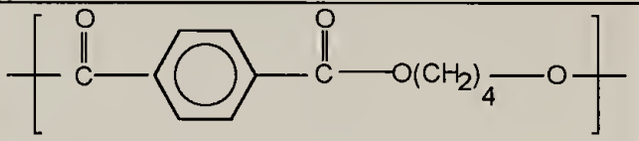
Polymer X_4 TRN-4(2:4:7)	0.65	4	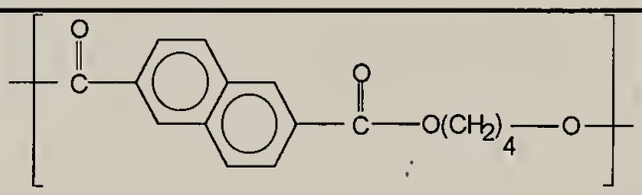

Table 3.2. Variation of substituents for Class Y alternating copolyesters.

	R_A	R_B
Polymer Y_1	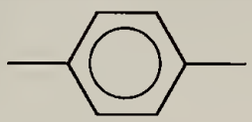	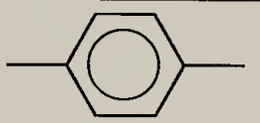
Polymer Y_2		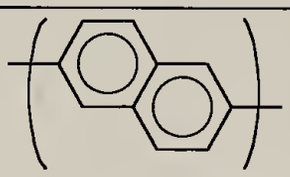
Polymer Y_3	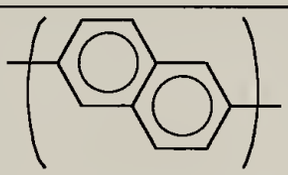	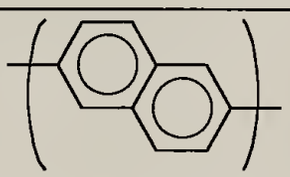

Table 3.3 Variation of substituents for the first type of Class Z random (statistical) copolyesters.

	S
Polymer Z_1	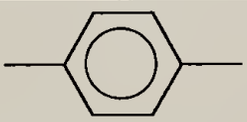
Polymer Z_2	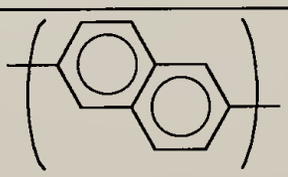

Table 3.4. Characterization of the pure materials.

Polymer	Comment	Origin	η_{inh} (dl/g)	Estimated M_n	Mesogen conc. (wt %)	T_g (°C)	[a] T_m (°C)	[b] T_{k-n} (°C)	[c] T_{n-i} (°C)	[d] $T_d^{5\%}$ (°C)	LC phase
PEN		Kodak	0.67	14 k	0	119	258	.	.	400	none
X_1	TR-2(2:4:7)	Choi	insoluble	.	55	.	218	302	.	347	nematic
X_2	TR-4(2:4:7)	Jo	0.72	16 k	54	.	208	283	.	340	nematic
X_3	TR-4(2:4:7)	Choi	1.30	38 k	54	.	211	286	.	343	nematic
X_4	TRN-4(2:4:7)	Choi	0.65	13 k	50	.	237	289	.	359	nematic
Y_1	R_A= phenylene R_B= phenylene	Choi	0.52	09 k	55	.	.	251	268	343	nematic
Y_2	R_A= phenylene R_B= naphthalene	Choi	0.60	12 k	51	.	.	245	306	359	nematic
Y_3	R_A= naphthalene R_B= naphthalene	Choi	0.53	10 k	54	.	.	211	300	353	nematic
Z_1	S = phenylene	Choi	insoluble	.	35	.	220	260	.	346	nematic
Z_2	S= naphthalene	Choi	insoluble	.	35	.	226	270	.	359	nematic
Z_3	side-chain flexible	Deak	1.10	30 k	75	.	.	293	.	383	nematic

All transition temperatures correspond to those at transition peaks during 2nd heating at 10°C/min under an N_2 atmosphere.

[a] melting of PBT (or PBN) domains of the polymers

[b] crystal-to-nematic transition

[c] nematic-to-isotropic transition

[d] temperature at which 5% weight loss occurs while heating at 10°C/min under N_2

CHAPTER 4

MECHANICAL PROPERTIES OF THE TLCP BLENDS

4.1 Introduction

In recent years, blends of TLCPs with traditional thermoplastics have attracted substantial academic and industrial attention. This chapter discusses the results of practical studies of PEN with specially designed TLCPs for compatibilized blends. These studies are based on prior knowledge determined within the Farris group with PET / TLCP polyblends and published methods [Bassett and Yee, 1990] [Joslin, 1994]. As previously stated, a compatibilized blend refers to a polyphasic structure with interaction at the phase boundaries. Within the practical context of processing studies, blend compatibilization first entails transforming particles intended for blending from 1 mm to 1 μm in diameter within approximately one minute through a process of droplet deformation, flow alignment, and coalescence within a matrix [Macosko, 1995]. Using a "polydomain" representation for the initial melt, when the structure is subjected to a flow field, the domain texture is ideally converted into a monodomain in which all of the molecules assume the same preferred orientation [Federico, 1989].

Thermotropic liquid crystalline polymers such as Vectra® A which contain *para*-linked aromatic units have the ability to form nematic phases. Orientational order and rigidity of the nematic phase persist in the solid phase as determined through macroscopic mechanical properties and theoretical predictions.

The first report of the existence of thermotropic copolymers appeared in the early 1970's [Roviello and Sirigu, 1975]. Since that time, many researchers have studied the mechanical prop-

erties of *in-situ* composites made with TLCPs, especially those containing thermotropic copolyesters. Frequently, a commercially available copolyester Vectra® A, is used in such studies. A wealth of generalizable processing information from studies on Vectra® A blended with a matrix of polycarbonate were also done at the University of Massachusetts [Federico, 1989]. *In- situ* composites of thermotropic copolyesters are the subject of several review papers which provide good historical summaries of such work [Kiss, 1987] [Economy and Goranov, 1995] [Handlos and Baird, 1995].

Much of the cited *in-situ* blending work studies blend systems ranges between 20% to 80% TLCP addition. Fewer studies focus on very small concentrations (i.e., less than 10% TLCP content). The reason for this possibly stems from the assumed route for mechanical property enhancement.

4.2 Background for In-Situ Composites

The model for *in-situ* reinforcement using a nematic TLCP such as Vectra® relies on the presence of a stiffer reinforcing phase developing within an inherently more compliant matrix, which remains unchanged. It differs from conventional modes of reinforcement such as those employing inorganic (glass) fiber in that the *in-situ* reinforcing phase develops during processing. Nematic phases are easily aligned within an applied flow field and in no other polymer forming process are the advantages of an included nematic phase more intuitive and more apparent than in (one-dimensional) fiber extrusion and drawing processes. In practice, the actual methods used to develop and retain a nematic phase lead to differences in its final role in the mechanical performance of the *in-situ* composites.

Hoechst Celanese reports a value of 66 GPa for the Young's modulus of commercially available Vectran HS® fiber (spun from pure Vectra® A). A survey of published literature, however, reveals many other values reported for the modulus of Vectra® A. These values range from as low as 2.2 GPa [Chapleau et al., 1992] to as high as a theoretically-determined value of 110 GPa [Lin et al., 1993] [Lin and Yee, 1994]. The explanation for the existence of this wide range once again stems from the dependence of TLCPs such as Vectra® on processing conditions, particularly on the degree of drawing.

A widely held notion about *in-situ* composites is that, other things being equal, mechanical enhancement should scale with the amount of a needle-like TLCP added. This is the reason that models such as rule of mixtures (ROM) and Halpin-Tsai [Halpin and Kardos, 1976] relations are commonly used to make quantitative comparisons of stiffness data in order to remark on the quality of a composite formed *in-situ*. If a particular composite fails to achieve its predicted modulus, it is usually attributed to reasons that the nematic phase is poorly dispersed, elongated, or adhered.

In itself, however, there is nothing about a (molecular) composite formed *in-situ* through the inducement of needle-like phases that suggests it should outperform its neat matrix counterpart. The popular notion about *in- situ* composites is valid only if the molecular needles are much stiffer than the matrix; this is the same concept behind conventional composites. Otherwise, an *in-situ* composite containing a compliant nematic phase (crudely, "floppy needles") can not greatly reinforce the matrix through non-synergistic means, regardless of how well the nematic phase is dispersed, elongated, or adhered.

As discussed in detail in §3.6, the copolyesters synthesized for these blending studies are not fully aromatic like Vectra® A. Rather, as semi-flexible TLCPs, their mesogen contents are calculated to fall between 35% to 75%; they are inherently more compliant due to the presence of flexible spacers. Because the total amount of TLCPs synthesized for blending studies was typi-

cally less than 10 g each, it was not possible to independently evaluate the mechanical properties of the pure TLCPs by spinning and drawing pure TLCP fibers.

While there was not enough of each pure TLCP for characterization to unequivocally state that they do not have the same potential for high stiffness as commercial Vectra® A, there is sufficient evidence to assume it true. Existing characterization work on a pure thermotropic copolyester containing flexible spacers very similar to those investigated here reveals that the Young's modulus of the pure TLCP fiber is 13 GPa [Shin and Chung, 1990]. (This value of 13 GPa is also approximately half of the modulus for post-treated pure PEN fibers.)

In light of the above, the most reasonable assumption for the actual modulus values of the pure TLCPs investigated here is that they lie somewhere between the extremes of 13 and 66 GPa. The importance of defining a bracketed range becomes more apparent in analysis of the data.

4.3 Models for In-Situ Composites

The following models describe two methods to estimate composite modulus which only take mechanical reinforcement effects into account. Analytically, they are not independent. The rule of mixtures (ROM) arises as a special limiting case of the more generalized Halpin-Tsai relations. Together they make up the two most common models used to address the predictions for *in-situ* composites.

4.3.1 Rule of Mixtures

The rule of mixtures offers in the most optimistic predictions for composite stiffness. The ROM calculation also allows a convenient way to estimate the mechanical properties of a compos-

ite. Using ROM as a method to calculate the expected stiffness of a binary composite (E_c) results in a linear combination of the Young's modulus of the reinforcing fiber phase (E_f) with that of the matrix phase (E_m) according to the following expression:

$$E_c = V_f E_f + (1 - V_f) E_m \qquad (4)$$

where V_f is the volume fraction of the reinforcing phase.

For example, the stiffness of PEN for most of the cases discussed herein is 24 GPa. Assuming perfect adhesion at the interface of the phases in a matrix free of voids or other impurities, a 30% blend of Vectran HS® fiber (66 GPa) within this matrix would result in a composite having a predicted modulus of 37 GPa according to ROM. Similarly, a 30% blend of pure TLCP having a modulus of 13 GPa, supposedly results in a composite modulus of 22 GPa. Given the variation in the range of possible values for E_f, the ROM predictions thus form a region as shown in a plot of ROM for all compositions TLCP in PEN in Figure 4.1.

The rule of mixtures is a generalized model used to account for the weighted contributions of an ensemble of items. Applied to composites, ROM contains no parameter to account for the structure or spatial distribution of the reinforcing phase within the matrix. It assumes a perfectly formed composite with equal strains in both the fibrillar and the matrix phase. This can only occur with perfectly aligned and adhered (continuous) fibers. It is evident, however, that the E_f cited for Vectra® A fiber depends strongly on how well the needle-like mesophase forms.

The next section addresses the issue about the relevance of the rule of mixtures as a comparative benchmark for measured properties in these studies.

4.3.2 Halpin-Tsai Model

The Halpin-Tsai relations for predicting composite modulus for a (cylindrical) fibrillar reinforcing phase within a continuous matrix contain a parameter ξ which is directly proportional to the aspect ratio (A) of the fibrils. The aspect ratio is equal to the length, l, of the included fibril divided by its diameter, d. The Halpin-Tsai relations yield the rule-of-mixtures as an analytical result in the limit of infinite draw ratio. For a formal proof of this limit, the reader is referred to the reference by Halpin [1984].

The Halpin-Tsai relations are the result of a mathematical model for a binary composite system containing perfectly straight fibrillar phase embedded in a matrix. The composite modulus is given as the product of the matrix modulus multiplied by a factor which depends on the volume fraction of the fibrillar phase according to the following equation:

$$E_c = E_m \frac{1+\xi\eta V_f}{1-\eta V_f} \qquad (5)$$

$$\text{where } \eta = \frac{\frac{E_f}{E_m} - 1}{\frac{E_f}{E_m} + \xi} \qquad (6)$$

$$\xi = 2\left(\frac{l}{d}\right) \qquad (7)$$

Figure 4.2 shows an example of how E_c varies as a function of volume fraction of a reinforcing phase having a number of different aspect ratios (A) within a PEN matrix (using E_f= 66 GPa for the fibrillar phase). It is apparent that as the aspect ratio increases, the predicted modulus values rapidly resemble the curve for ROM.

TLCPs are known for efficiently aligning with a flow field. This is also true of blended fibers of semi-flexible TLCPs studied herein as shown in Figure 4.3. These are polarized optical micrographs of fibers of 20% X_3 in PEN. Figures 4.3(a) and 4.3(b) show as-spun fibers upon heating on a hot stage. The as-spun 20% fibers shown in Figure 4.3(b) clearly contain TLCP fibrils oriented along the fiber axis. The intensity of the birefringent nematic portions of the hot-drawn fiber in Figure 4.3(c) remains bright and also shows fibrils aligned about the axis of the fiber. The intensity of the birefringent nematic phase seems to increase further for hot-drawn (fully post-treated) fiber of the same composition. These sample micrographs taken at 200X indicate that the aspect ratio of the dispersed phase is sufficiently high such that either high aspect ratio estimates using Halpin-Tsai relations or simplified ROM can serve as an appropriate comparison for all similar cases.

4.3.3 Processing Basis

The following sections provide a descriptive rationale for the methods used to form and draw the fibers.

4.3.3.1 Fiber Formation

There is one additional step in sample pre-treatment (as described in § 2.2.1.1) for TLCP/PEN polyblends: powders of TLCP and PEN are first tumble-mixed for 48 hours prior to drying at 90°C. Otherwise, the same equipment and procedures for melt-spinning were used for the blends as for pure PEN.

There were two batches of PEN received and used for blend studies. The first batch (PEN^1) showed different thermal behavior in the as-received state than the second batch (PEN^2). PEN^1 was used in blending studies with only two of the TLCPs. (The highest achieved modulus value for PEN^1 was 26 GPa. The highest modulus achieved for PEN^2 was 24 GPa. These values are taken into account when comparing the actual modulus values of the polyblends with those predicted by theory)

Spinning fibers properly from the melt-state is a critically important task. If malformed, the as-spun fibers prove unworkable and untransformable by drawing methods. To prevent this, the exiting fiber stream must flow steadily, containing a minimal amount of impurities.

Blends of naphthalene-substituted TLCPs with PEN allowed melt-extrusion at lower temperatures compared to those for phenylene-substituted TLCPs. (Specific die temperatures are mentioned in the discussion for each type of TLCP in the sections to follow.)

The die was kept as low in temperature as possible to prevent degradative reactions and to minimize transesterification reactions. Though unquantified in the course of these studies, transesterification reactions are unavoidable under these high temperature conditions [Stewart et al., 1993] [Jo et al., 1995] [Backson et al., 1995].

Typical problems encountered were the appearance of bubbles and degraded or unmelted particles in the melt stream. In the case of bubbles and degraded particles, the screw speed was increased until degradation was no longer visible. Die temperatures were changed only as a last resort. The appearance of unmelted particles in the melt usually results in near-cessation of flow after prolonged periods of time. In these cases, unmelted particles adhered to the surface of the feed screw were usually found (mostly in the Zone 1) upon dismantling the extruder for cleaning with a bore-cleaning kit fitted with a bronze brush. (Note that no solvents were used to clean any portion of the apparatus.)

4.3.3.2 Post-Treatment

All of the fibers were drawn such as to attain the highest draw ratio possible. The ability to attain higher stiffness values by maximizing the draw ratio is similar to the effects with neat PEN discussed in Chapter 2. Figure 4.4 is a multi-dimensional plot which describes the effect of several parameters on the stiffness values of two systems of TLCPs (Y_1 and Z_1) with PEN. The color of each point indicates the magnitude of the final stiffness value attained. There are two main conclusions here. The first is that for any given TLCP concentration level, the highest Young's modulus always appears at the highest level of draw -- which reaches a maximum of λ=12-15 for most of the polyblended fibers. Secondly, it is evident that without the benefit of post-treatment, fibers containing different levels of TLCP in PEN all have the same stiffness as that of neat PEN. These observations contrast with those of pure Vectra® or Vectra® blends exceeding 10% TLCP; these fibers are generally very stiff. Attempts to strengthen the such fibers through post-treatment generally fail because drawing the fiber beyond a few per cent strain quickly results in fiberline breakage.

All cold-drawing took place at temperatures between 145°C-150°C which is slightly warmer than those used in neat PEN studies (140°C-145°C) as described in Chapter 2. Many of the fiber compositions were undrawable at lower temperatures. Hot drawing was, however, done at the same temperature, 210°C, as for neat PEN. Neat PEN fibers spun side-by-side with the blends were therefore post-treated in the same manner as the blends in order to compare their behavior.

4.4 Testing Procedure

Fiber specimens of 50 mm gage length were mounted onto paper tabs with an adhesive to facilitate specimen handling and testing alignment as per Allen [1983]. Fiber diameters were averaged over a minimum of five measurements per specimen using an Olympus microscope equipped with a calibrated scale accurate to ± 0.5 μm. Tensile tests were performed using an Instron 5564 tensile tester programmed with a cross-head speed of 5 mm/min, giving a strain rate of 10% min^{-1}. The tester unit is linked to a personal computer running Instron Series IX software which sampled tensile data at 56 Hz for initial modulus measurements. The Young's modulus was determined from the best linear fit through the initial (elastic) region of the stress-strain beginning from the origin. Instrument compliance tests, done in accordance with ASTM Standard D3379-75 for the Instron 5564 using a series of Kevlar 149 fiber, yielded a result of 0.12 mm/N. Such a low value for machine compliance means that apparent moduli reported throughout this thesis are negligibly (0.01% to 0.015%) lower than the true moduli. Other measured tensile properties were ultimate strain and stress. Each tensile property was averaged over twelve tests performed at ambient conditions in the laboratory. Data for tests exhibiting grip failure or slip were omitted for ultimate property or modulus measurements.

The above methods are the same as those used to determine the tensile properties of fibers of pure PEN and PET and its blends from previous work.

4.5 Results

Table 4.1 presents a summary of all of the mechanical properties for the various blend systems investigated. The TLCPs were blended with PEN which arrived in two batches. Since

these batches exhibited different thermal and mechanical characteristics, the use of each type of PEN is denoted by a superscript. In Table 4.1, the number in boldface represents the Young's modulus in GPa. A cursory view of this table reveals that moduli for almost all of the 1% blends are nearly the same.

Figures 4.5 and 4.6 plot the actual measured stiffnesses of all the blends compared to the rule-of-mixtures prediction. These plots graphically summarize all the Young's modulus values for blends of TLCPs with PEN. Many of the points overlap on Figure 4.6 at 1% composition. Error bars are purposely omitted for points on Figure 4.6 to reduce the amount of visually-inseparable information. Typical values for standard deviation of the Young's modulus are less than 5% of the mean.

Lacking a known value for E_f for each case, the ROM calculations were done using stiffness values corresponding to that of commercial Vectra® A fiber (Vectran HS® tradename) and pure semi-flexible TLCP cited in literature [Shin and Chung, 1990]. This leads to a region of estimated values for the stiffness of the "ideal" composite.

For the purposes of discussion, data points corresponding to modulus values which lie above the upper bound are defined as "synergistic." Points corresponding to modulus values falling beneath the lower bound are defined as "non-synergistic." Points which lie somewhere in between the two bounds correspond to blend systems which have plausibly formed *in-situ* composites in the conventional sense using these TLCPs. Note that the ROM line appears curved in figures for which the x-axis is given on a log-scale.

Many of the results at 1% and at some of the other compositions evidence synergistic effects not predicted by composite theory. The remaining sections deal with each of the systems separately and draw comparison to blends with PET where possible.

4.5.1 Class X: Segmented Diad/Triad Copolyesters

X_1 and X_2 were the only TLCPs studied as polyblends within PEN[1]; all other TLCPs were blended with PEN[2]. Figure 4.5 shows that the moduli of treated blends of X_1, a TR-2 (2:4:7) type polymer in PEN[1]. In this case, the modulus of the pure material is 26 GPa. Modulus values for X_1 polyblends fall far lower than that of prediction by about 40%. The series of X_1 as-spun fibers, all extruded at a die temperature of 304°C, were very brittle and as a consequence, very difficult to draw. The 1% X_1 as-spun fiber was completely unworkable, prone to breakage with any handling and this is the reason that no value appears at 1% inclusion for X_1.

On the other hand, the moduli of treated blends of X_2 in PEN[1] also spun at 304°C gave rise to positively synergistic elastic properties. X_2 is a TR-4(2:4:7) type polymer, differing from X_1 only by the presence of two additional methylene spacers in the Triad sequence. While their chemistry is similar, their molecular weights are not: X_2 has a lower estimated molecular weight of 16,000 g/mole based on viscosity measurements compared to X_1 which was insoluble.

Figure 4.7 shows the results of TR-4(2:4:7) type polymer used in studies with PET with its respective ROM predictions. This data with polyblends of PET is adapted from [Joslin, 1994]. The stiffness properties of PET polyblends of TR-4(2:4:7) indicate that they fall into the range for properly-formed *in-situ* composites. Together, Figures 4.6 and 4.7 show that the shifts toward synergistic behavior occur at lower TR-4(2:4:7) concentration in PEN than in PET. This shifting effect is not, however, unbounded at very low concentration (< 1%).

Like X_2, polymer X_3 is also a TR-4(2:4:7) type polymer blended with PEN. Figure 4.8 plots values for its Young's modulus in blends with PEN[2]. There are two important points to consider when comparing X_3 data with that of X_2. The first is that the stiffness value for the post-treated PEN[2] matrix used for X_2 is slightly lower than that of PEN[1] used for X_3. These modulus

differences are therefore taken into account in with each theoretical curve. The second point to consider is that the molecular weight of X_3 (38k) is likely more than twice that of X_2 (16k), as estimated from viscosity measurements. In spite of this, the final stiffness values of X_2 and X_3 blends are almost the same at the same concentrations (1%, 2%, and 5%). This suggests that the effect of higher molecular weight of an otherwise chemically-identical TLCP phase can perhaps compensate for an inherently more compliant matrix.

X_3 blends (also spun at 304°C) are the most thoroughly studied of all blend systems discussed herein, spanning a range of ¼% to 20%. There is a large difference in Young's modulus for blends at just ½% and 1% TLCP inclusion; the shift from negative to positive synergy is striking. Positively synergistic effects for the X_3 system are bracketed at intermediate TLCP concentration. (This effect is later seen in side-chain flexible random TLCPs as well)

Polymer X_4, designated by an alternative nomenclature designation of TRN-4(2:4:7), contains a naphthalene unit in the Triad mesogen and flexible PBN spacers. The placement of these naphthalene-based moieties within the repeat unit were designed to enhance chemically compatibility with PEN. Polymer X_4 is more chemically similar to the PEN matrix than any other in its class. X_4 blends were melt-spun at temperatures between 295°C - 300°C. In terms of optical clarity, the as-spun fibers of the X_4 polyblends appeared the most glassy and transparent compared to all of the other fibers spun. The addition of X_4 copolymer noticeably aided the melt-spinning procedures over that of neat PEN for all TLCP contents except that of 5%. This was seen in the motor current and resulting screw speed necessary to extrude the fiber at a constant rate. More specifically, the screw speed varied from 25-45 rpm for the blends versus the maximum of 55 rpm for neat PEN. As shown in Figure 4.9, the resulting stiffnesses of X_4 blends are comparable to those of X_3, which contains only phenylene units in the Triad mesogen and flexible PBT spacers. Again, a lower modulus results at higher TLCP concentration.

Two trends seen thus far are that (1) modulus values at 1% are nearly the same, and (2) modulus values of blends shift toward lower, non-synergistic values with increasing TLCP content.

Elaborating on the first point, a back calculation using ROM for 1% inclusion shows that the reinforcing phase would need to possess a modulus value over 700 GPa to affect reinforcement through mechanical means alone. (Note: this sample calculation result is given to presage later discussion of synergistic effects rather than to suggest that an extremely stiff nematic phase was somehow formed *in-situ*.) These trends are not isolated to X class TLCPs. They are evident throughout all classes examined presently.

4.5.2 Class Y: Alternating Copolyesters

Like class X, class Y polymers also exhibited strongly synergistic effects at lower concentrations.

Y_1 copolymer contains no naphthalene units within its alternating structure and was spun at 305°C with PEN. As shown in Figure 4.10, blends of Y_1 with PEN^2 show positively synergistic effects with modulus values 125% to 130% greater than that of the neat PEN^2 matrix at a loading level as low as 1%. While the modulus does drop at the highest loading level of 5%, the resulting stiffness still lies within the range of that of an ideally formed *in-situ* composite. The addition of Y_1 also served as a processing aid for PEN. Screw speeds were typically near 35 rpm for all Y_1 blends.

Y_2 copolymer contains one naphthalene unit in the non-mesogenic (PBN) sequence of the alternating structure. Y_2 polyblends were spun at 290°C with PEN^2. Again, the placement of a naphthalene (versus phenylene as with Y_1) was meant to increase chemical compatibility with the PEN matrix. Figure 4.11 shows the measured stiffnesses for this series of fiber. Like the previous

case, synergistic effects amounting up to 130% improvement in modulus over the neat matrix are seen at low concentrations.

The modulus values at 1% for Y_1 and Y_2 are both 31 GPa, which is close to those found for class X polymers.

4.5.3 Class Z: Random Copolyesters

There are two types of random copolyester discussed below: main-chain flexible and side-chain flexible. Their physical behavior appears to differ using this additional classification.

4.5.3.1 Main-Chain Flexible Random Copolyesters

Z_1 is a fully phenylene-substituted random copolyester which was spun with PEN^2 at 305°C. Figure 4.12 shows the results for post-treated blends of Z_1 with PEN^2. All Z_1 blends exhibited notable synergy effects. It is for the Z_1 series that the highest modulus value of any blend system investigated was obtained at 2% inclusion. This corresponds to 133% enhancement of the modulus over that of neat PEN^2. Scanning electron microscopy (SEM) of the cross-section of cryogenically-fractured Z_1 as-spun fibers reveals that TLCP domains form on a variety of length scales, as shown in Figure 4.13, within both the "skin", and "core" regions. Figure 4.13(a) shows the cross-section of 1% as spun fiber. (The diameter of this cross-section is about 100 μm.) The TLCP phase, whose light-colored appearance contrasts with that of the matrix in the SEM micrographs, does not give rise to typical skin-core effects. For example, comparing Figures 4.13(b) and 4.13 (c) of 2% Z_1 polyblends shows that TLCP domain diameters within the same skin region

can vary from about 1½ μm to less than $^{1}/_{10}$ μm. The same $^{1}/_{10}$ μm domain diameter is found in the core region of 5% Z_1 polyblends as shown in Figure 4.13(d).

Z_2 is a fully naphthalene-substituted random copolyester which was spun with PEN[2] at 290°C. Figure 4.14 shows the results for blends of Z_2 with PEN. As with Z_1, all compositions of Z_2 show strongly synergistic effects which exceed the rule-of-mixtures by margins well outside experimental error.

Interestingly, the absolute highest value for any blend system (32 GPa) occurs at a 2% blend of the *phenylene-substituted* random copolymer. While this value is very close to other near-maximum values, one might expect the highest modulus value to have occurred with an inherently stiffer naphthalene-substituted TLCP polyblend with other parameters being equal. This observation supports the claim that mechanisms other than *in-situ* reinforcement dominate mechanical property enhancement.

4.5.3.2 Side-Chain Flexible Random Copolyesters

Figure 4.15 and Figure 4.16 show that the side-chain flexible random copolyester polyblends of Z_3 in PEN[2] exhibited bracketed synergistic behavior similar to its analogs in PET. The synergistic effect of side-chain flexible TLCP addition is more pronounced for blends in PET than in PEN. In PET, a difference between just 5% to 6% addition shifts the behavior from strongly positive to negative synergy.

The Z_3 copolyester is unique in both its chemical character and processing character compared to all of the other TLCPs discussed thus far. Although the intent of placing ethoxy hydroquinone as flexible side chains in the copolymer was to facilitate its "solubility" with aliphatic units of the PEN matrix (in the molten state), the effect was not clearly observed during the critical

stages of fiber formation during steady melt-spinning at 75 m/min. While melt-spinning the blends of Z_3 at 305°C also led to decreased settings for screw speeds from 47 rpm to 26 rpm (for 1% to 5% blends respectively), the apparent melt viscosity was observed to increase over this range as indicated by the current required to drive the motor. This suggests the presence of some type of chemical changes during spinning.

The 2% Z_3 blend composition showed the largest synergistic effect in this series. SEM micrographs of cryogenically-fractured as-spun fibers of Z_3 polyblends are shown in Figure 4.17. The main difference between the hot-drawn 2% Z_3 fiber shown in Figure 4.17(b) and the other as-spun fibers is that the hot-drawn fiber appears highly crystalline. This set of micrographs illustrates that the TLCP domain sizes are at the same approximate sub-micrometer size within both as-spun and hot-drawn fiber. That is, the diameter of the TLCP phase is not dramatically changed. The most noticeable change is crystalline modification of the matrix.

4.6 Summary

The most significant factors influencing the mechanical properties of the fiber blends are presented below.

4.6.1 Effects of Processing History

The foremost conclusion from these studies is the that mechanical stiffness and strength rely more heavily on the net draw ratio than on any other parameter, including TLCP content. Without post-treatment, all fibers tested (i.e., in the as-spun state) give rise to modulus values of 2 GPa. This is the same stiffness value seen for fibers of as-spun PEN, as-spun PET, and all as-

spun TLCP blends of PET (as reported by Joslin [1994]). Both POM and SEM micrographs of representative samples reflect that the characteristic length and aspect ratio of the TLCP domains do not change appreciably upon post-treatment.

4.6.2 Presence of Synergistic Effects

There are several striking trends evident from a survey of the mechanical properties found in this chapter. The first is that many of the blends give rise to synergistic effects well outside the plausible range predicted by composite theory for *in-situ* reinforcement using nematic TLCPs.

Notably, all 1% blends of main-chain flexible TCLPs give rise to nearly identical modulus results. Clearly, synergy effects at 1% TLCP inclusion are indifferent to the chemical architecture as the effects are seen in segmented block, alternating, and random TLCPs. The effect at 1% also appears indifferent to molecular weight of the TLCP.

Using class designations, however, the type Z (random) TLCPs served as the most effective agents for property enhancement. Unlike the other classes, all random TLCPs (both main-chain flexible and side-chain flexible) gave rise to Young's moduli higher than or equal to the upper bound of prediction at all levels of inclusion. Random copolymers were also seen to cause the greatest degree of modulus enhancement in PET where similar classes of TLCPs were also studied.

Synergistic effects are formidable to predict in a quantitative manner. They result in non-linear combinations of properties of the pure materials. For instance, if the TLCP physically modifies the matrix modulus by virtue of its very inclusion, then the Young's modulus of the pure matrix becomes a less relevant parameter and benchmark, particularly at higher loading levels. The exact behavior is, however, non- intuitive and depends on the physical processes that occur.

Apart from the work presented in this thesis, the only reported case of synergistic effects in mechanical properties of a TLCP / PEN blend occurs for composites of 10% -70% Vectra® A950 injection molded into rectangular rods (ca. 12 mm^2 cross-section) [Jang and Kim, 1995]. These workers reported a flexural modulus of 5.8 GPa for pure Vectra® A950 specimens. For their blends of Vectra® A in PEN, the highest reported modulus is 6.5 GPa which occurs at 70% Vectra® loading. They attribute the synergy effects in flexural modulus to the development of skin-core morphology. Their argument for the presence of a thickly formed skin layer containing more-highly oriented, *stiffer* TLCP fibrils which affect greater load-bearing capacity is plausible. The "effective" flexural modulus for pure Vectra® A within their polyblends, when back-calculated from ROM, is 8 GPa at the highest level of synergy achieved for their blends. This effective value lies well in the range of possible stiffnesses reported for pure Vectra® A.

As stated in §4.5, however, the TLCP discussed in this thesis would need to possess a Young's modulus over 700 GPa in order to affect the typical level of reinforcement seen at 1%. This effective modulus not only exceeds the theoretical stiffness value for perfectly axially aligned crystals of Vectra® A (110 GPa) but it exceeds the highest stiffness value determined experimentally for any polymer fiber (which is 300 GPa for poly[benzobisthiazole] [PBZT]). Further, the modulus of high performance graphite fiber (519 GPa) amounts to less than 75% of this calculated value. Thus, even the presence of ideally formed *in-situ* composites is insufficient to account for modulus enhancements in the broad case. This is the reason that none of the data points were subjected to an empirical curve fit within the framework of ROM.

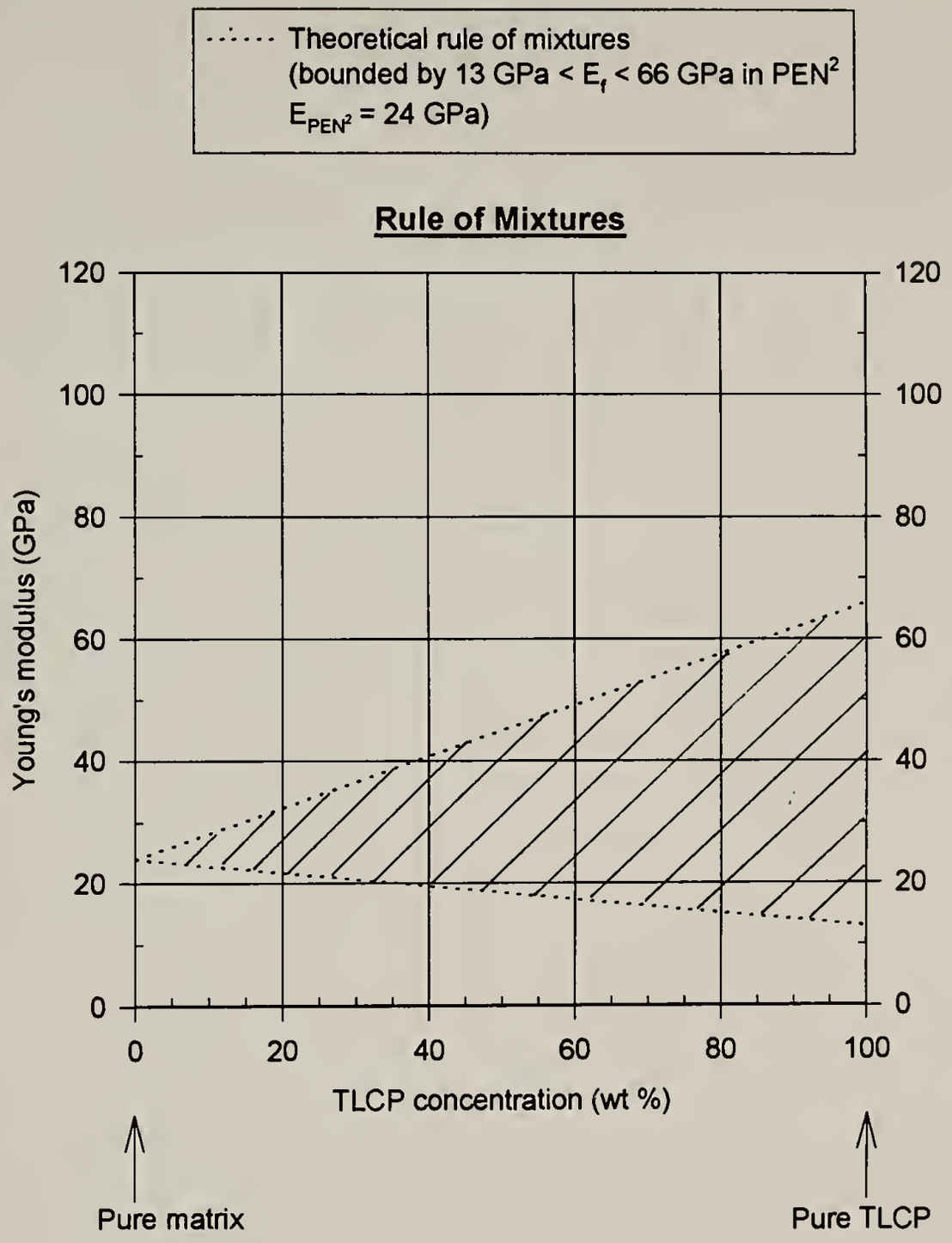

Figure 4.1. Predicted range of Young's moduli as defined by the theoretical rule of mixtures.

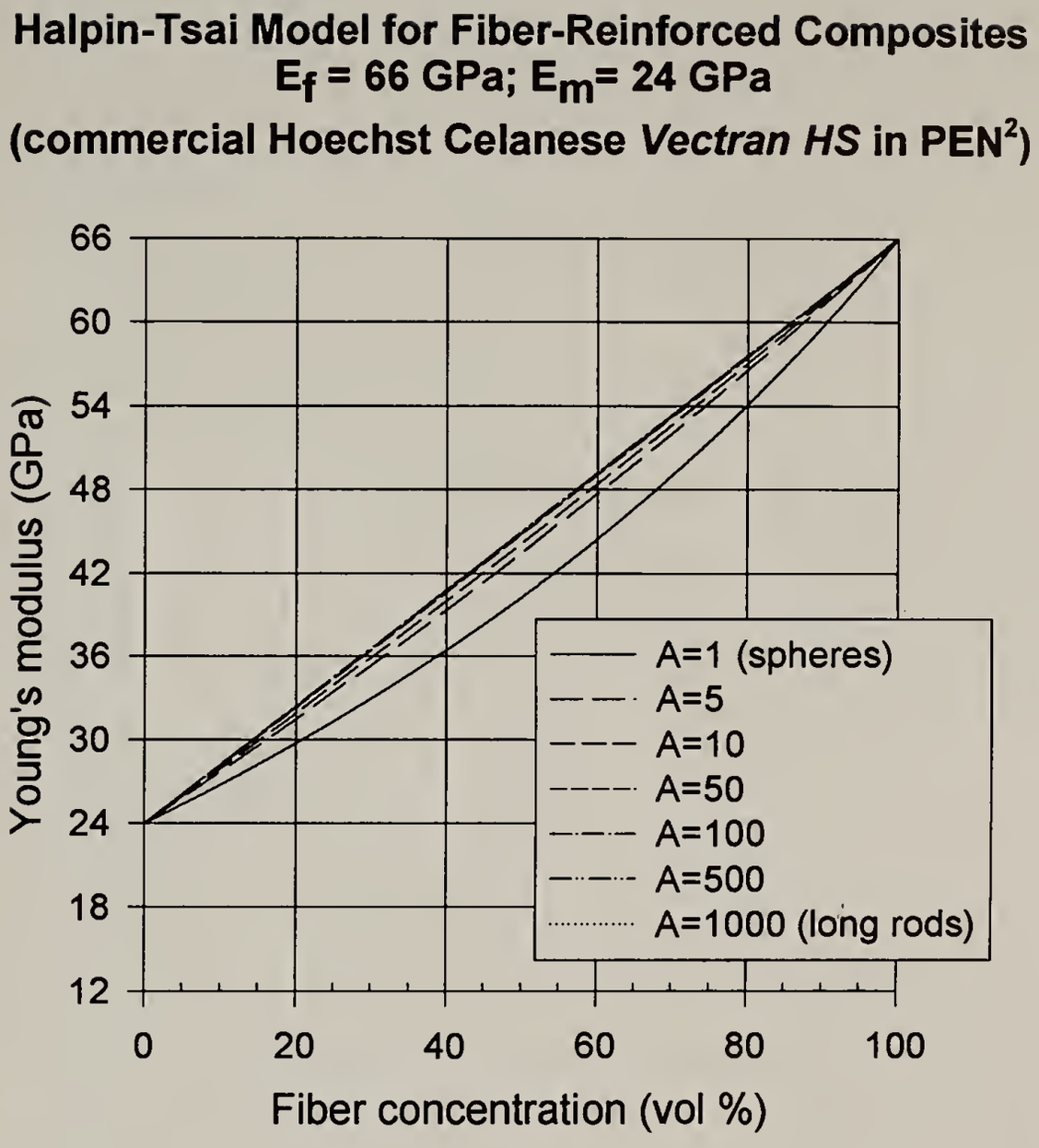

Figure 4.2. Halpin-Tsai predictions using relevant values for TLCP/PEN blend systems.

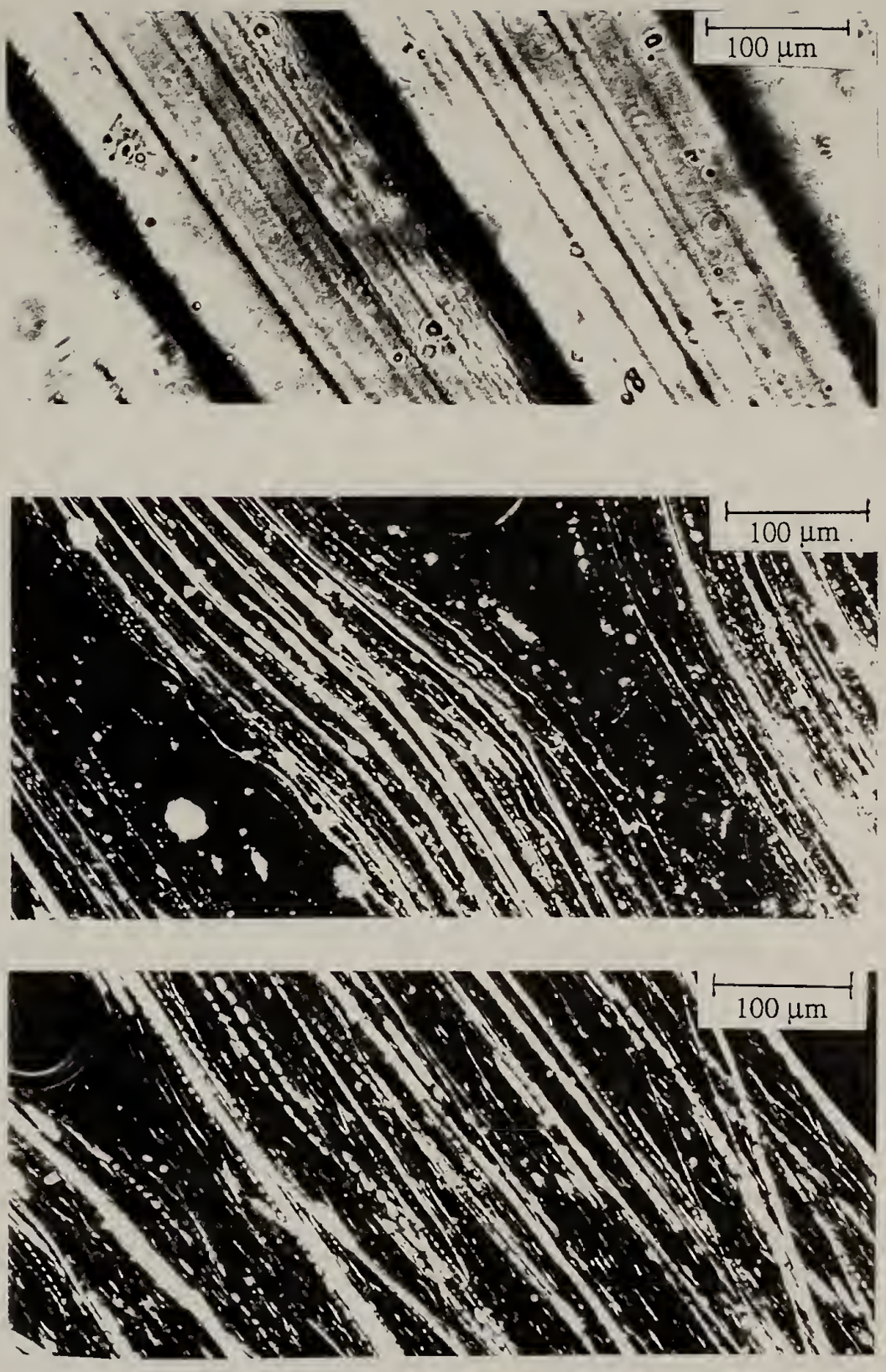

Figure 4.3. Polarized light micrographs of fibers of 20% X_3 in PEN (at 200x). (a) As-spun fibers at 255°C; (b) As-spun fibers at 280°C; (c) Hot-drawn fibers at 280°C.

Black: Young's modulus above 25 GPa
Gray: Young's modulus between 5 GPa and 25 GPa
White: Young's modulus below 5 GPa

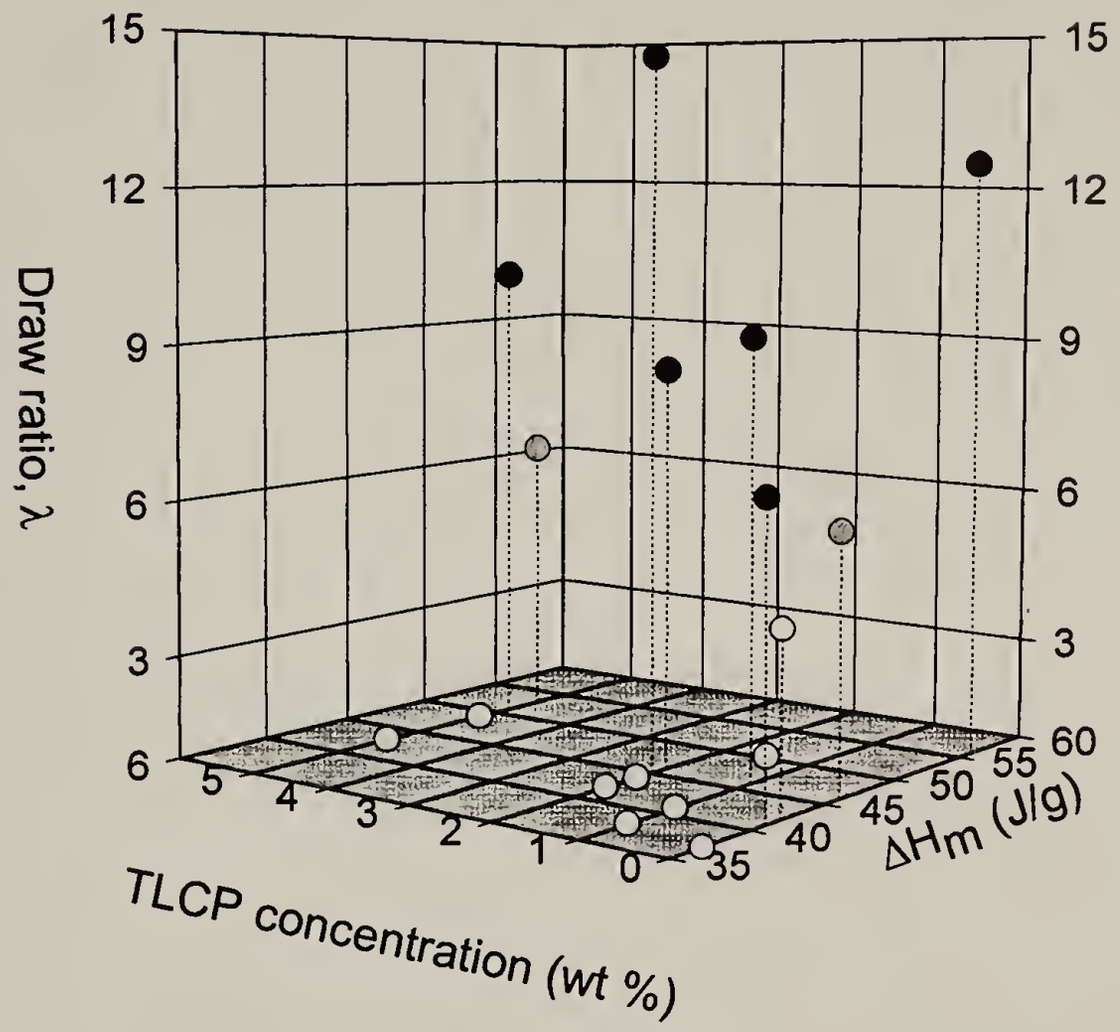

Figure 4.4. Master plot for the effects of several parameters on Young's modulus. Two TLCP systems (Y_1 and Z_1) are represented here in addition to neat PEN.

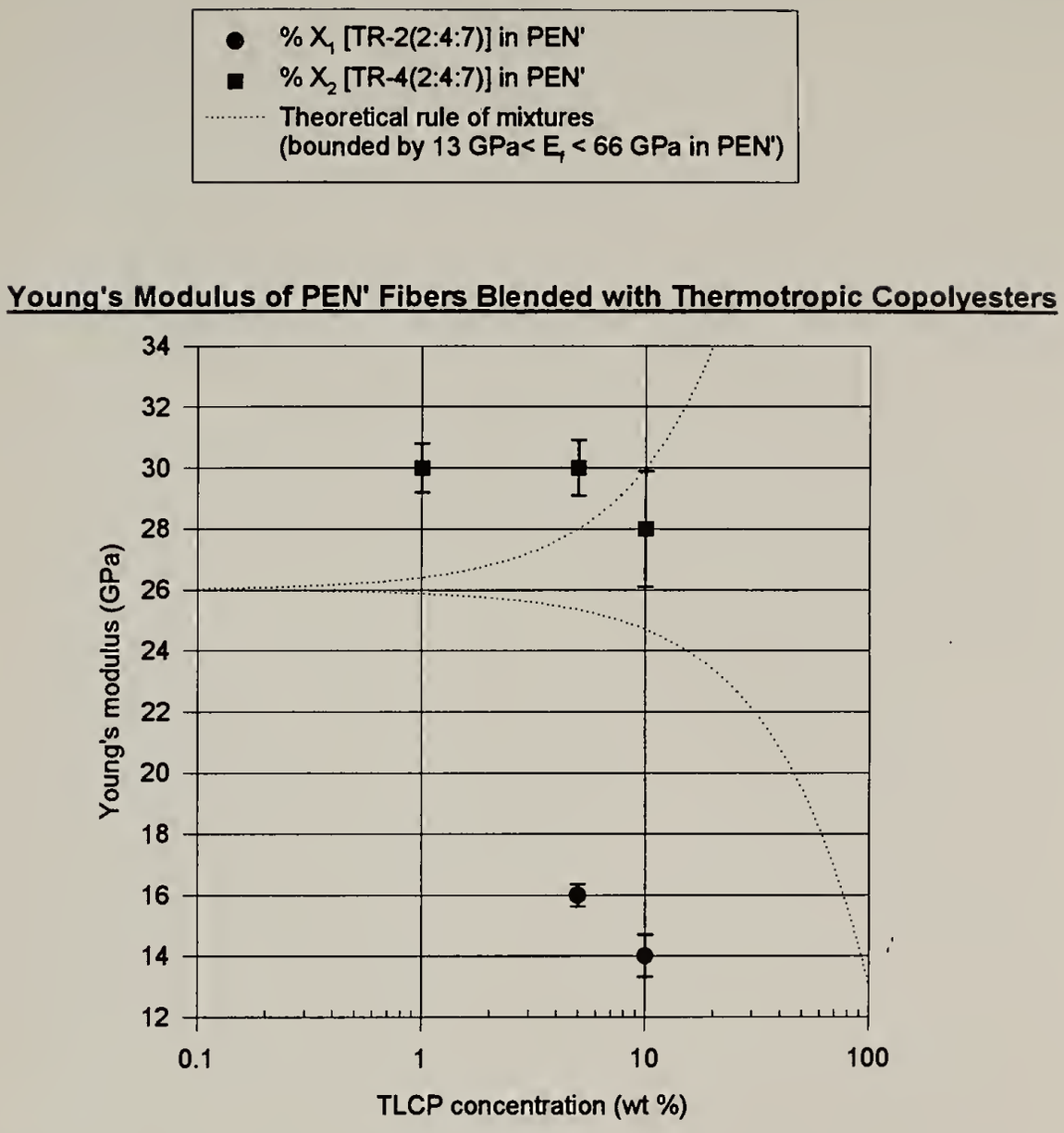

Figure 4.5. Young's moduli of hot-drawn fibers of X_1 and of X_2 blended with PEN[1].

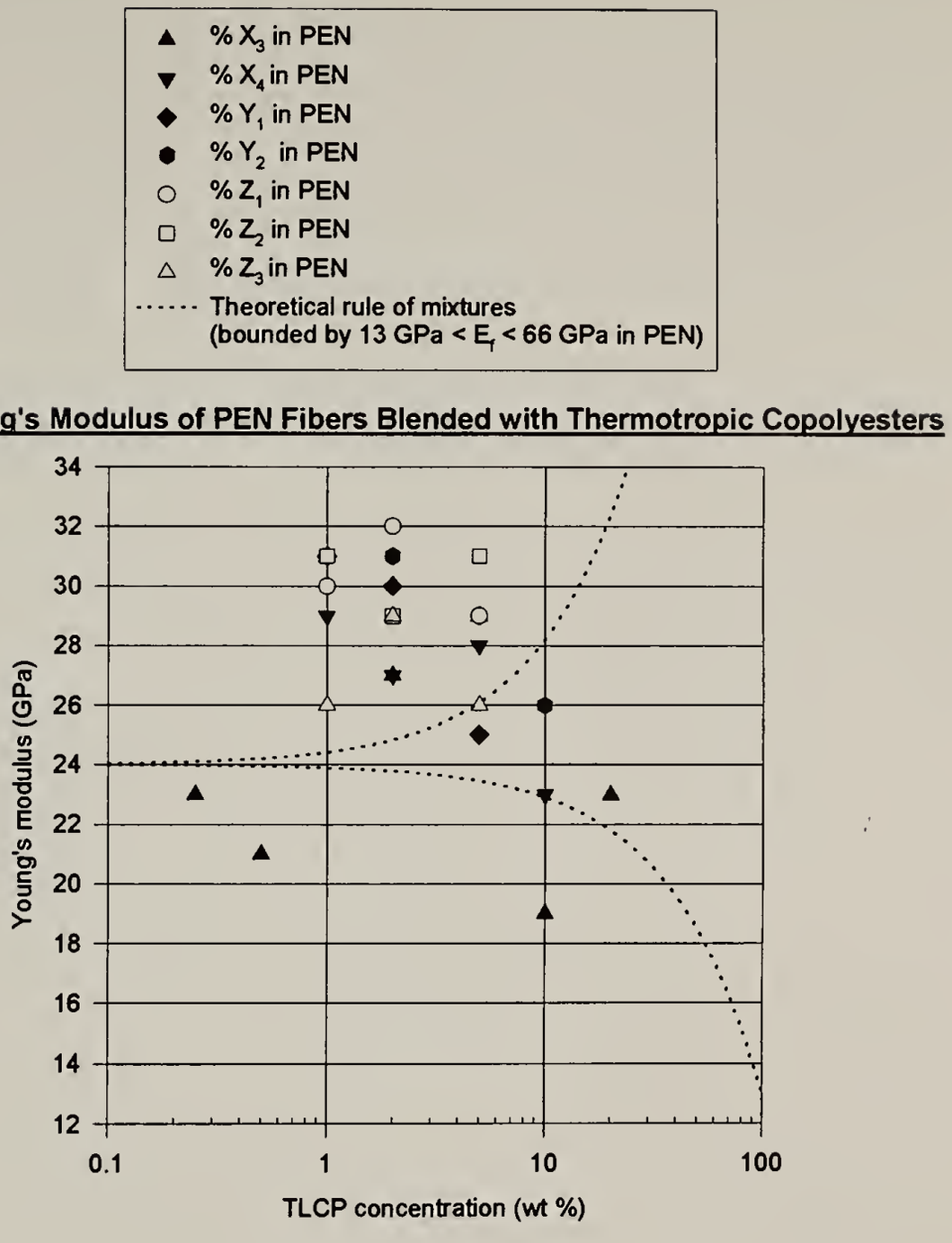

Figure 4.6. Young's moduli of hot-drawn fibers of all TLCPs blended with PEN[2]. Note that many data points overlap at 1%.

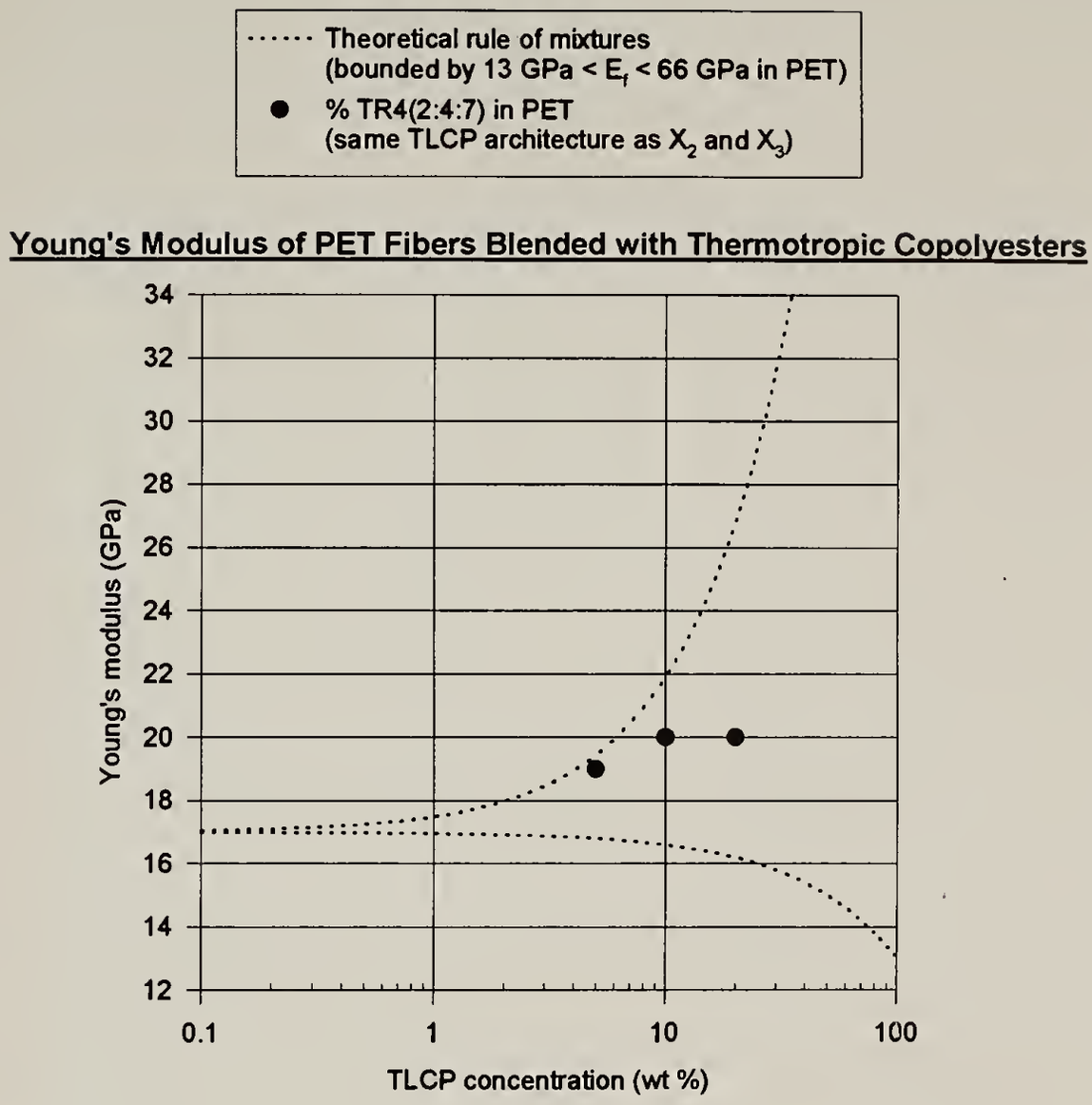

Figure 4.7. Young's moduli of hot-drawn fibers of a TR-4(2:4:7)-type TLCP blended with PET.

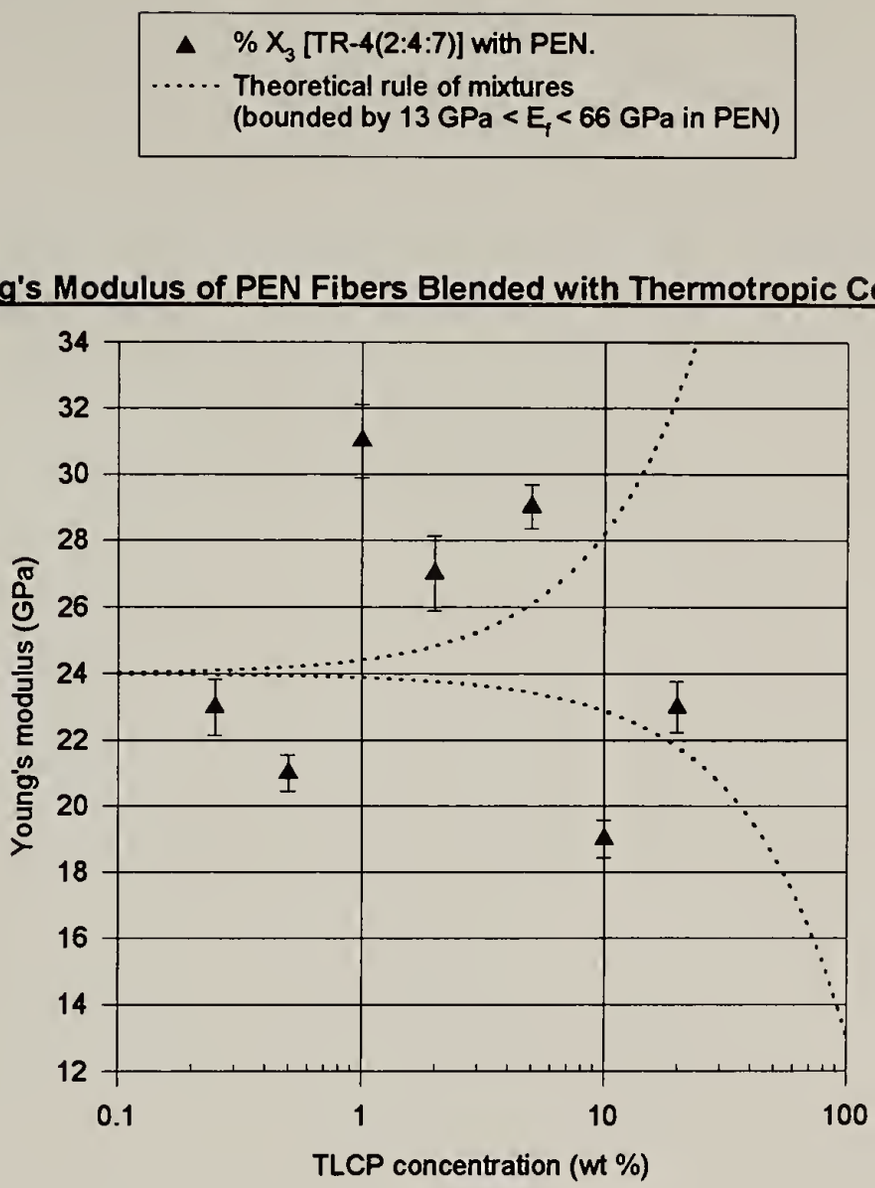

Figure 4.8. Young's moduli of hot-drawn fibers of X_3 blended with PEN[2].

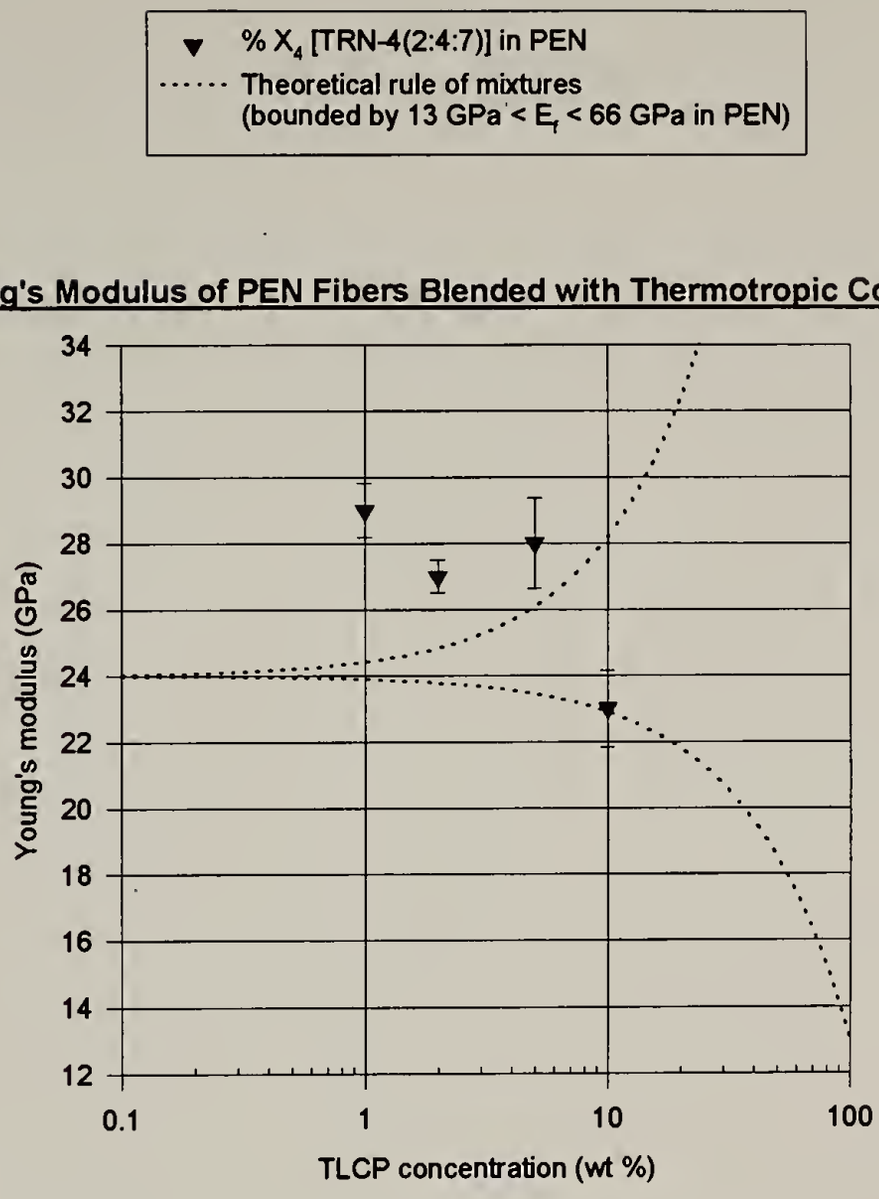

Figure 4.9. Young's moduli of hot-drawn fibers of X_4 blended with PEN[2].

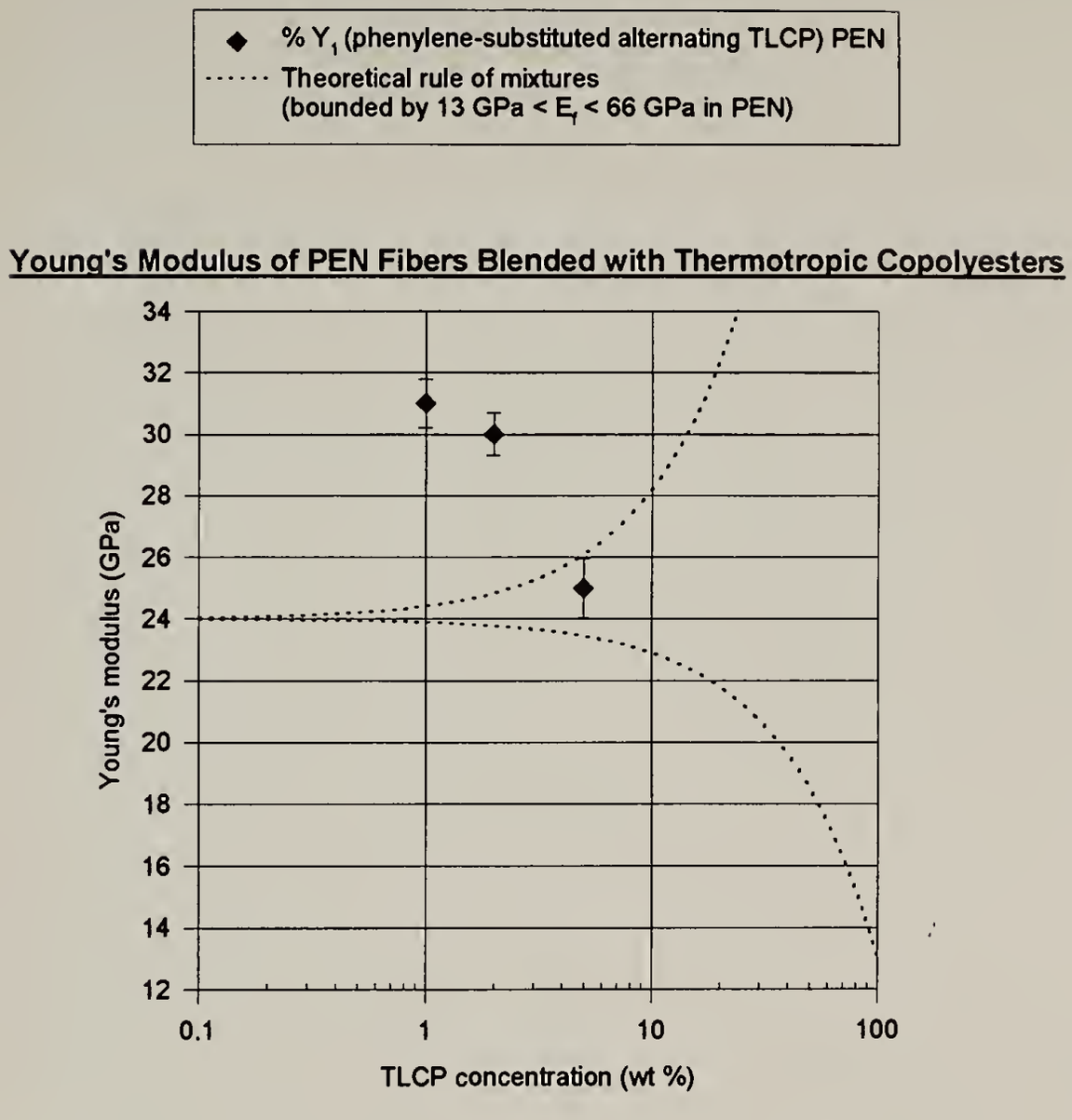

Figure 4.10. Young's moduli of hot-drawn fibers of Y_1 blended with PEN[2].

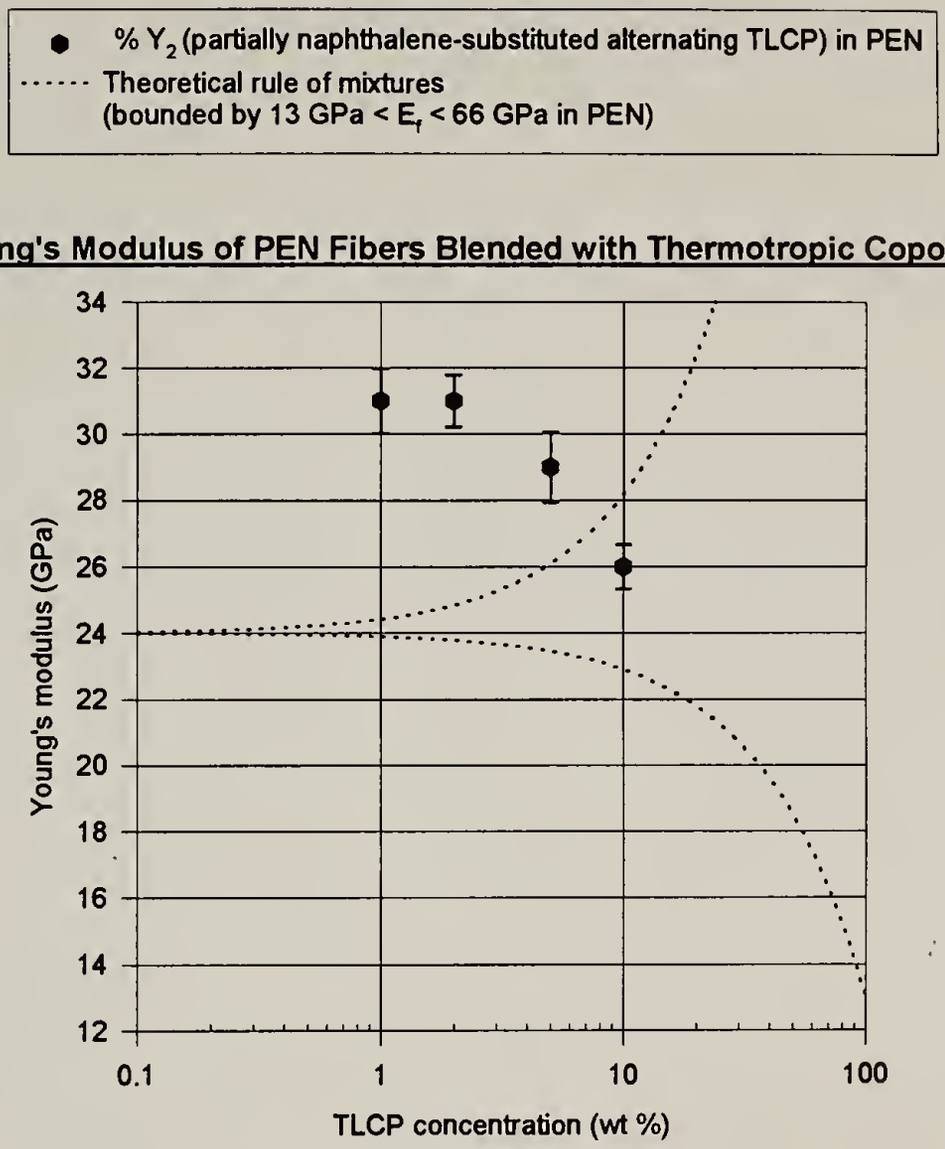

Figure 4.11. Young's moduli of hot-drawn fibers of Y_2 blended with PEN[2].

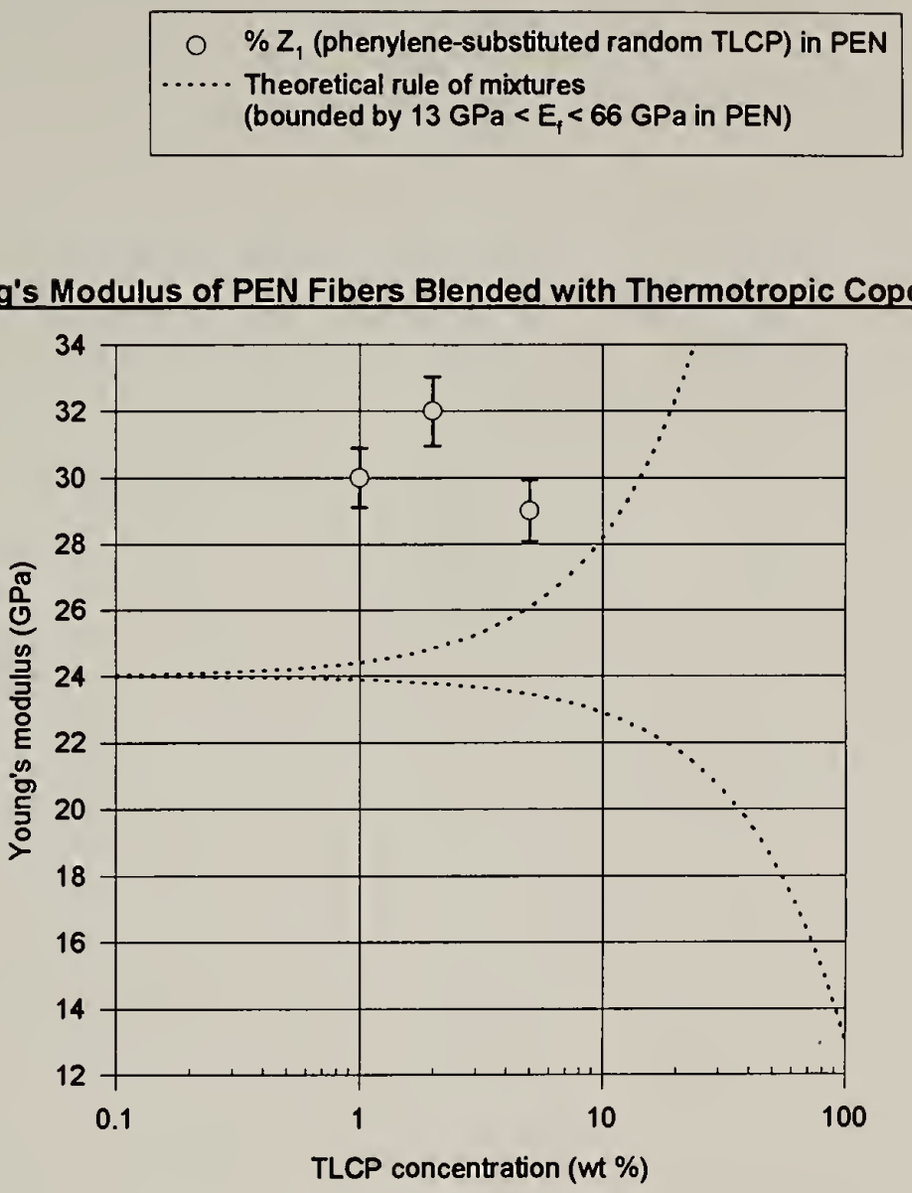

Figure 4.12. Young's moduli of hot-drawn fibers of Z_1 blended with PEN[2].

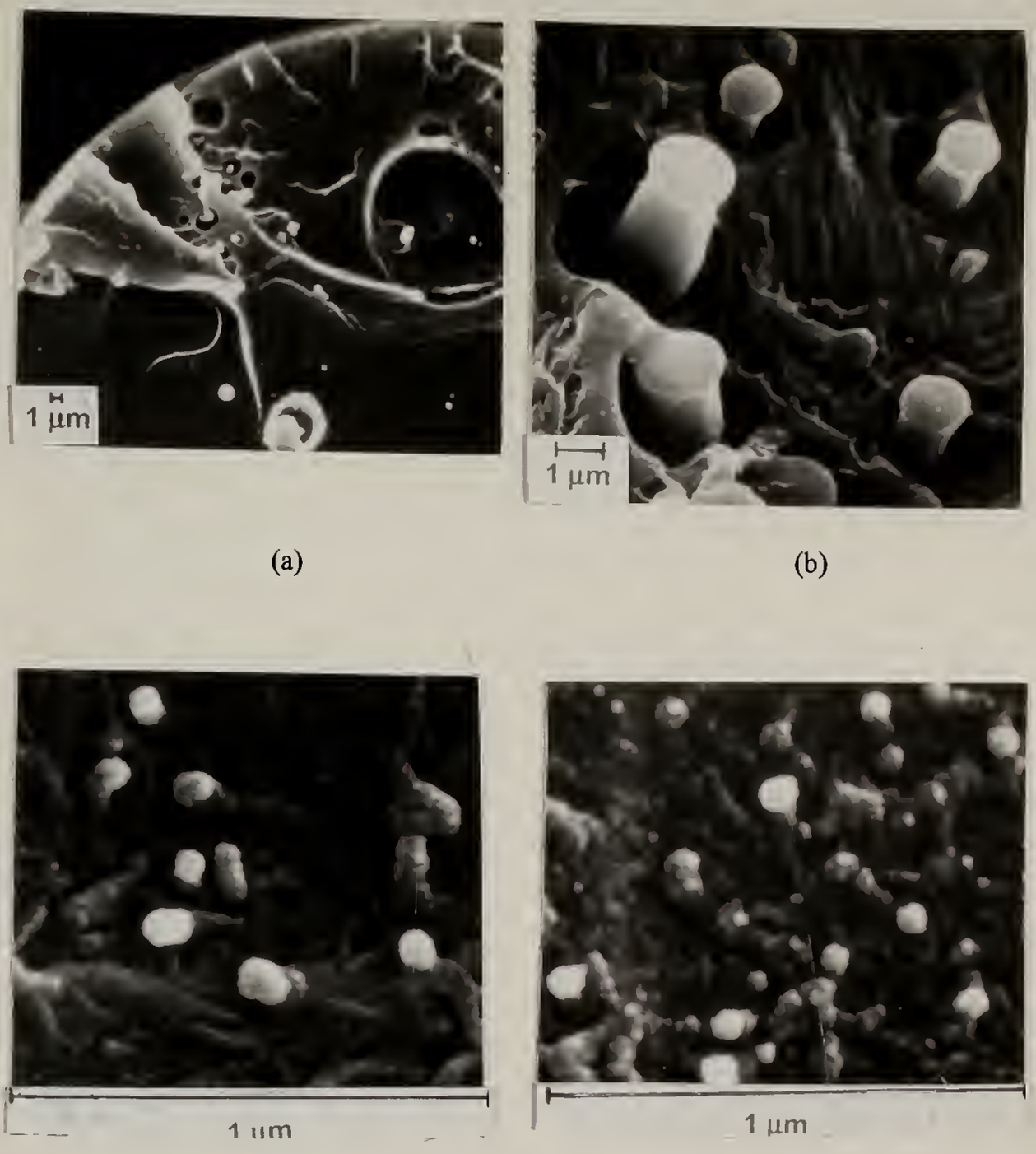

Figure 4.13. SEM micrographs of the cross-section of cryogenically-fractured as-spun fibers of Z_1 blended with PEN. These micrographs illustrate that while fibrillation occurs over a wide domain scale, the as-spun fibers do not exhibit marked skin-core effects. (a) As-fiber containing 1% Z_1; (b) Outer skin region of as-spun fiber containing 2% Z_1 showing fibril diameters above one micron; (c) Outer skin region of as-spun fiber containing 2% Z_1 showing submicron inclusions; (d) Inner core region of as-spun fiber containing 5% Z_1 showing submicron inclusions.

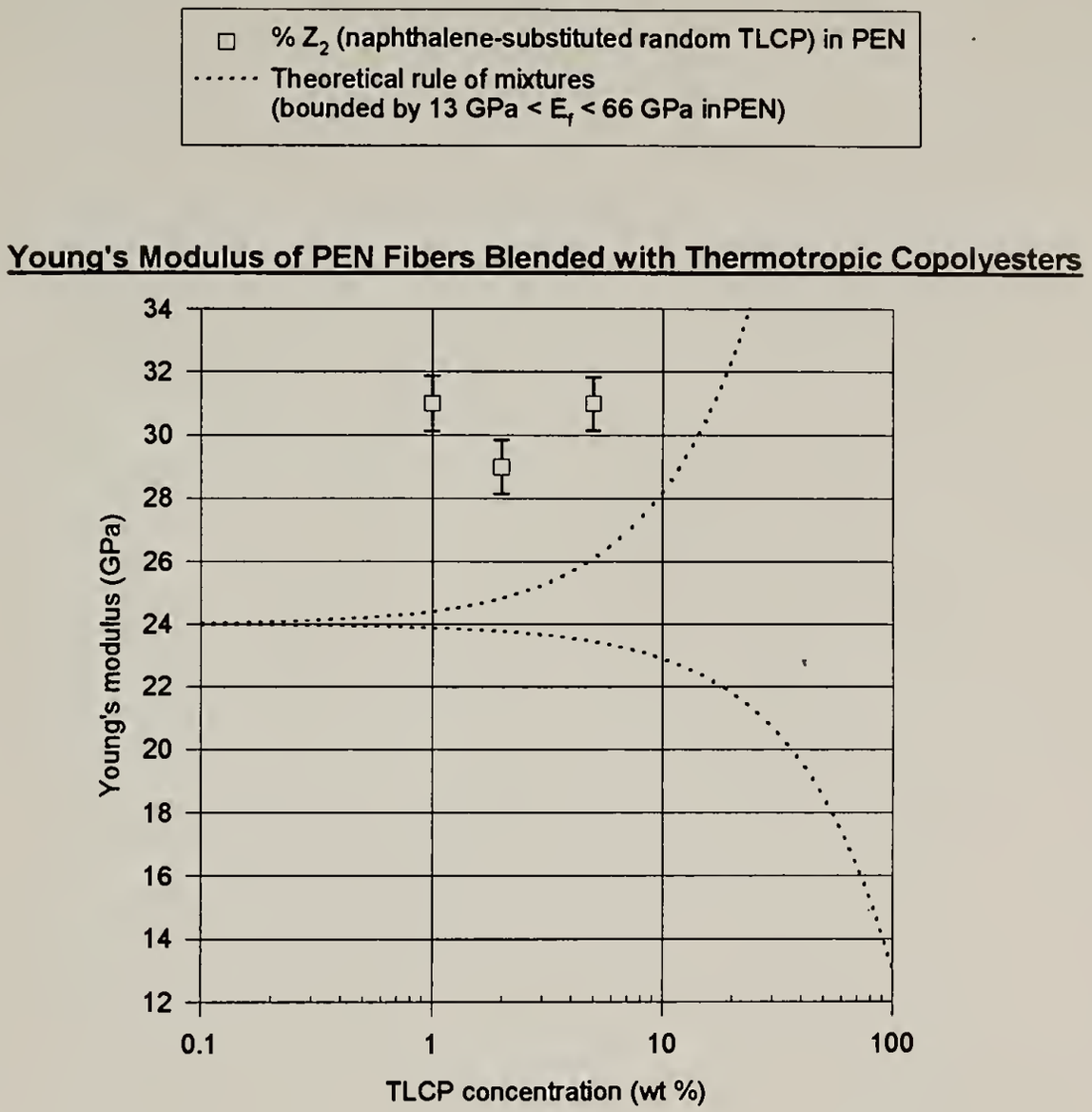

Figure 4.14. Young's moduli of hot-drawn fibers of Z_2 blended with PEN[2].

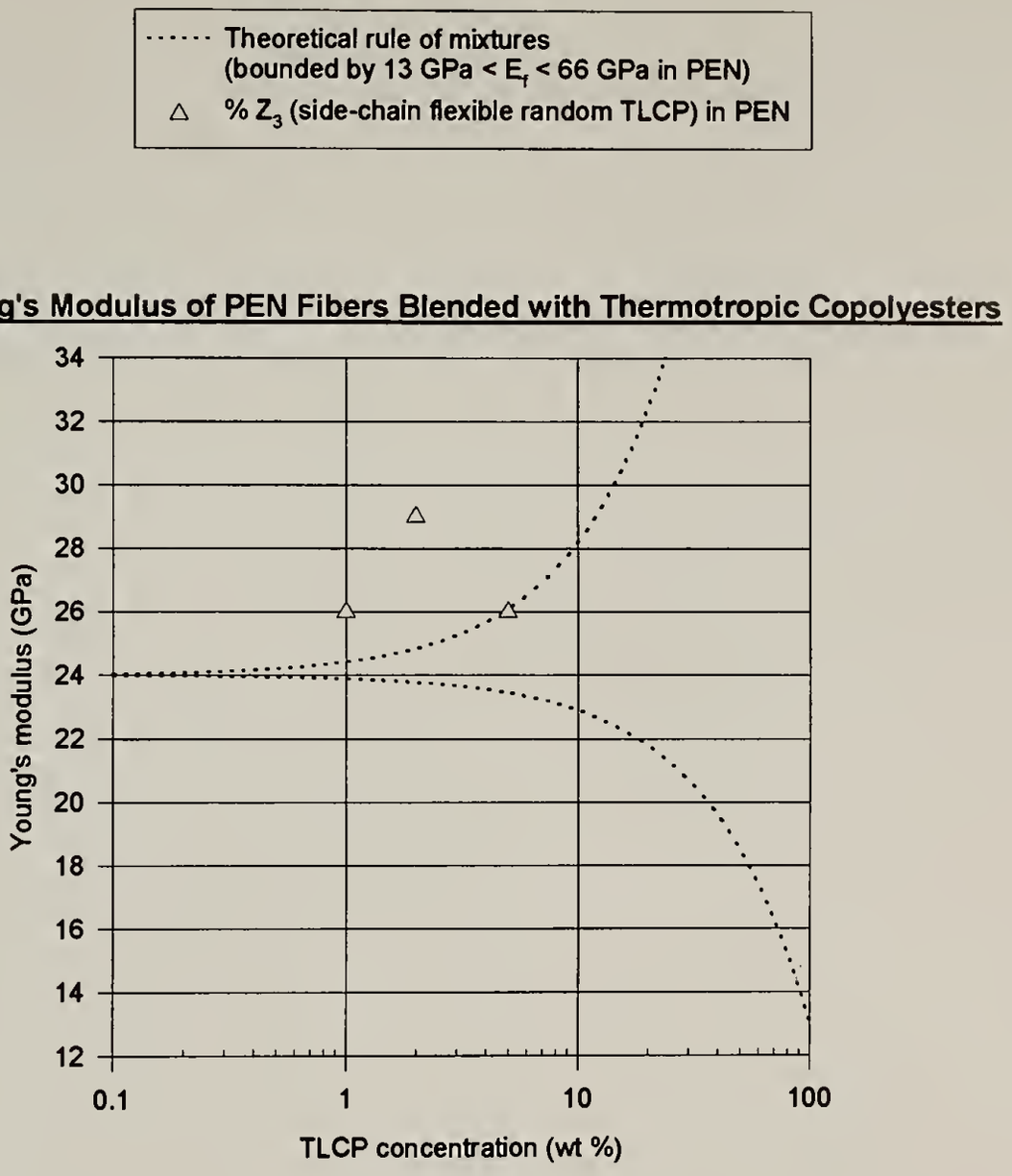

Figure 4.15. Young's moduli of hot-drawn fibers of Z_3 blended with PEN[2].

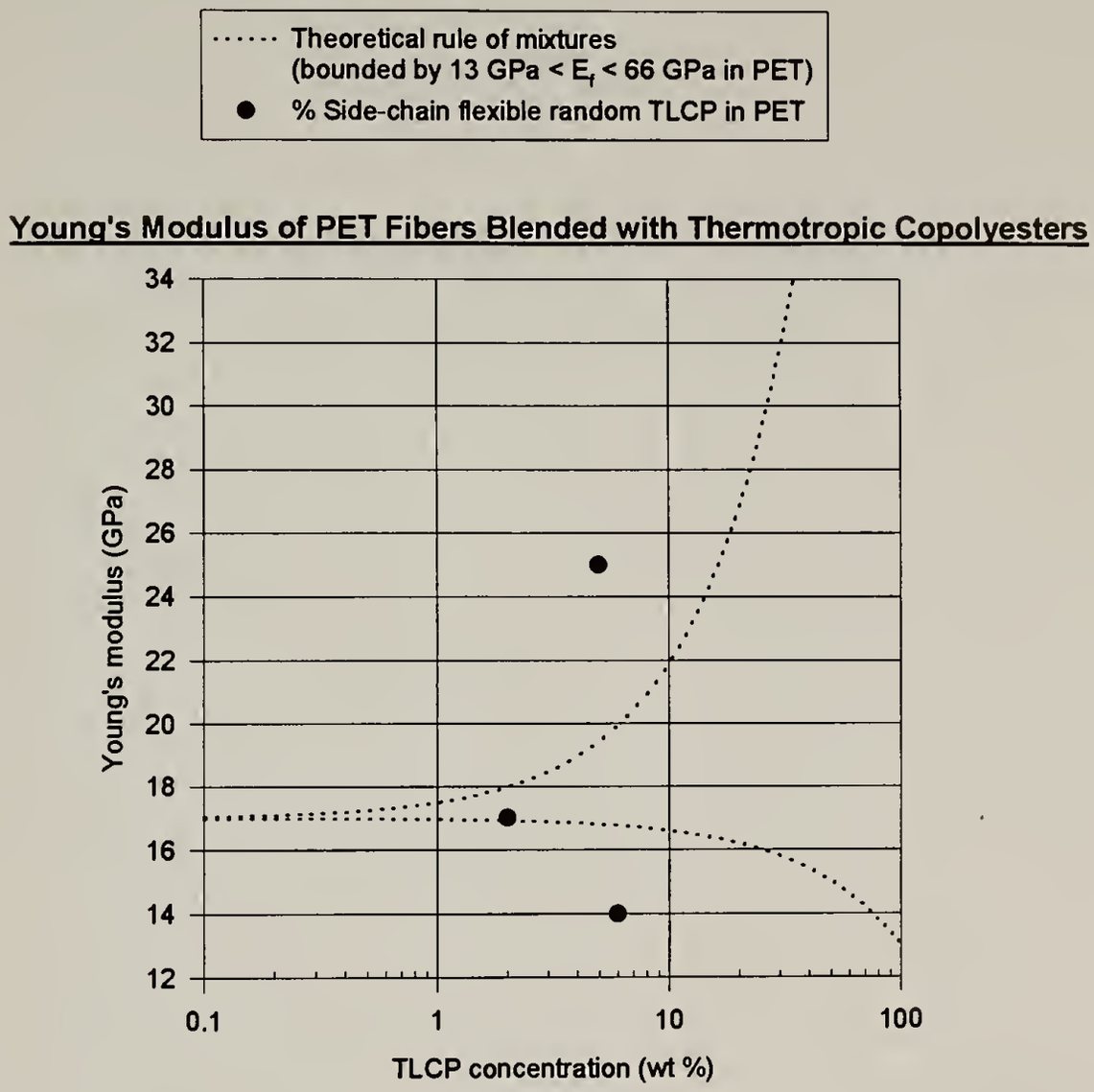

Figure 4.16. Young's moduli of hot-drawn fibers of a side-chain flexible TLCP blended with PET.

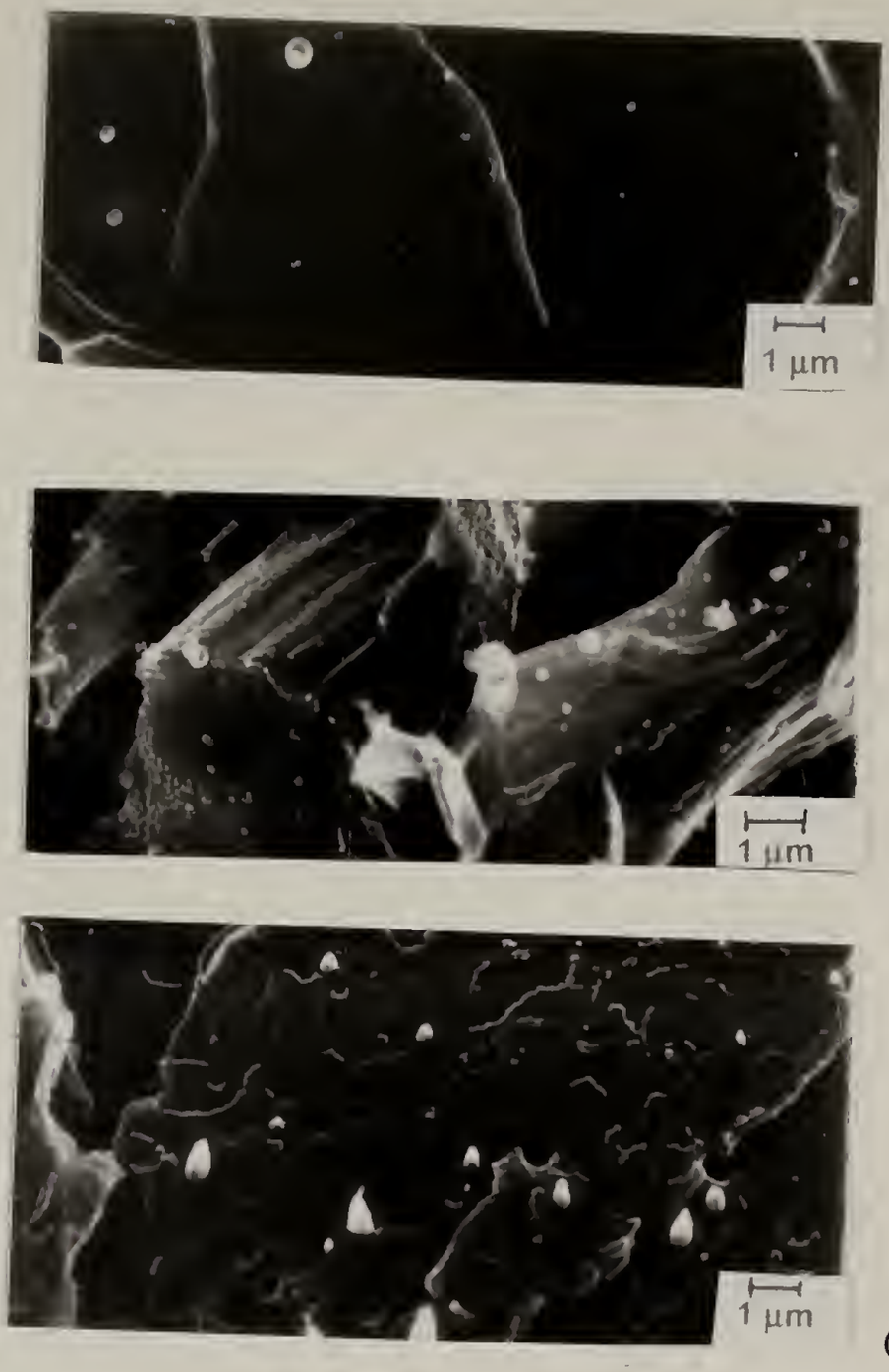

Figure 4.17. SEM micrographs of the cross-section of cryogenically-fractured fibers of Z_3 blended with PEN[2]. These micrographs illustrate that the most striking difference between as-spun and hot-drawn fibers is not the degree or scale of fibrillation, but the apparent crystallinity of the matrix. (a) As-fiber containing 1% Z_3; (b) Hot-drawn fiber containing 2% Z_3; (c) As-spun fiber containing 5% Z_3.

Table 4.1. Mechanical properties for hot-drawn fibers of all investigated polyblends of TLCP with PEN. TLCP concentrations are given in weight per cent.

Polyme	¼%	½%	1%	2%	5%	10%	20%
*X_1					**16**, 7, 6	**14**, 7, 7	
*X_2			**30**, 9, 4		**30**, 8, 4	**28**, 6, 4	
†X_3	**23**, 7, 5	**21**, 6, 6	**31**, 9, 4	**27**, 8, 6	**29**, 9, 4	**19**, 3, 10	**23**, 5, 3
†X_4			**29**, 9, 4	**27**, 7, 5	**28**, 8, 4	**23**, 5, 8	
†Y_1			**31**, 8, 3	**30**, 9, 4	**25**, 7, 7		
†Y_2			**31**, 8, 3	**31**, 8, 3	**29**, 7, 3	**26**, 4, 6	
†Z_1			**30**, 8, 4	**32**, 8, 3	**29**, 7, 4		
†Z_2			**31**, 8, 4	**29**, 8, 4	**31**, 8, 3		
†Z_3			**26**, 9, 6	**29**, 9, 5	**26**, 7, 5		

[**E (GPa)**, σ_u (GPa x 10), ε_u (%)]

*PEN[1] matrix: E=26 GPa

†PEN[2] matrix: E=24 GPa

CHAPTER 5

THERMAL PROPERTIES OF THE TLCP BLENDS

5.1 Introduction

The last chapter discussed evidence of synergistic mechanical effects with the addition of TLCP to PEN where a binary mixture was presumed. Barring the presence of transesterification reactions -- which effectively change the number of components within this system -- the thermal role of the TLCPs may also be considered within this context. Many of the results indicate that the TLCP has the ability to affect the PEN matrix as a function of concentration. Some of these effects of compatibilization and matrix modification are also seen for TLCP blends with PET where mechanical property synergy was observed as well [Joslin, 1994].

5.1.1 Compatibilization

The aim of all of the blending studies was to form compatibilized blends consisting of a polyphasic structure with interaction at the phase interface. Both POM and SEM micrographs have already shown cases of distinct phase separation for the TLCP phase within PEN.

Coupled with the above, the detection of a single T_g suggests partial miscibility of the matrix with the TLCP [Chapleau et al., 1992]. The TLCPs can thus plasticize the matrix if the T_g of the TLCP is lower than that of the matrix [Turek et al., 1995]. As previously stated, the T_gs of the TLCPs were indeterminable using DSC as a technique. Other authors have, however, reported

a T_g of 47°C for semi-flexible TR-4 type thermotropic copolyesters and a T_g of 39°C for a side-chain flexible TLCP similar to Z_3 [Chang et al., 1995] [Chang and Farris, 1995].

A single T_g is significant as evidence for compatibilization only if the individual T_g of the two phases are widely separated. This was not the case for the aforementioned TLCPs within a PBT matrix as cited above. The cited TLCP temperatures are, however, markedly different from the T_g of pure PEN, which is 119°C. Thus, if the addition of TLCP as a plasticizing agent lowers the apparent T_g of the PEN blends, then a degree of phase compatibilization is likely.

5.1.2 Nucleation of PEN

An additive serves as matrix modifier if it can nucleate or enhance the crystallization of a matrix in which it resides. Crystalline nucleation and growth can occur as the material is heated to its melting point and when it is cooled from its melt state into a solid.

There are several reports of crystalline nucleation effects stemming from liquid crystalline polymers in polymer blends. Misra and coworkers showed that Vectra A® can increase the crystallization rate of PET; similarly, Joseph and coworkers described the role of main-chain flexible thermotropic copolyesters as nucleating agents for PET [Dutta et al., 1990]: Increased heats of fusion have been reported for blends of PET/PHB copolymer with PET, and for blends of semi-flexible thermotropic copolyester with PET [Sukhadia et al., 1990] [Shin and Chung, 1990]. Similar results are found using Vectra® in PET [Shin and Chung, 1990]. More recently, Chang and Farris [1995] presented examples of how a side-chain flexible thermotropic copolyester nucleates crystallization of a PBT matrix.

Other reports, however, present evidence to the contrary. After observing little concentration dependence of the TLCP of recrystallization temperatures of PET, El-Amouri and Skoulios

[1995] concluded that binary mixtures of a thermotropic copolyester prove inept as nucleating agents for PET. In some cases, the authors report lowered re-crystallization temperature of PET when blended with more than 40% by weight of a thermotropic copolyester. Other fiber studies suggest that a supercooled LCP mesophase actually restricts PET chain mobility, thereby frustrating (instead of hastening) PET crystallization [Mehta and Deopura, 1993].

5.2 Experimental

The thermal studies presented were done on as-spun fiber samples that had been quenched from the melt. The motivation was to study inherent thermal effects present in TLCP polyblends melt-extruded with PEN into monofilaments. As a result, it was necessary to remove possible artifacts (such as stored strain) associated with fiber forming processes.

Thermal transitions for each TLCP blend were detected using DuPont DSC 2910 equipment at a heating rate of 10°C/min under a stream of N_2. DSC transitions were highly dependent on the thermal history of the sample, and thus all samples were studied with identical thermal histories. Unless otherwise specified, the procedure consisted of four steps. First (1) as-spun fiber samples were heated from 30° to 300°C at 10°C/min. Once equilibrated at 300°C, they were then (2) quenched in liquid N_2, (3) re-heated to 300°C at 10°C/min, and (4) cooled back to room temperature at -10°C/min.

All thermal data were recorded during steps (3) and (4). Glass transition temperatures were taken at curve inflection during step (3). Other reported temperatures correspond to those at transition peaks during steps (3) and (4). The temperature and enthalpy changes were calibrated using an indium standard.

5.3 Results

The body of thermal data overwhelmingly points to the role of compatibilized TLCPs as nucleating agents for PEN. Thermal data for each topic is presented separately.

5.3.1 Compatibilization

For every TLCP investigated, except for the side-chain flexible copolyester, incremental addition of TLCP generally shifted the T_g of the blend toward lower values. This plasticization effect is anticipated because the T_g of the semi-flexible TLCP is likely far lower than that of PEN. The glass transition temperature of pure PEN (T_g°) is 119°C for all cases unless otherwise noted. The T_g of the TLCP cited from literature is under 50°C. At any a particular TLCP concentration, the deviation of the glass transition temperature of the blend (T_g^{blend}) from T_g° is defined as ΔT_g such that $\Delta T_g \equiv T_g^{blend} - T_g^\circ$. The maximum plasticizing effects are seen for class X and Y TLCPs. For example, 10% blends of these TLCPs lower T_g by 7-10 degrees C. Class Z gave rise to the smallest plasticization effects.

5.3.1.1 Class X: Segmented Diad/Triad Copolyesters

Figure 5.1 compares two sets of T_g data for X_3 and X_4. The T_g lowering effect of X_3 in PEN is the largest observed for any of the copolyesters investigated. Also, the data points for X_3 copolymer nearly exactly match those for ROM predictions for T_g. (This calculation uses the polymer weight fractions as weight factors for individual T_gs and the earlier cited value of 47°C for

the T_g of Triad-based thermotropic copolyester.) There is a large difference in the behavior of the X_3 [TR-4(2:4:7)] compared to X_4 [TRN-4(2:4:7)].

The TCLPs discussed in Figure 5.1 differ subtly in their chemical structure with the presence of naphthalene substitution in X_4, versus phenylene substitution in X_3. The overlayed T_g data for X_4 polyblends shows higher values for nearly all compositions. Because naphthalene-substituted X_4 is comparatively rigid, a reasonable hypothesis is that its T_g is higher that of phenylene-substituted X_3.

Figure 5.2 compares the effects of Triad-based polymer in PEN and in PET. The lower curve corresponds to that of X_3 while the upper curve corresponds to that of a segmented copolyester, TR-2 (2:6:7), very similar to X_3. Both reflect a degree of compatibilization of the TLCP with the matrix. The nomenclature of TR-2 (2:6:7) shows that its architecture contains fewer flexible methylene spacers and a higher percentage of rod-like mesogenic Triad units than X_3, whose designation is TR-4 (2:4:7). This supports another reasonable hypothesis that the T_g of the intrinsically less rigid TLCP is higher than that of X_3.

Figure 5.3 compares data for other X class segmented TLCPs which also affect T_g lowering when blended with PEN. While these samples and their neat as-spun fiber comparisons were heated to a final melting temperature other than 300°C (as described in the procedure), it is nevertheless instructive to examine the effects of these TLCPs on T_g of the blend. In fact, the T_g lowering trends are the same.

Again, the data supports the idea that the intrinsically more rigid component, X_1 which contains fewer methylene spacers than X_2, has a higher T_g than X_2. This is the reason that T_g lowering effects of X_1 are relatively less pronounced at any particular concentration.

5.3.1.2 Class Y: Alternating Copolyesters

While similar in molecular weight, the alternating copolymers displayed T_g lowering effects different from those observed in the segmented copolymers. In the previous cases, the intrinsically stiffer TLCP appeared to have a higher T_g.

Figure 5.4 shows that the fully phenylene-substituted TLCP Y_1 exhibited negligible effect on T_g when blended with PEN. On the other hand, the same concentrations of Y_2, which contains one naphthalene-substitution in the non-mesogenic (PBN) sequence of the alternating structure, shows marked T_g depression with increasing Y_2 content.

Other things being equal, this would suggest that the T_g of Y_1, the more flexible TLCP, lies well above the T_g of Y_2, the more rigid TLCP. This conclusion is non-intuitive based on chemical structure arguments alone. In fact, the explanation for this effect has less to do with chemical structure than with the presence of an induced nematic state for each TLCP during the course of the DSC experiment.

Y_1 copolymer was the only one of all ten TLCPs examined which fully isotropized (cleared) at a temperature under 300°C. (Table 3.1 showed that it undergoes nematic-to-isotropic transition at 268°C.) This means that Y_1 was quenched as an isotropic glass after it was ramped to 300°C in step (3) of the DSC procedure. In contrast, Y_2 was quenched below its isotropization temperature. Studies by Zachmann et alii on thermotropic copolyesters and terpolyesters of PET, PEN, and PHB reveal that the T_g of these polymers in the isotropic phase is sharply higher (by 30°C to 35°C) than their T_g in the liquid crystalline state. Using deuteron nuclear magnetic resonance (NMR) techniques, Zachmann and coworkers showed that trans-gauche jumps of CH_2 groups in the elongated chains of the LC state can occur at lower temperatures than in the coiled chains of the isotropic state [Zachmann et al., 1992] [Zachmann et al., 1993] [Spies and Zach-

mann, 1994]. Thus, the results with alternating class Y TLCPs, which suggest that the T_g of Y_1 is higher than that of Y_2, are consistent with those findings.

Although SEM of as-spun Y_1 / PEN fibers does show the same sub-micron size scale for a sparsely distributed dispersed phase, it is not possible to tell from DSC studies that Y_1 has compatibilized with PEN.

5.3.1.3 Class Z : Random Copolyesters

Figure 5.5 shows the results of Z_1 and Z_2 main-chain flexible concentration on the T_g of blends. Compatibilization effects are evident in both cases. Here as expected, the intrinsically stiffer TLCP (Z_2) appears to have a slightly higher T_g than phenylene-based Z_1. The effect of T_g lowering, presumably through compatibilization, is more evident at higher concentration.

There are no evident plasticization effects for either Z_3 (side-chain flexible copolymer) in PEN or for a similar side-chain flexible TLCP in PET. Figure 5.6 shows that unlike the others in its class, the ethoxy substituted hydroquinone TLCPs do not affect the T_g of their blends within a matrix of either PEN or PET. In another study involving polyblends of PBT, a similar type of trioxyethylene substituted hydroquinone side-chain flexible thermotropic copolyester was also reported to have no effect on T_g [Chang and Farris, 1995].

5.3.2 Nucleating Effects on Heating

Evidence for the copolyesters acting as nucleating agents for the matrix appears in both heating and cooling behavior during DSC runs. In the heating portion, the quantities of interest are the cold-crystallization temperature (T_{cc}), the melting point of PEN on heating (T_m) and their asso-

ciated heats of transition. ΔH_{cc} is an exothermic (energy releasing) transition while ΔH_m is endothermic (energy absorbing). All heats associated with thermal transition are normalized by the total amount of PEN within each blend.

Figure 5.7 is a series of DSC heating thermograms (for blends of X_3) which illustrate the typical and unmistakable effects that TLCP concentration can have on T_g, T_{cc}, T_m and their associated heats. A primary observation is that in all cases, the TLCPs as a group have virtually no effect on the melting temperature of PEN at any concentration. (The melting point of PEN, whether pure or blended with TLCP, remains at 258 °C.) All of the TLCPs are, however, able to raise ΔH_m of PEN with increasing TLCP concentration; the implication is that the presence of the TLCP can impart higher crystallinity of the matrix.

Another broad observation is that within each class, the TLCPs have nearly the same effect on T_{cc} lowering as a function of concentration. Again, an exception exists for Z_3 polymer which does not depress T_{cc} to the same degree that both Z_1 and Z_2 do.

5.3.2.1 Class X: Segmented Diad/Triad Copolyesters

Starting again with a comparison of X_3 and X_4, Figure 5.8 shows that neither has much effect on T_m but both show markedly similar drops in T_{cc}. This means that the solid-state ordering transition of cold-crystallization is hastened by the addition of segmented copolymer. That is, cold-crystallization occurs at lower temperatures on heating in step (3) of the DSC procedure. While the T_{cc}s for both types of polyblends are noticeably reduced , these trends are similar in spite of intrinsic stiffness and molecular weight differences of the additives. Figure 5.9 plots the associated heats for cold-crystallization and melting of X_3 and X_4. It shows, however, that naphthalene-substituted X_4 (represented by hollow points) generally allows for a higher heat of melting at lower

compositions. Perhaps due to its chemical similarity with PEN, X_4 seems a slightly better nucleating agent than X_3 for PEN.

Figure 5.10 shows the effects of concentration of a TR-2 (2:6:7) type copolyester used on the transition temperatures of PET. It shows the same trends as Triad-type copolyesters in PEN -- notably that T_m remains unaffected. Within the PET matrix, however, T_{cc} lowering effects appear to quickly reach a plateau value at higher concentrations. PET appears to cold-crystallize at a temperature 40 degrees lower than it otherwise would without the addition of TR-2(2:6:7). As was shown in Figure 5.8, the addition of TR-4 type polymers in PEN resulted in comparatively smoother variation in T_{cc} lowering. The effects of TR-2(2:6:7) on the heats of these transitions for PET are shown in Figure 5.11. The effects of TR-2 (2:6:7) on the heats of cold-crystallization and melting of PET are also similar to effects of TR-4 (2:4:7) and TRN-4 (2:4:7) in PEN. Again there is a characteristic rise in ΔH_m and a corresponding drop in ΔH_{cc}.

Figure 5.12 shows the effects of TR-*m* (2:4:7) incorporation within the PEN matrix. These samples were heated to a temperature other than 300°C during the DSC heating ramp. Nevertheless, for $m = 2$ and $m = 4$, the trends in melting point stasis and cold-crystallization lowering were the same as all of the others in class X.

5.3.2.2 Class Y: Alternating Copolyesters

The aggregate effects of phenylene-substituted Y_1 alternating copolyester in PEN on heating are shown in Figure 5.13 and are similar to those observed in the segmented copolyesters. The results for Y_1 are perhaps more interesting when directly compared with those of naphthalene-containing Y_2 as shown in Figure 5.14. When these plots are overlayed, the points plotted for Y_1

fall almost exactly onto those of Y_2. Given that the molecular weights of Y_1 and Y_2 are similar, these results indicate that chemical structure plays a small role for this class of TLCP.

5.3.2.3 Class Z: Random Copolyesters

Figures 5.15 and 5.16 respectively plot the effects of Z_1 and Z_2 main-chain flexible TLCPs on the PEN matrix on heating. The temperatures for both melting and cold-crystallization are nearly exactly the same for both types of TLCP polyblends. In terms of ΔH_m , the nucleating effects of naphthalene-substituted Z_2 rise more quickly than that of phenylene-substituted Z_1 but plateaus at 2%.

The effects of Z_3 side-chain TLCP are shown in Figure 5.17. Of all the TLCPs examined, Z_3 showed the least sizable effect on the crystallization parameters on heating.

5.3.3 Nucleating Effects on Cooling

The remaining sections discuss the ability of the TLCP to affect supercooling of the matrix. Supercooling, ΔT^*, is the difference between the temperature at which a substance melts (T_m) and the temperature at which it re-freezes (T_x) such that $\Delta T^* \equiv T_m - T_x$. Generally, ΔT^* is non-zero because $T_m > T_x$.

5.3.3.1 Background

Supercooling phenomena are found for a variety of crystallizable materials (including water). It is an important effect to note, for example, when casting ingots from molten metals. For

high molecular weight molecules, the degree of supercooling is especially rate dependent. Only in the theoretical limit of a static cooling rate (i.e., a cooling rate of 0°C/min) are macromolecules predicted to yield $\Delta T^* = 0$ when cooled from the melt. In contrast, in the results here, pure PEN material gives rise to $\Delta T^* = 76°C$ even when cooled at the relatively slow rate of -10°C/min. Thus, pure PEN melts at 258°C but does not re-solidify from the melt until it reaches 181°C.

While supercooling is inevitable, an effective nucleating agent reduces ΔT^*. This is the reason for examining cooling data as a function of TLCP concentration and type. To simplify matters somewhat, because T_m of the pure PEN matrix remained unchanged regardless of TLCP content and type, it is sufficient to note only T_x in order to make conclusions about supercooling for each TLCP. More specifically, for these studies on TLCP blends with PEN, the equation quantifying supercooling becomes $\Delta T^* = 258°C - T_x$.

In all cases, the presence of TLCP hastens re-crystallization of PEN from the melt. The TLCP also increases the amount crystallized from the melt, as indicated by the heat of fusion, ΔH_x, compared to that of neat PEN. Large effects are seen in most cases with as little as 1% (or less) of TLCP added. The heat of fusion for 100% crystalline pure PEN is 104 J/g [Ghanem and Porter, 1989]. The studies in this chapter show that the percent crystallinity of PEN can rise from 20% (for pure re-crystallized PEN) up to just under 50% when PEN is blended with a small amount of TLCP additive.

5.3.3.2 Results

The most exceptional example of a TLCP as a nucleating agent on cooling occurs for the segmented triad-diad class of TLCP. Figure 5.18 presents a series of cooling thermograms for the X_3 series of blends with PEN; the observed shifting toward higher T_x and larger ΔH_x with TLCP

content are typical for all TLCP systems. Figure 5.19 quantifies the supercooling and nucleating behavior of PEN blended with X_3 [TR-4(2:4:7)] on a plot. Figure 5.20 gives the corresponding effects for PEN blended with X_4 [TRN-4(2:4:7)]. In the presence of X_4 , which is an intrinsically stiffer material than X_3, PEN re-crystallizes from the melt at temperatures up to 34 degrees higher than it otherwise would as a pure material. The apparent heat of fusion ΔH_x for PEN is approximately doubled at just 1% X_4 inclusion; the percent of PEN re-crystallizing from the melt increases from 20% to just under 40%.

Also plotted on the same scale to ease comparison, Figures 5.21 and Figure 5.22 compare the effects of alternating copolyester inclusion on undercooling. In this case, phenylene-substituted Y_1 consistently gives rise to values of ΔH_x and T_x equal to or higher than that of naphthalene-substituted Y_2. For both cases within class Y, the heat of fusion ΔH_x is doubled at just 1% inclusion of alternating TLCP.

As a whole, the random TLCPs gave rise to more smoothly varying nucleating effects on cooling than the other classes. In particular, none of the class Z copolyesters were able to double the value for ΔH_x of pure PEN at any level of TLCP inclusion.

Figure 5.23 shows the nucleating effects on cooling for Z_1 (phenylene-substituted main-chain flexible random TLCP). Figure 5.24 shows the trends for Z_2 (naphthalene-substituted main-chain flexible random TLCP). While the actual magnitudes of maximum cooling effects are similar for both Z_1 and Z_2, phenylene-substituted Z_1 approaches these values more subtly. Examination of the trends for Z_3 (side-chain flexible random TLCP), shown in Figure 5.25, reveals that they are intermediate compared to those observed for Z_1 and Z_2.

5.4 Summary

These studies indicated that the TLCPs are compatibilized to a good degree with the PEN matrix as reflected in the detection of a single T_g within a binary system. Only class X of TLCPs blended with PEN yielded T_g results which decrease linearly with TLCP concentration in accordance with ROM calculations. In order to fit the T_g behavior of the other classes of TLCP, another model (such as Flory-Fox) should be considered. In either case, the actual T_g of the TLCP remains as a parameter which must be estimated. The trends in the apparent T_g decrease as a function of TLCP concentration for the blends are mostly consistent with existing work. Comparisons across all TLCP classes reveal that the more flexible the TLCP, the better it performs as a plasticizing agent for PEN.

The effects on supercooling coupled with observed increases in both the heats of melting and fusion with TLCP concentration are classic indicators that the TLCPs also assume the role of nucleating agents within the PEN matrix. In ten out of ten cases examined, the TLCPs can modify the PEN matrix to some extent by virtue of their inclusion. Nucleating effects are also seen with Triad-based TLCP in PET [Joslin, 1994]. There are not, however, any broadly-based trends relating molecular weight or mesogen content to the heat of fusion.

The relevant question is, "What is it about the TLCP that makes it an effective matrix modifier?" The intuitive response might be that the presence of a molecularly needle-like state can provide crystalline nucleation sites. The nematic texture itself is a collection of physical defects. Physical defects and impurities are common nucleators for crystallization in other materials. Implications of the results from the Y_1 alternating copolyester polyblends are thought-provoking when addressing the above question.

As discussed in §3.6.1, Y_1 is a fully phenylene-substituted copolyester that completely isotropized (at 268°C) prior to quenching in the melt state at 300°C. This means that at the beginning of the second heat and cooling [steps (3) and (4) of the DSC procedure], Y_1 existed as an isotropic polymer. Evidence that Y_1 was captured in an isotropic state was reflected in T_g properties for Y_1 (blended with PEN) which shows apparent glass transition behavior that would be characteristic of a thermotropic copolyester "frozen" in its isotropic-state. Yet it remains that Y_1 displayed cold-crystallization and melting behavior comparable to other TLCP systems which never had the opportunity to isotropize prior to degrading. Y_1 also shows sizable ability to reduce supercooling and nucleate a degree of re-crystallization of PEN from the melt; its role as a nucleating agent in some cases is superior to other TLCPs.

Copolyester Y_1 did not have another low temperature LC transition detectable using the procedures and methods applied. Considering the data, it seems an LCP in its isotropic phase also has the ability to act as a matrix modifier as it crystallizes. As a result, a fair conclusion is that the presence of the nematic state cannot solely account for the ability of the TLCPs to modify the matrix in which they reside.

The structure and rheology of the nematic state of thermotropic copolyesters are also very sensitive to thermal history [Han et al., 1994(a)] [Han et al., 1994(b)]. Slight differences in test procedures, particularly exposure to high temperatures, can affect not only the quality of the nematic state but can effectively alter the number of components in the blend if transesterification happens to a large extent [El-Amouri and Skoulios, 1994]. While transesterification was not investigated in the thermal studies of this chapter, its general effect is to chemically fuse (and alter) the existing structures of adjacent polyester chains. It is a common effect and is seen to occur appreciably in blends of PEN with PET [Stewart et al., 1993], blends of PEN with PBN [Yoon et al., 1994], and blends of PBT with a TR-4 copolyester [Jo et al., 1995].

The existence of complicating factors such as these mentioned above are possible reasons for the variety of results from different research groups who investigate the nucleating effects of TLCP.

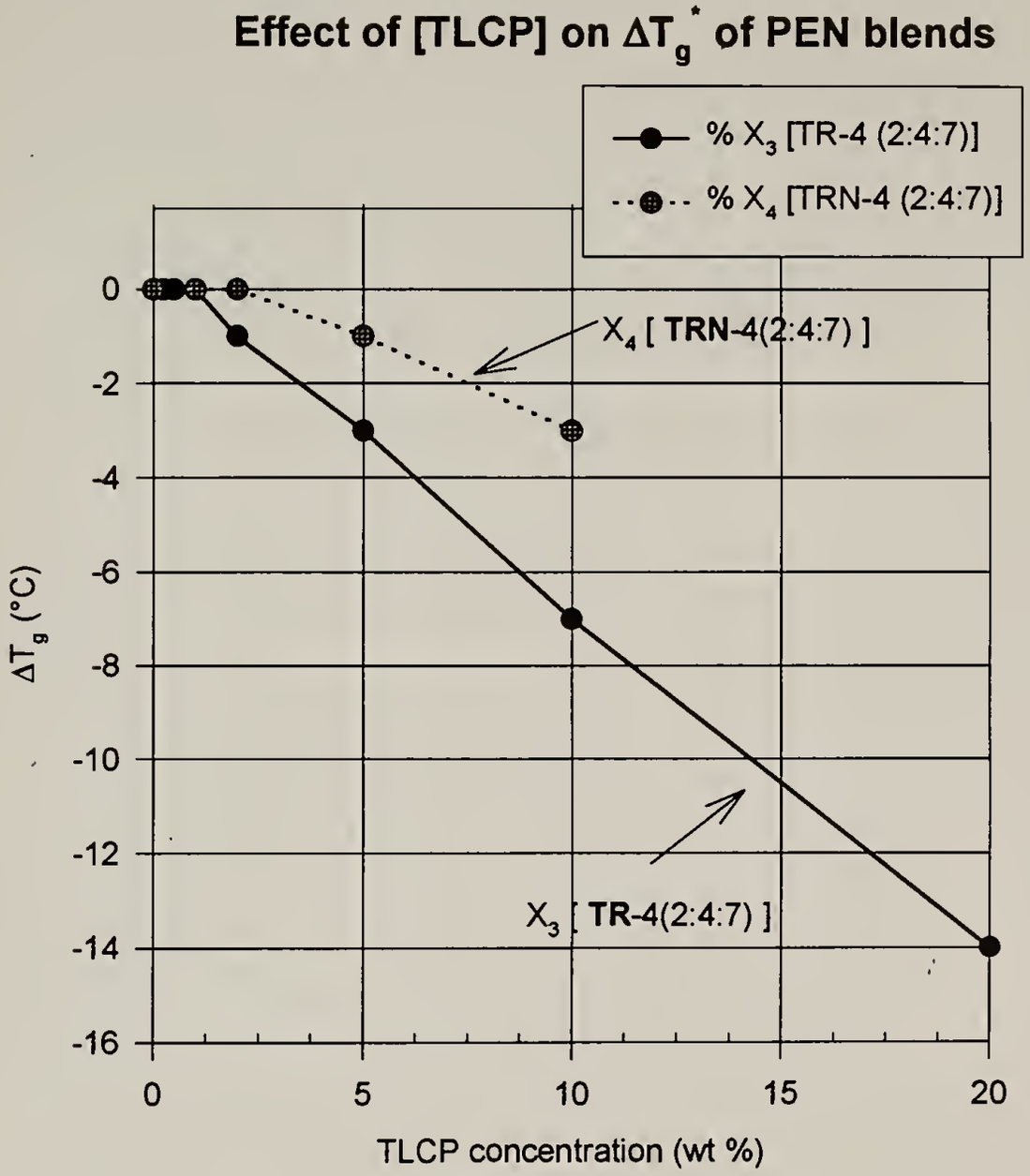

* obtained from 2nd heating of as-spun fiber at 10°C/min under N_2 following quench from melt state. T_g° (of pure PEN) is 119 °C.

Figure 5.1. Depression of T_g for blends of PEN with X_3 and X_4 segmented copolyesters.

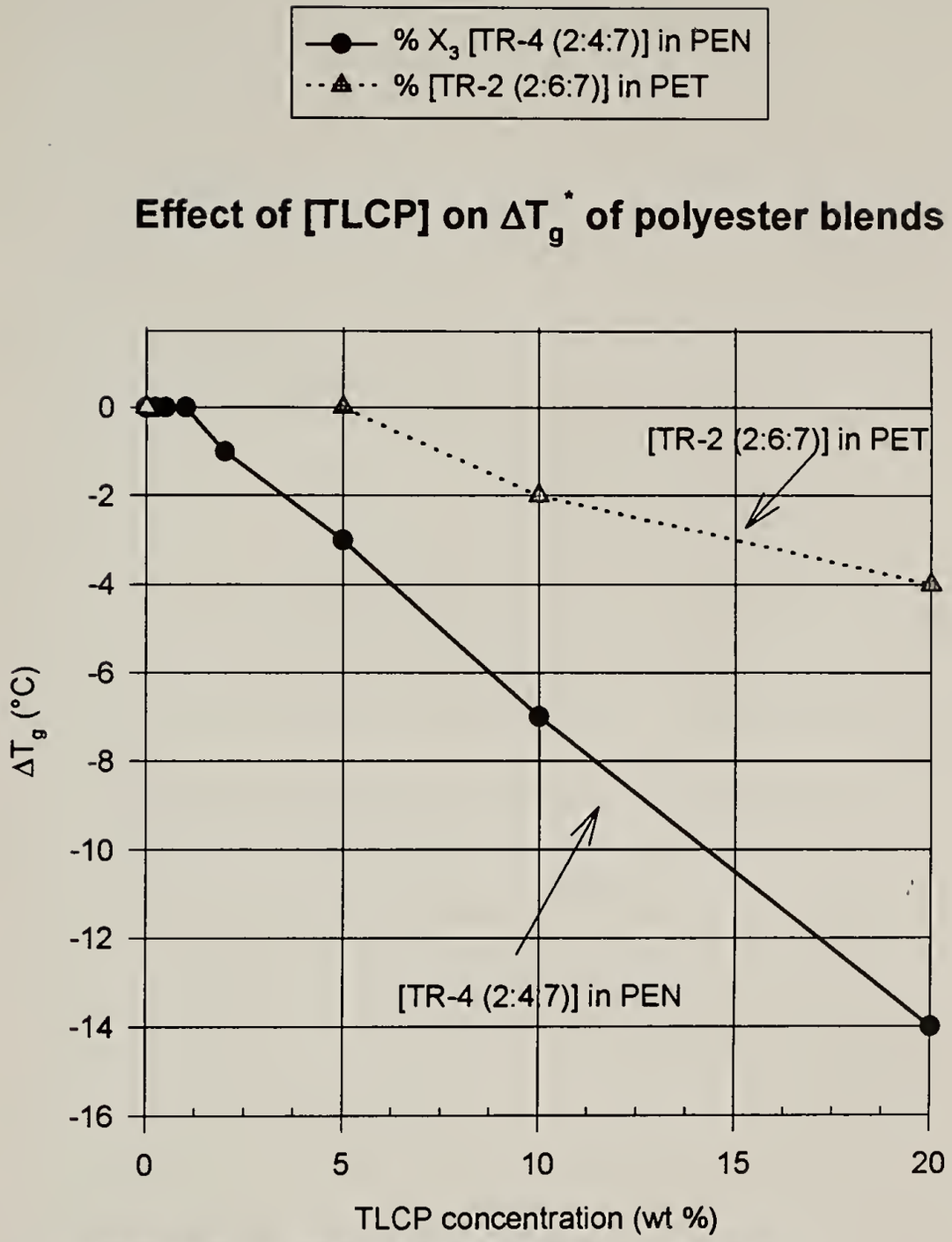

Figure 5.2. Depression of T_g for blends of PEN with X_3 and blends of PET with TR-2 (2:6:7) segmented copolyesters.

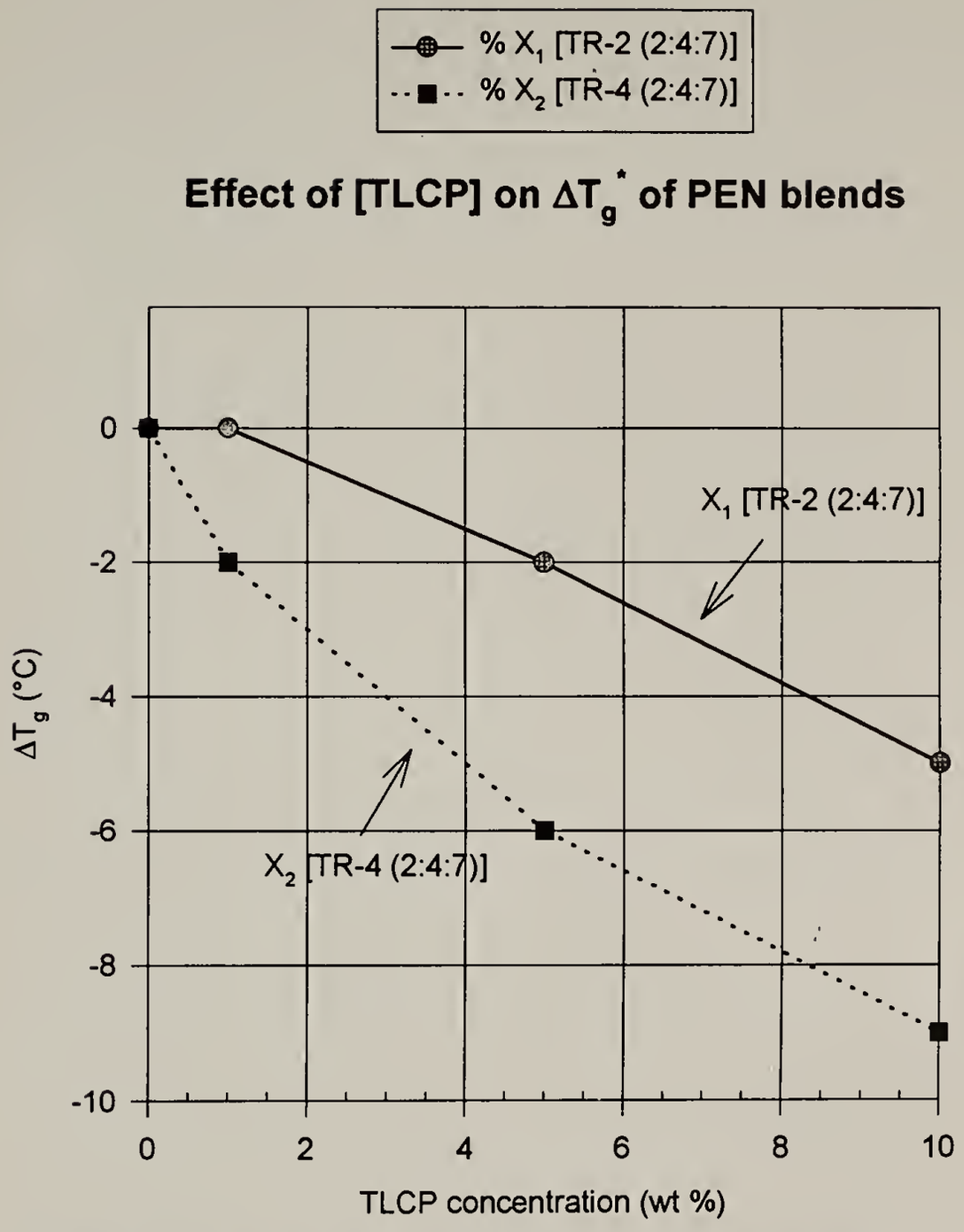

*obtained from 2nd heating of as-spun fiber at 10°C/min under N2 following quench from melt state. $T_g°$ for X_1 =120°C; $T_g°$ for X_2 =122°C

Figure 5.3. Depression of T_g for blends of PEN with X_1 and X_2 segmented copolyesters.

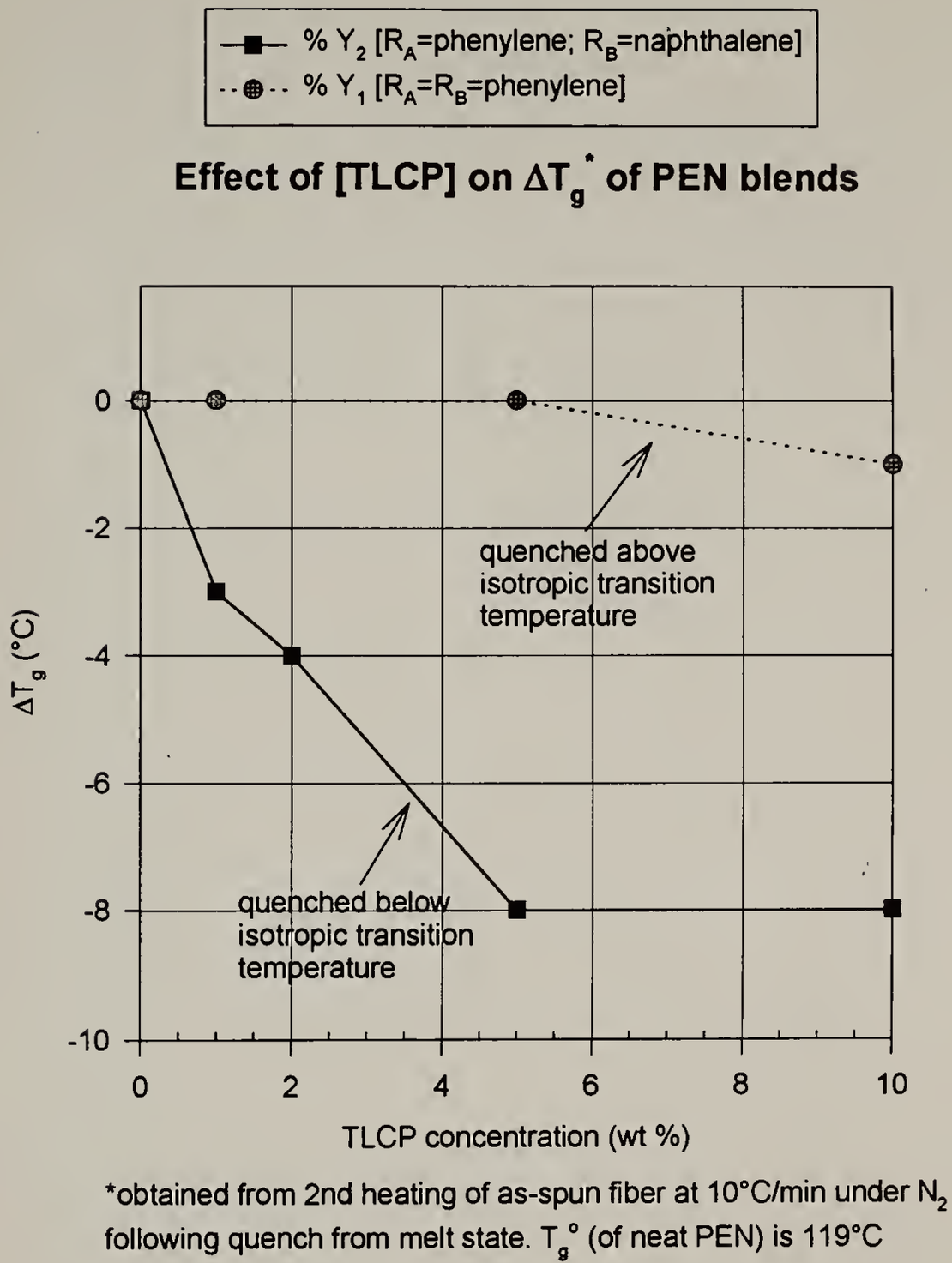

Figure 5.4. Depression of T_g for blends of PEN with Y_1 and Y_2 alternating copolyesters.

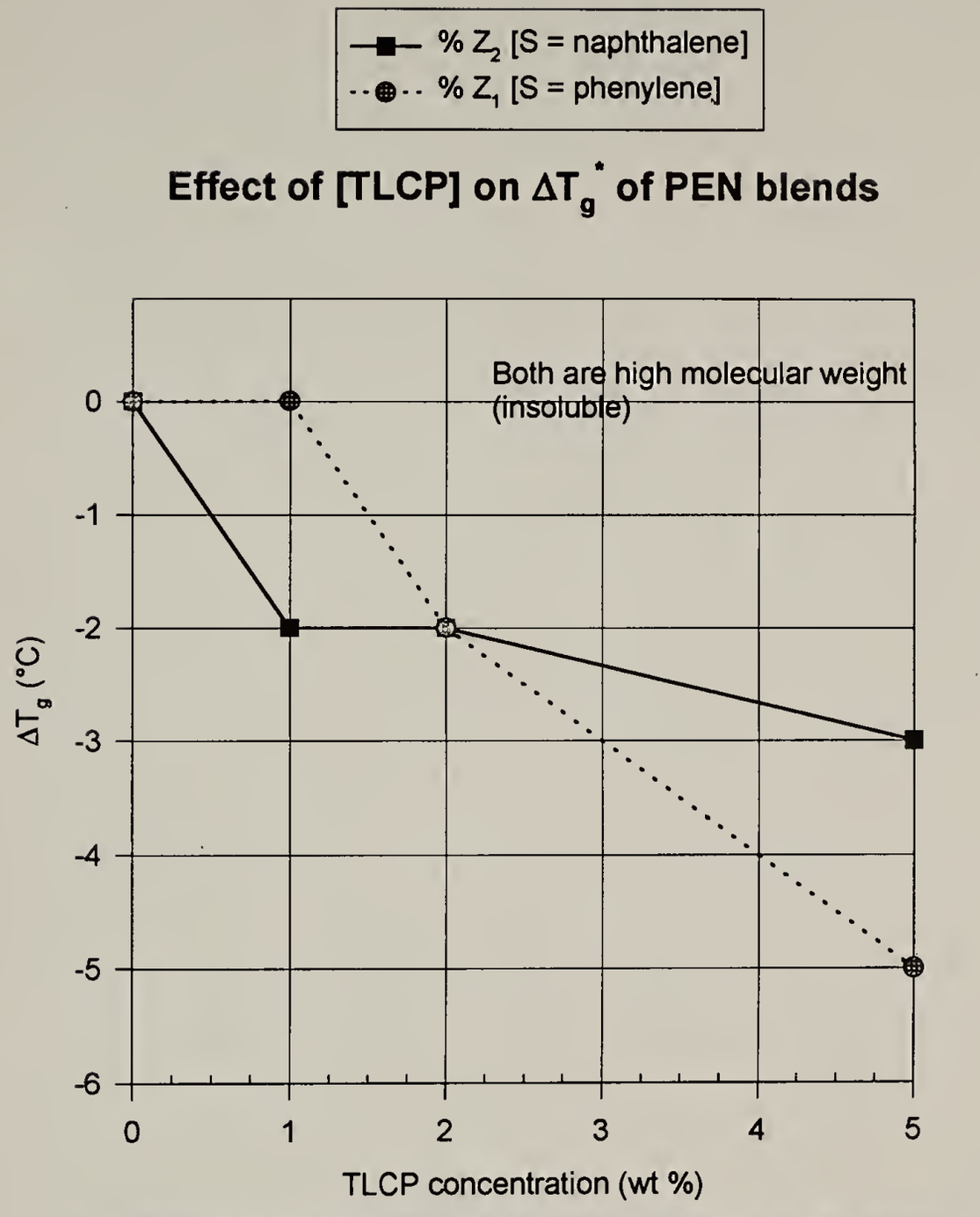

Figure 5.5. Depression of T_g for blends of PEN with Z_1 and Z_2 random copolyesters.

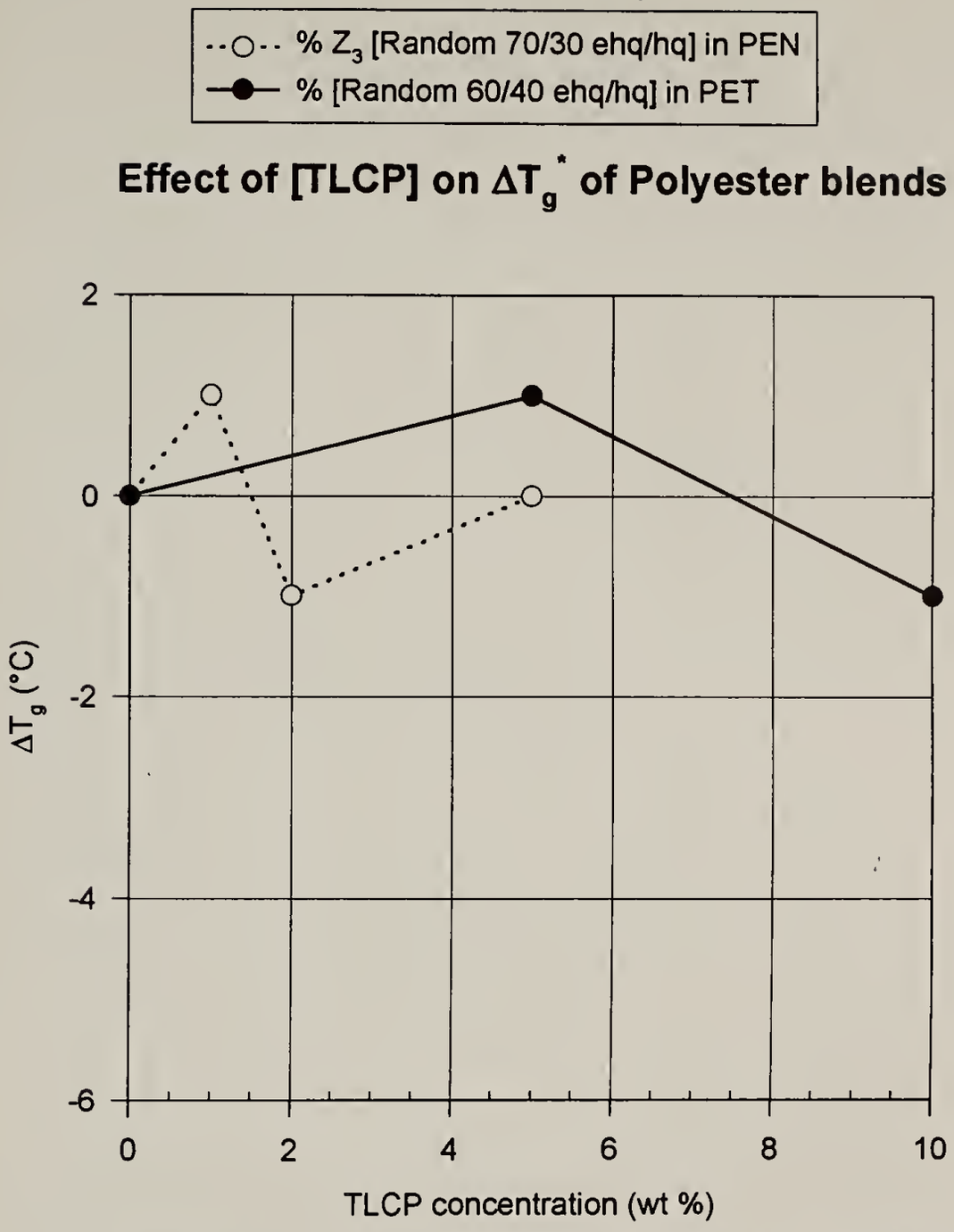

Figure 5.6. The negligible effects on T_g for blends of PEN with Z_3 and blends of PET with a related side-chain flexible random copolyester.

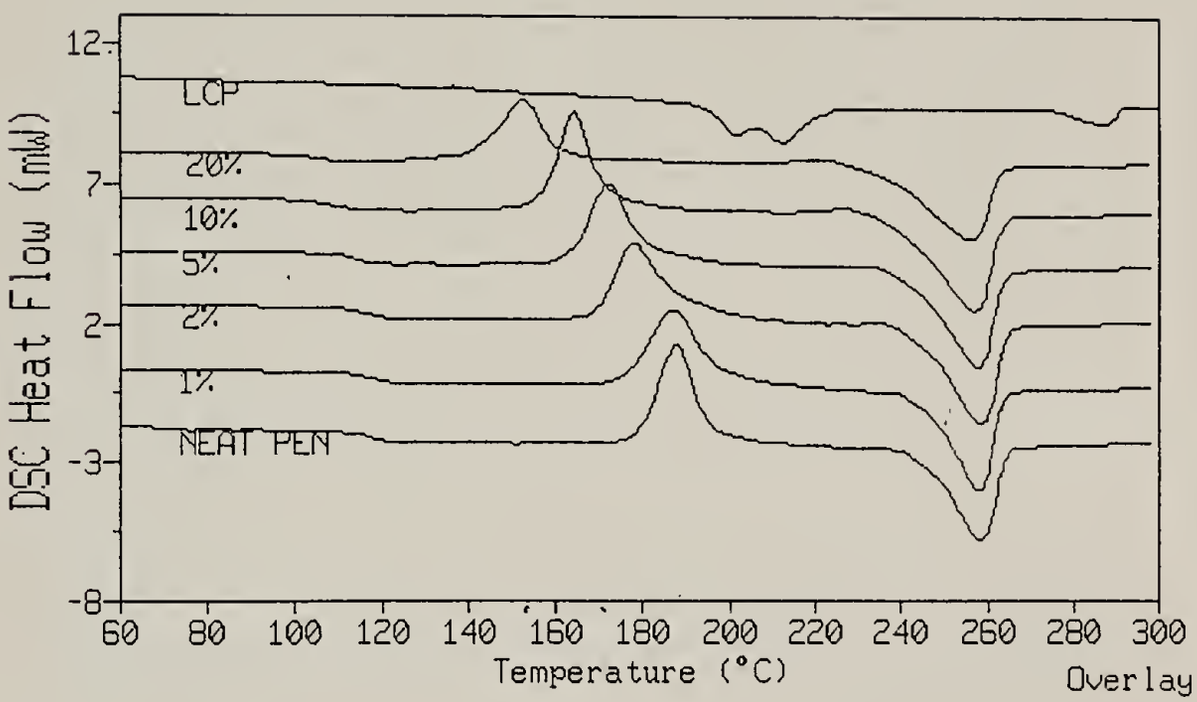

Figure 5.7. DSC heating thermograms for blends of PEN with X_3 segmented copolyester.

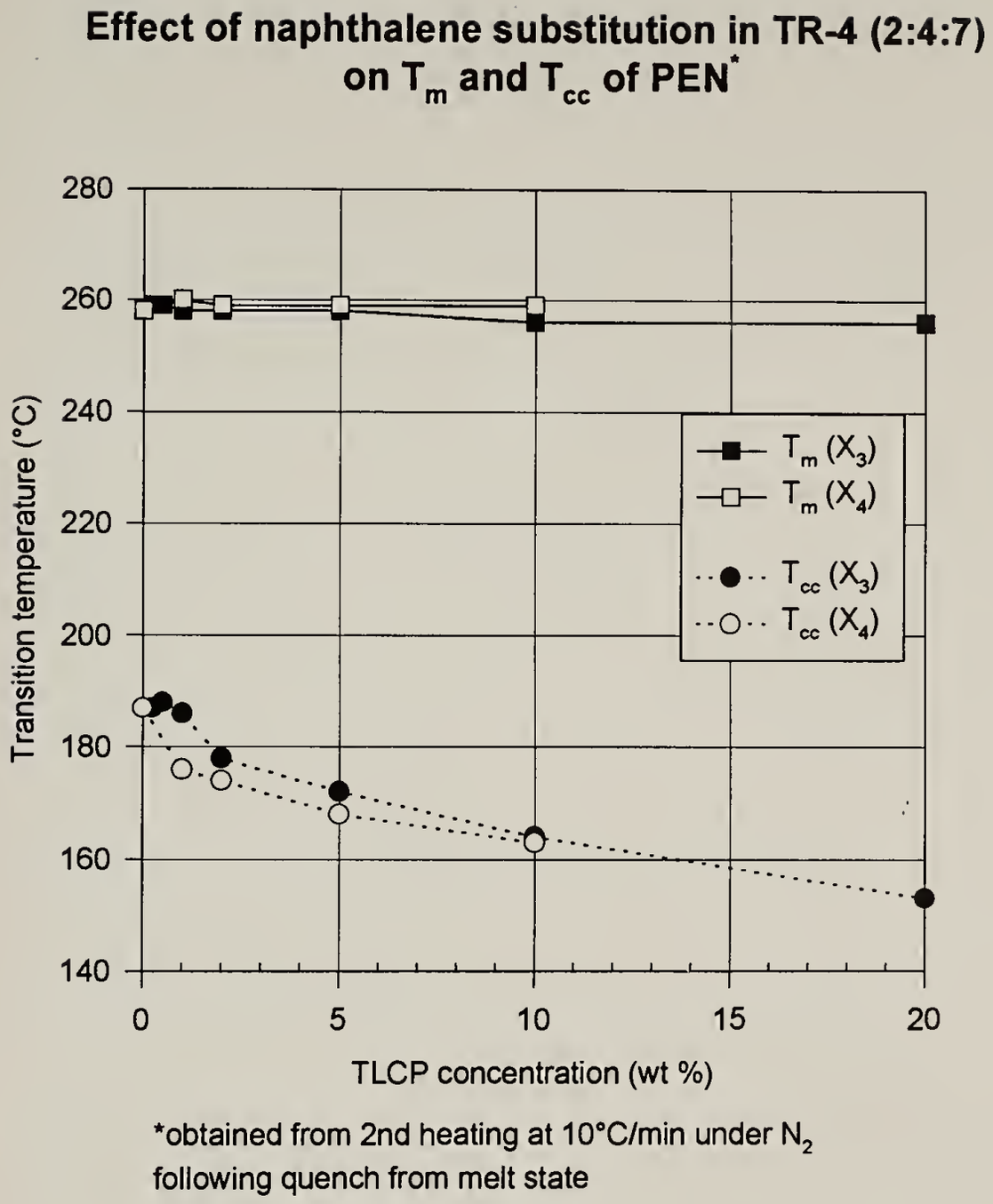

Figure 5.8. Effects of X_3 and X_4 segmented copolyester content on T_{cc} and T_m of PEN.

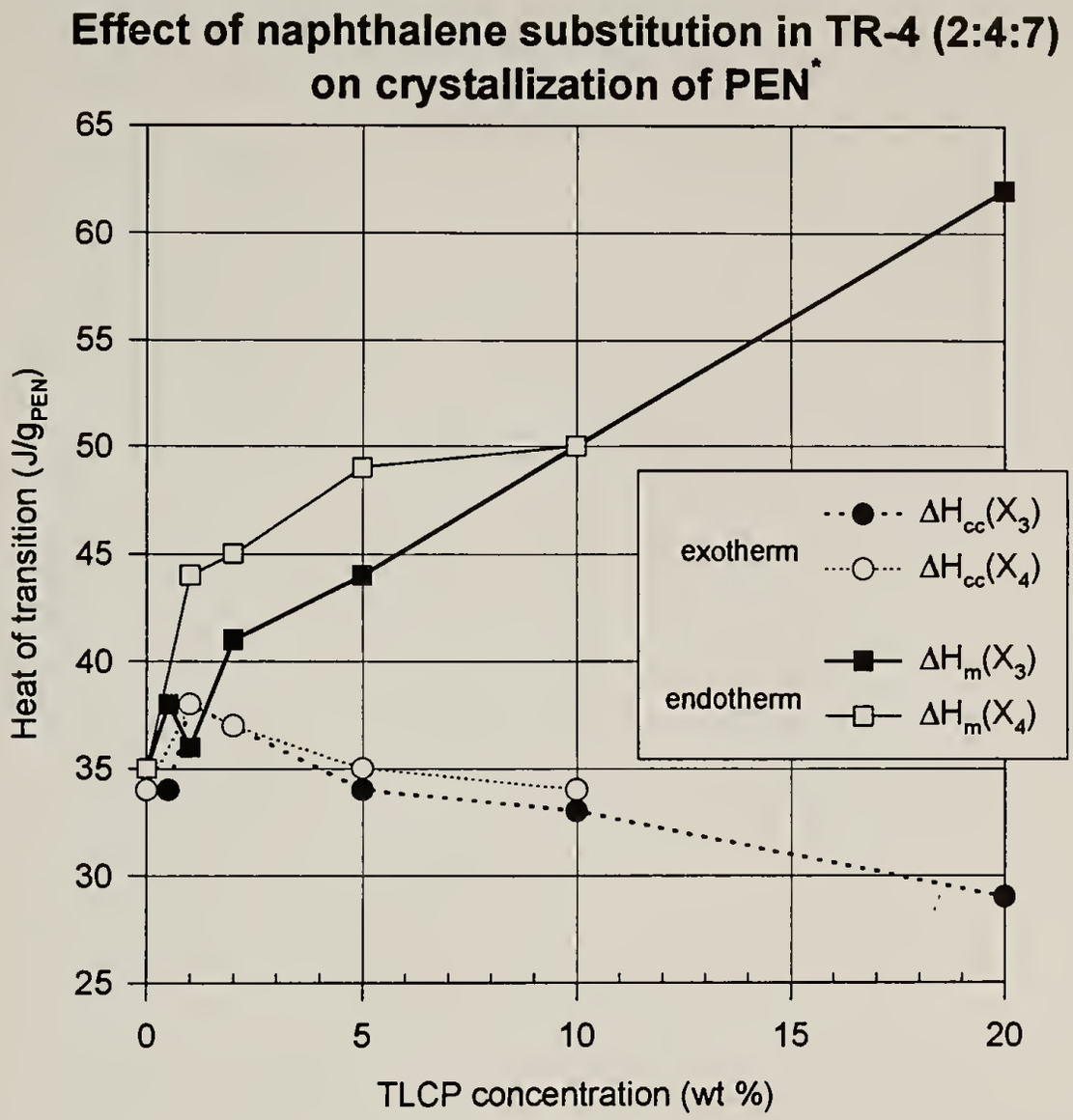

Figure 5.9. Effects of X_3 and X_4 segmented copolyester content on ΔH_{cc} and ΔH_m of PEN.

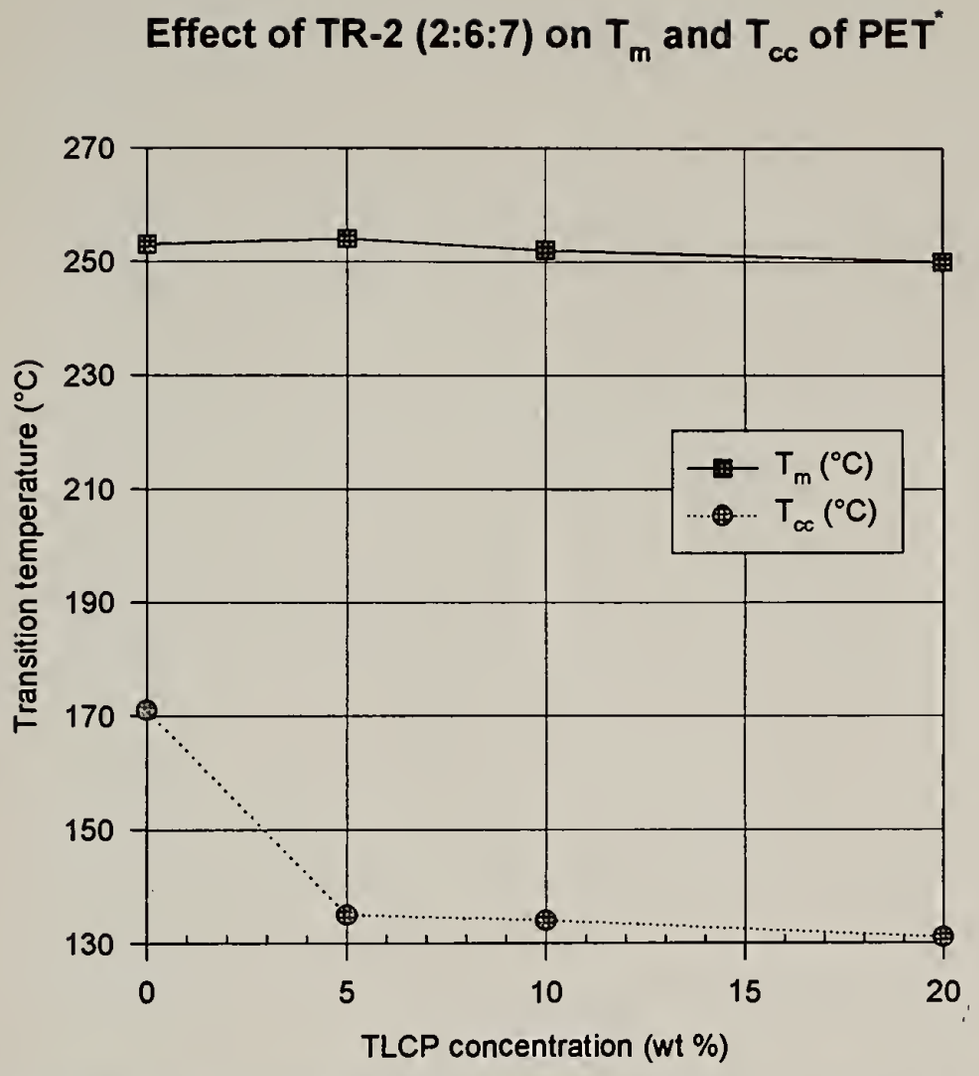

Figure 5.10. Effect of TR-2 (2:4:7) segmented copolyester content on T_{cc} and T_m of PET.

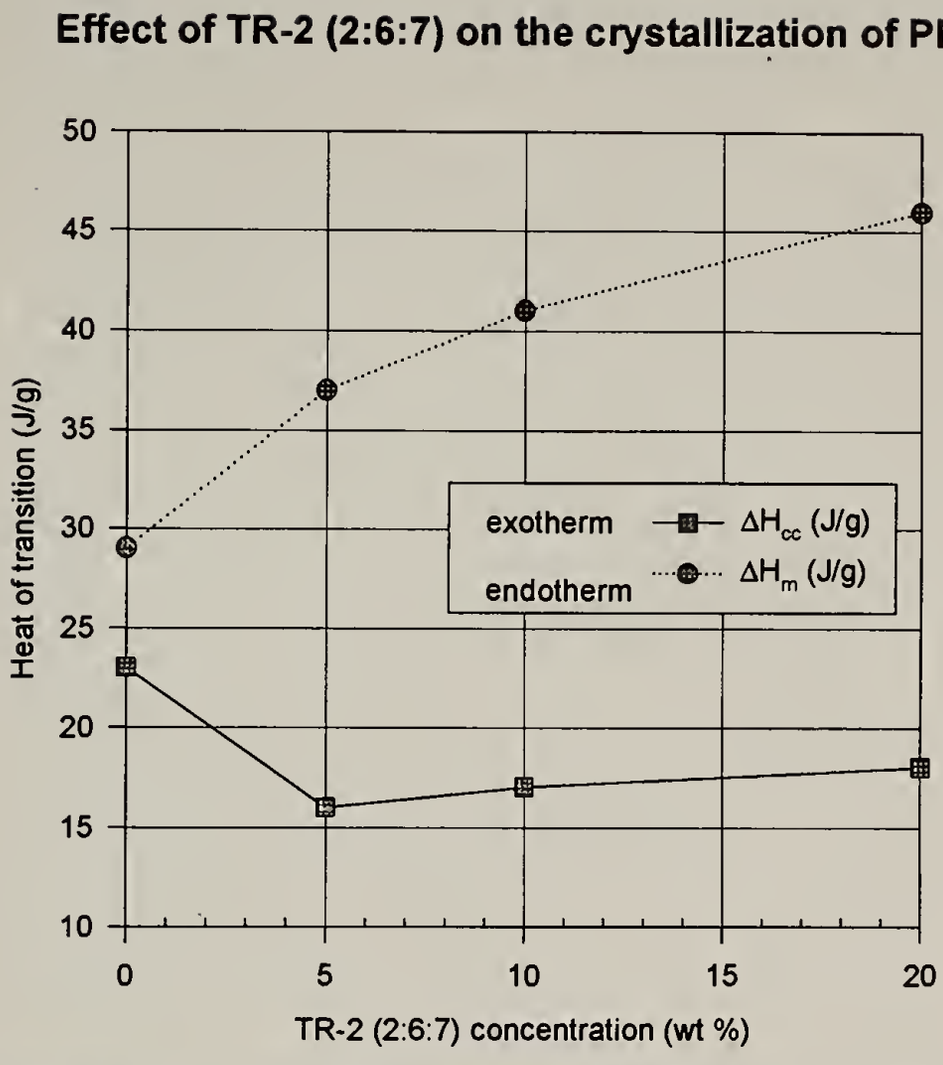

*obtained from 2nd heating at 10°C/min under N_2 following quench from melt state

Figure 5.11. Effect of TR-2 (2:4:7) segmented copolyester content on ΔH_{cc} and ΔH_m of PET.

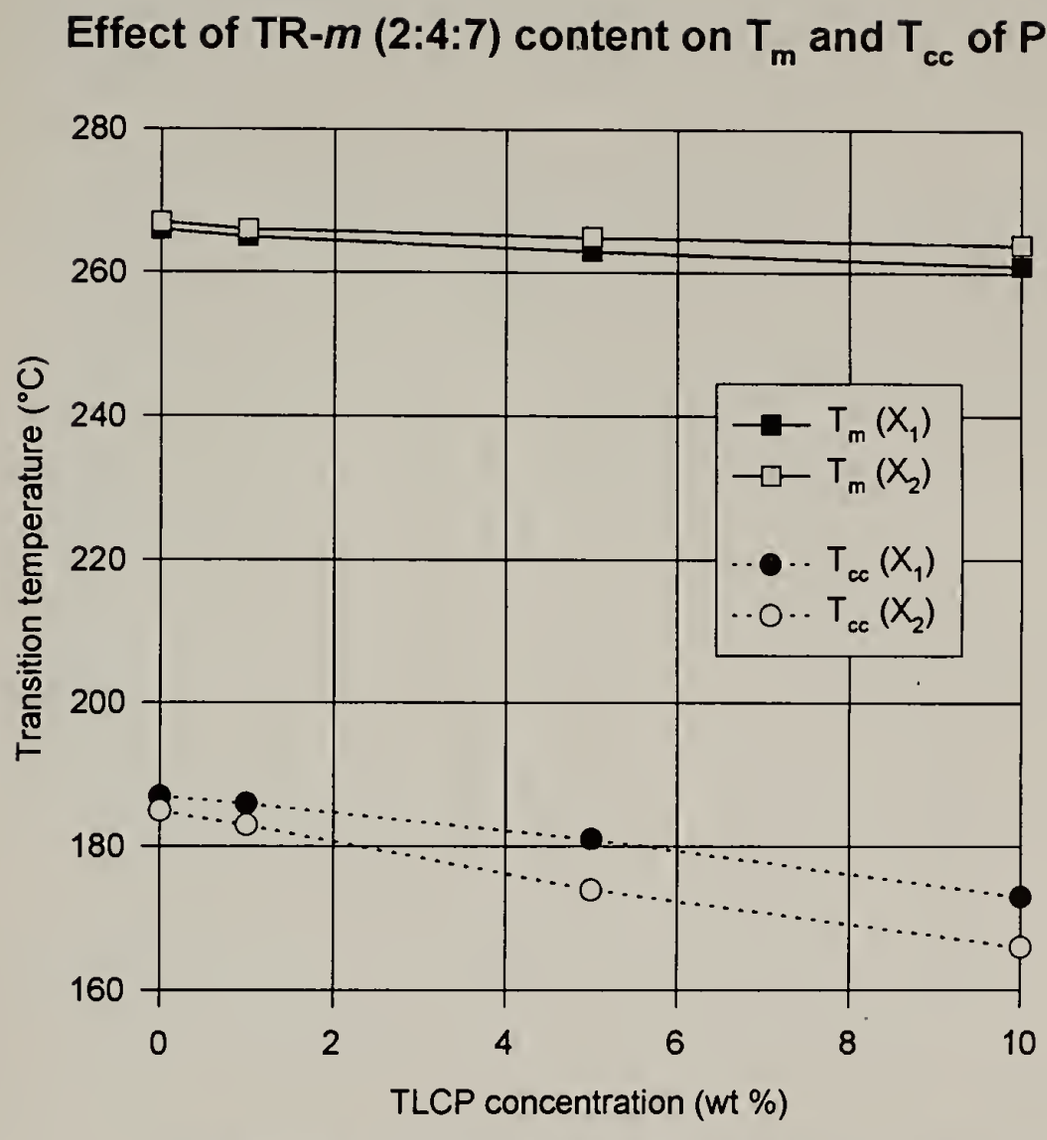

Figure 5.12. Effects of X_1 and X_2 segmented copolyester content on T_{cc} and T_m of PEN.

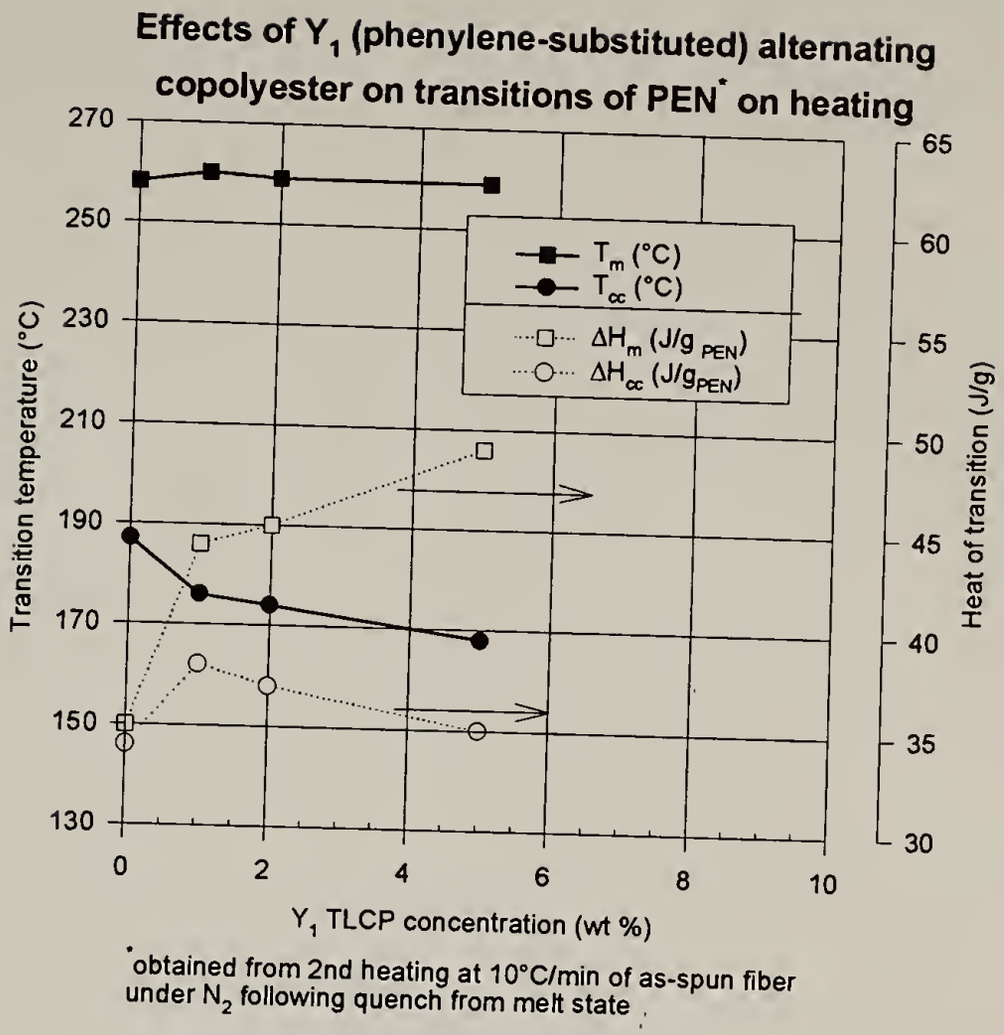

Figure 5.13. Effect of Y_1 alternating copolyester content on the crystalline transitions of PEN on heating.

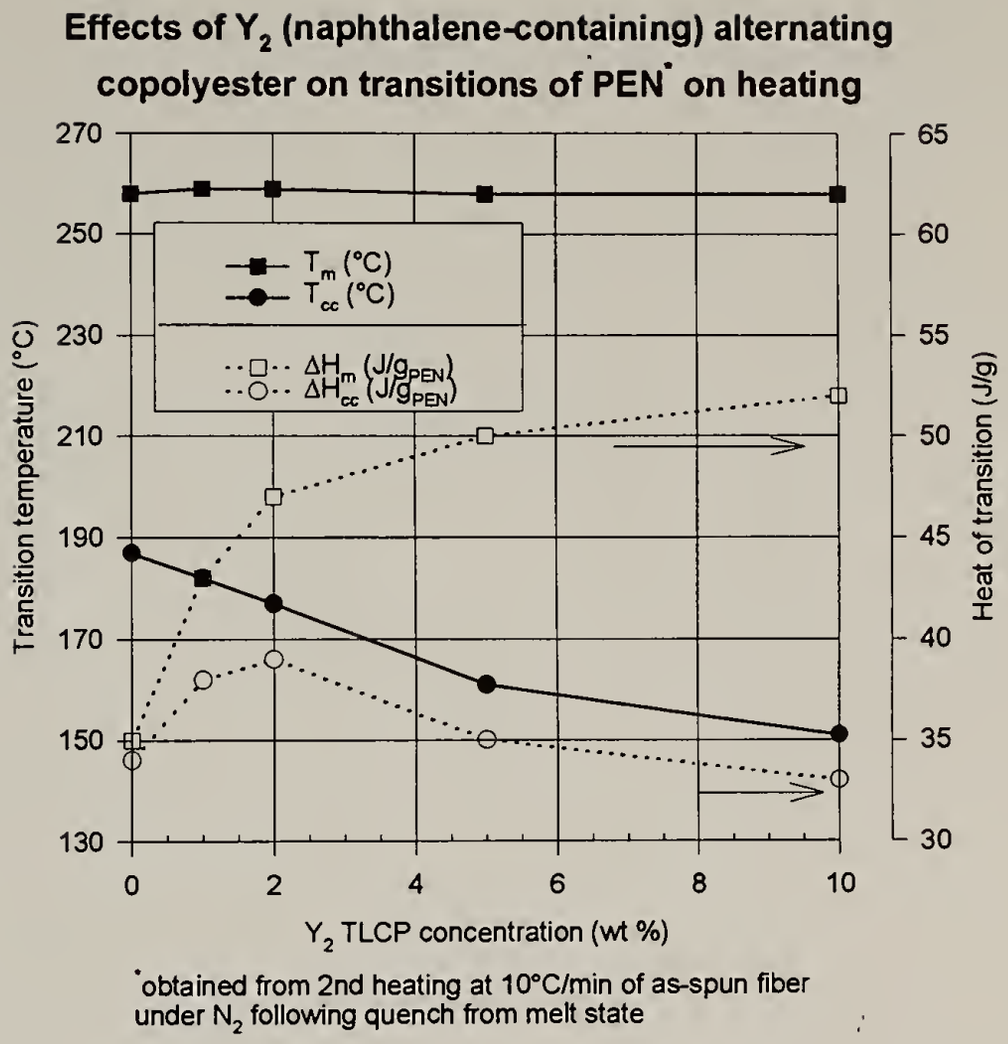

Figure 5.14. Effect of Y_2 alternating copolyester content on the crystalline transitions of PEN on heating.

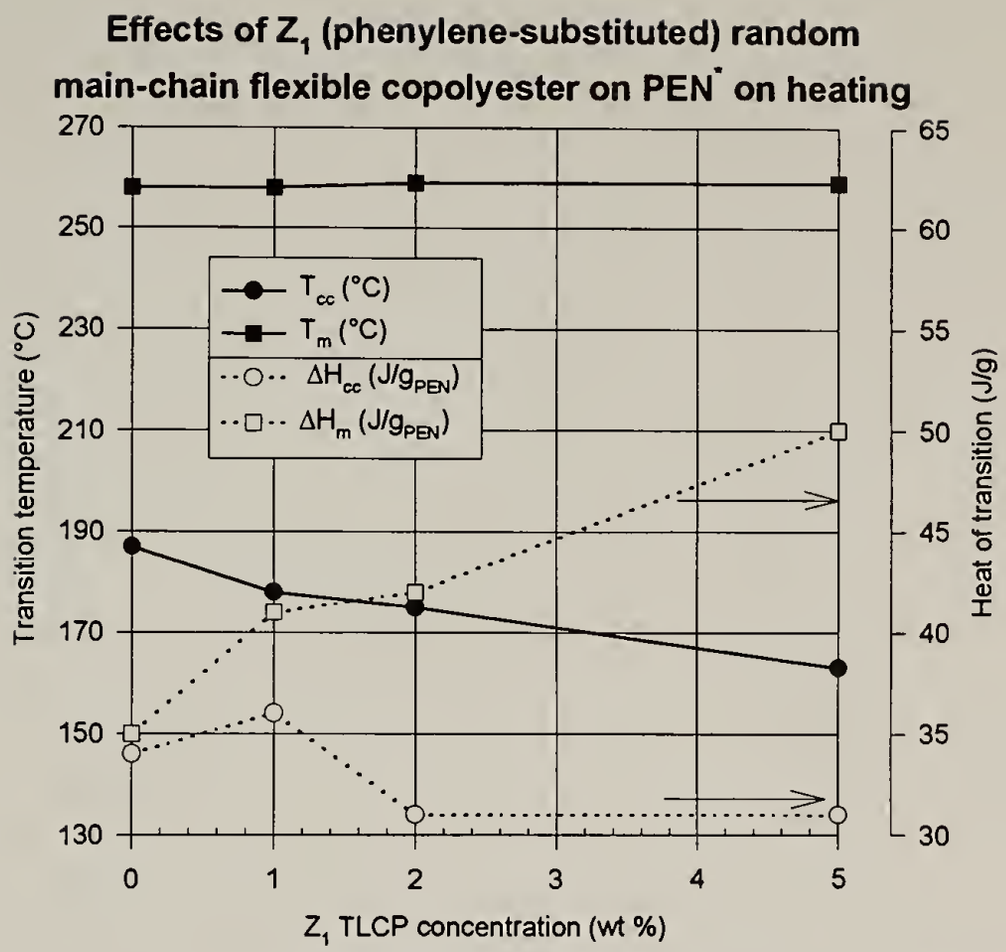

*obtained from 2nd heating at 10°C/min under N_2 following quench from melt state

Figure 5.15. Effect of Z_1 main-chain flexible random copolyester content on the crystalline transitions of PEN on heating.

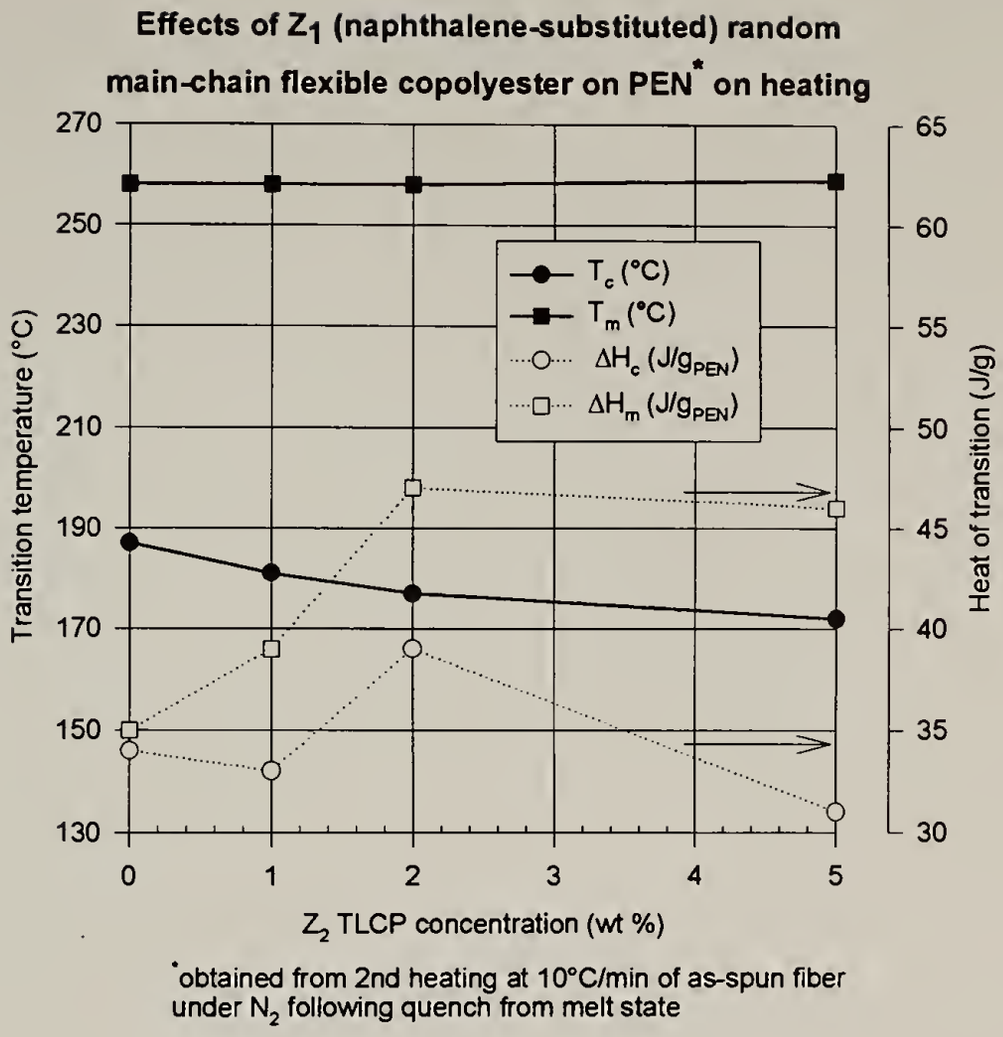

Figure 5.16. Effect of Z_2 main-chain flexible random copolyester content on the crystalline transitions of PEN on heating.

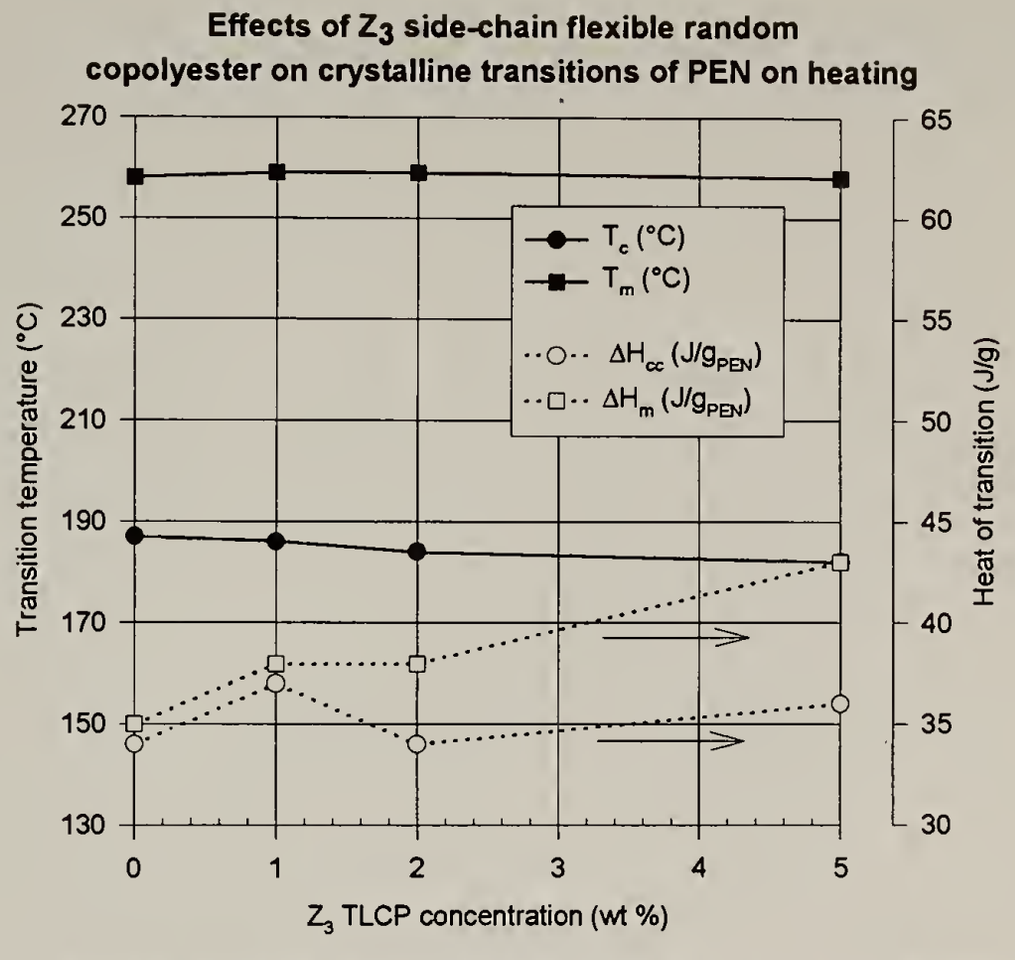

*obtained from 2nd heating at 10°C/min under N_2 following quench from melt state

Figure 5.17. Effect of Z_3 side-chain flexible random copolyester content on the crystalline transitions of PEN on heating.

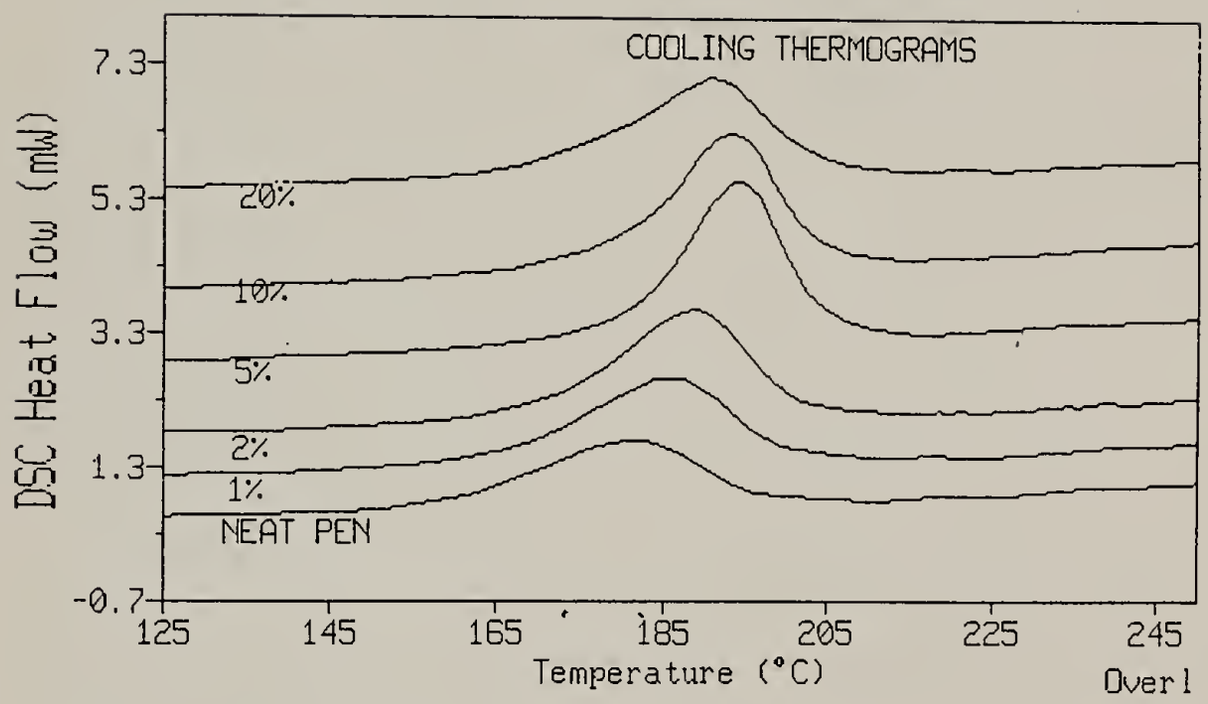

Figure 5.18. DSC cooling thermograms for blends of PEN with X_3 segmented copolyester.

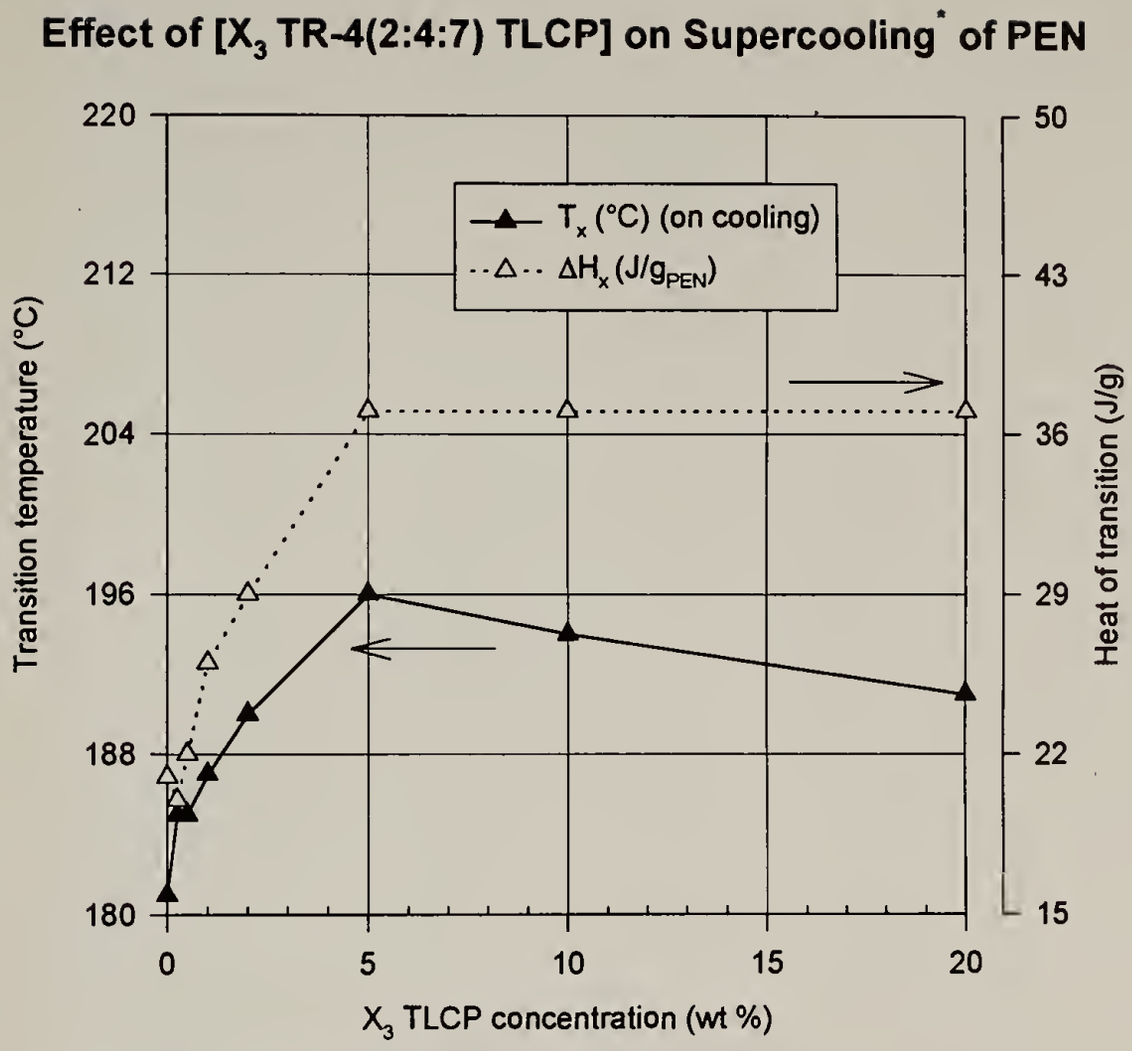

Figure 5.19. Supercooling effects of X_3 segmented copolyester in PEN.

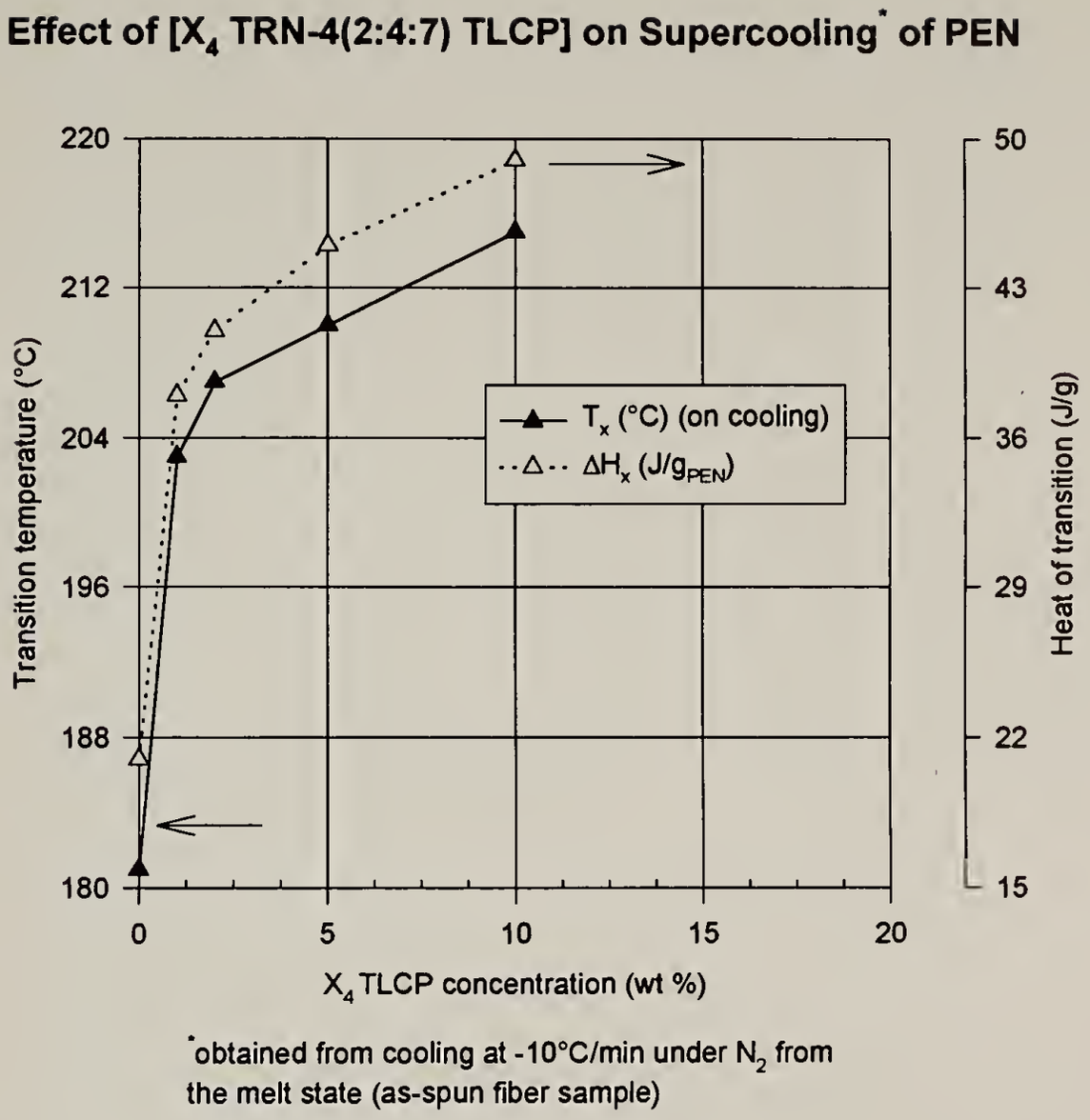

Figure 5.20. Supercooling effects of X_4 segmented copolyester in PEN.

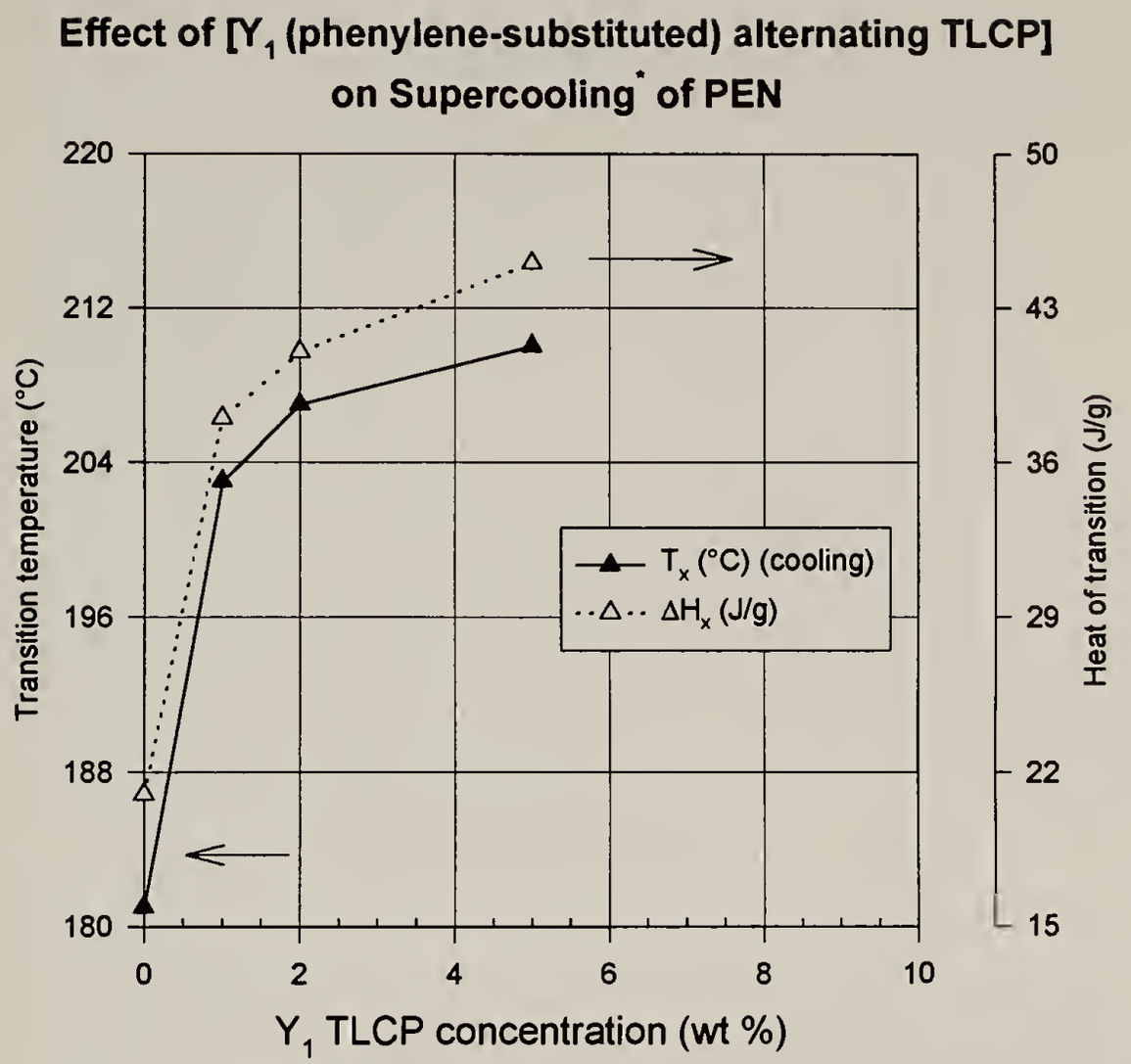

Figure 5.21. Supercooling effects of Y_1 alternating copolyester in PEN.

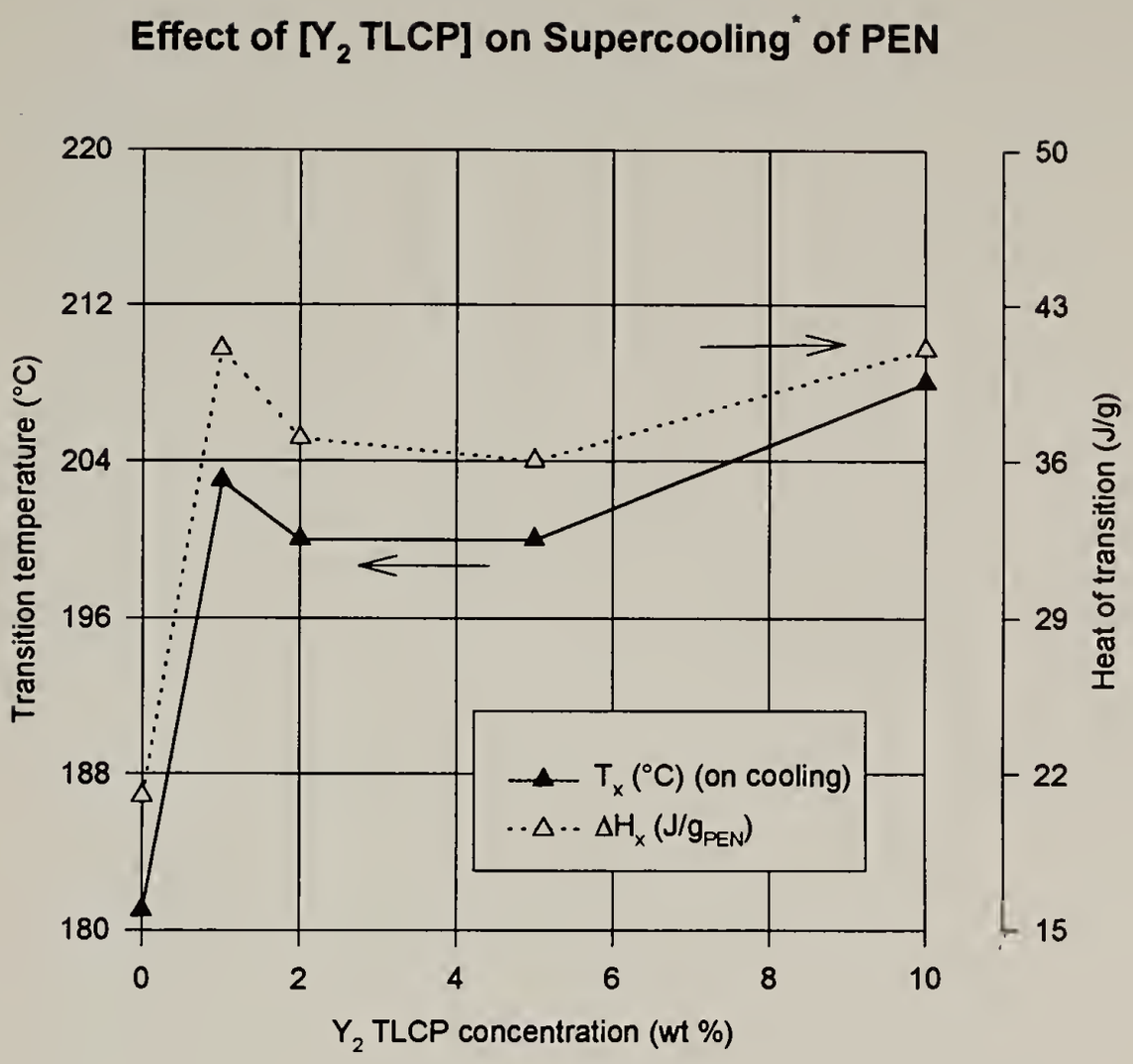

Figure 5.22. Supercooling effects of Y_2 alternating copolyester in PEN.

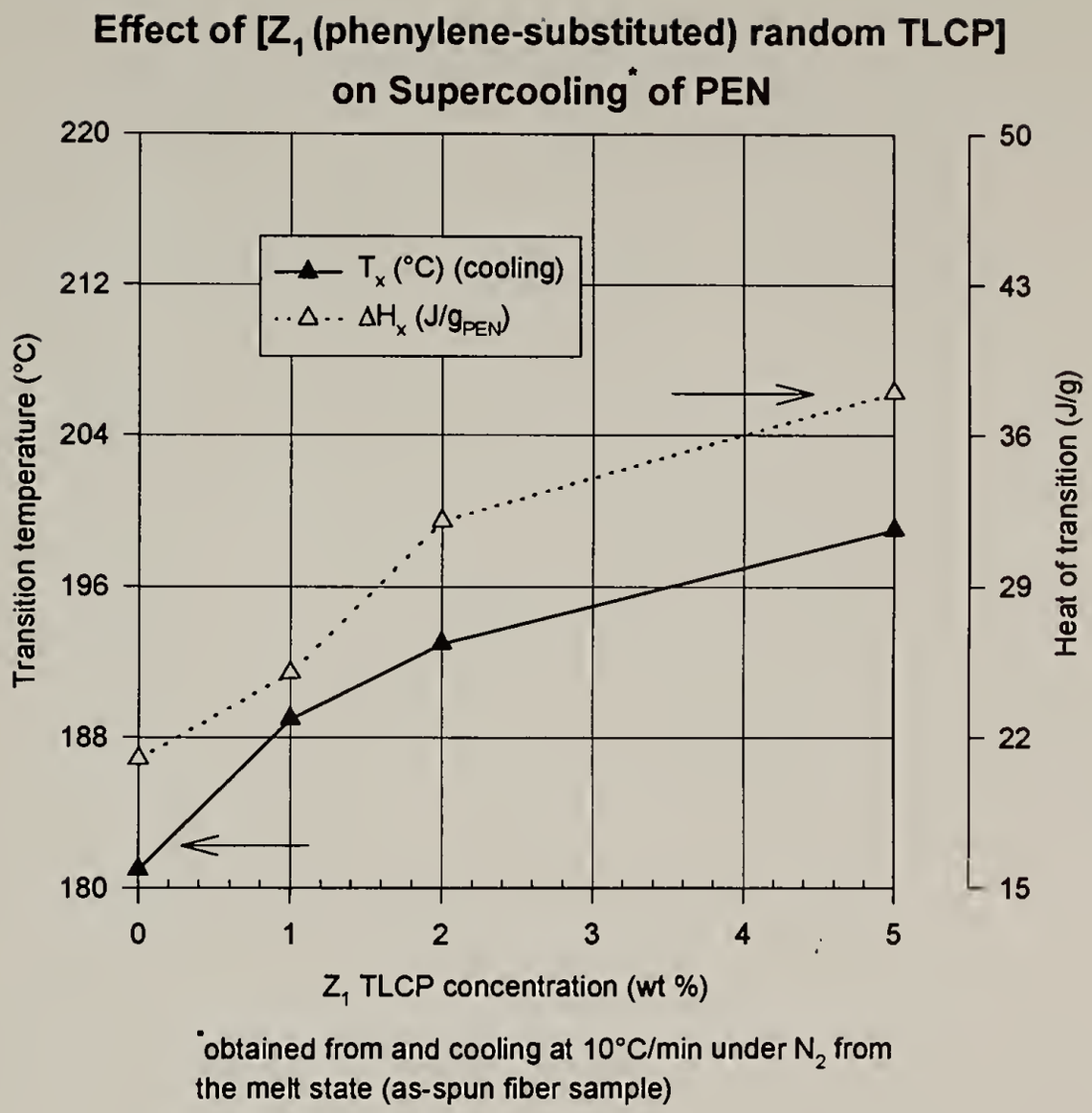

Figure 5.23. Supercooling effects of Z_1 main-chain flexible random copolyester in PEN.

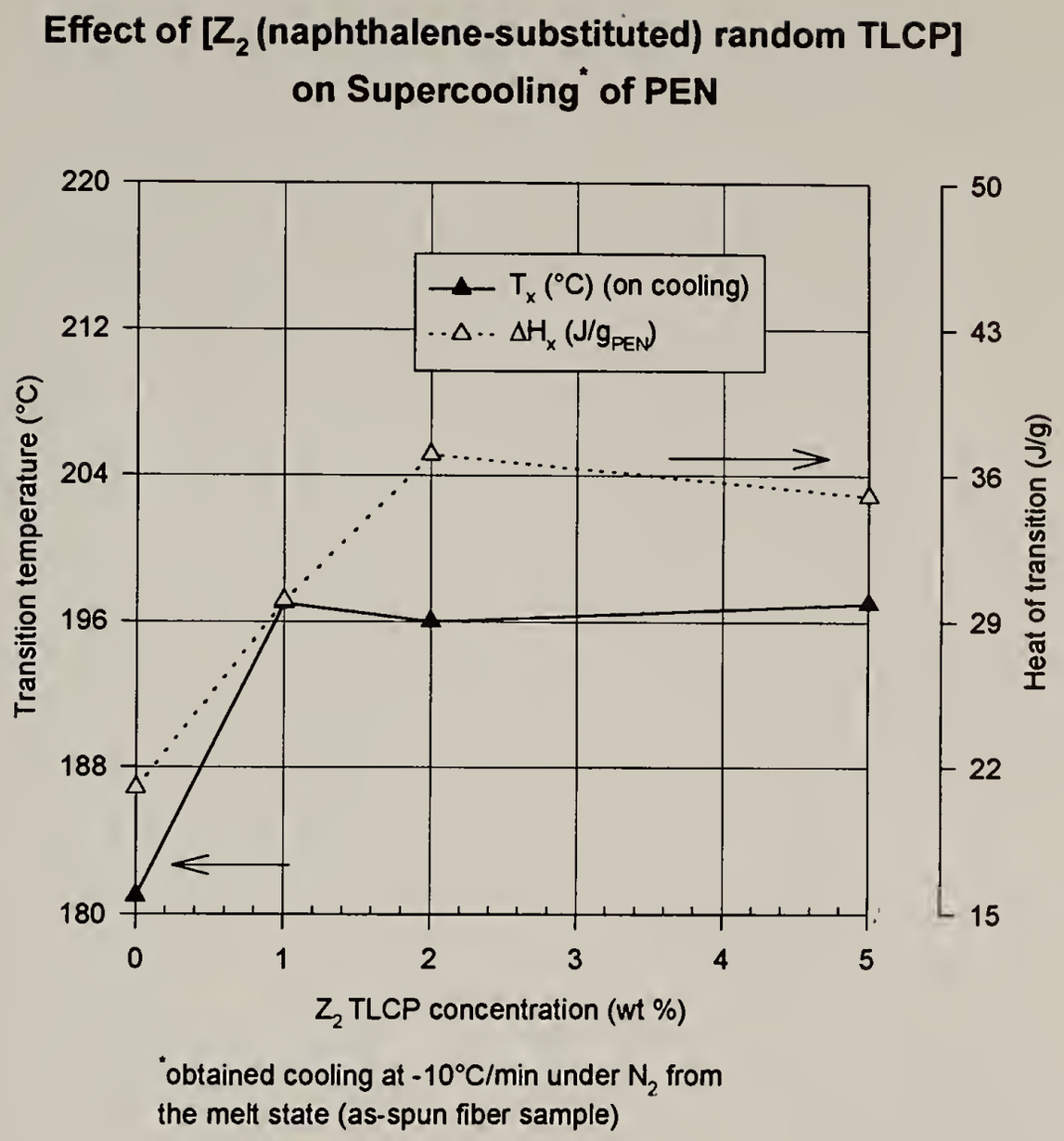

Figure 5.24. Supercooling effects of Z_2 main-chain flexible random copolyester in PEN.

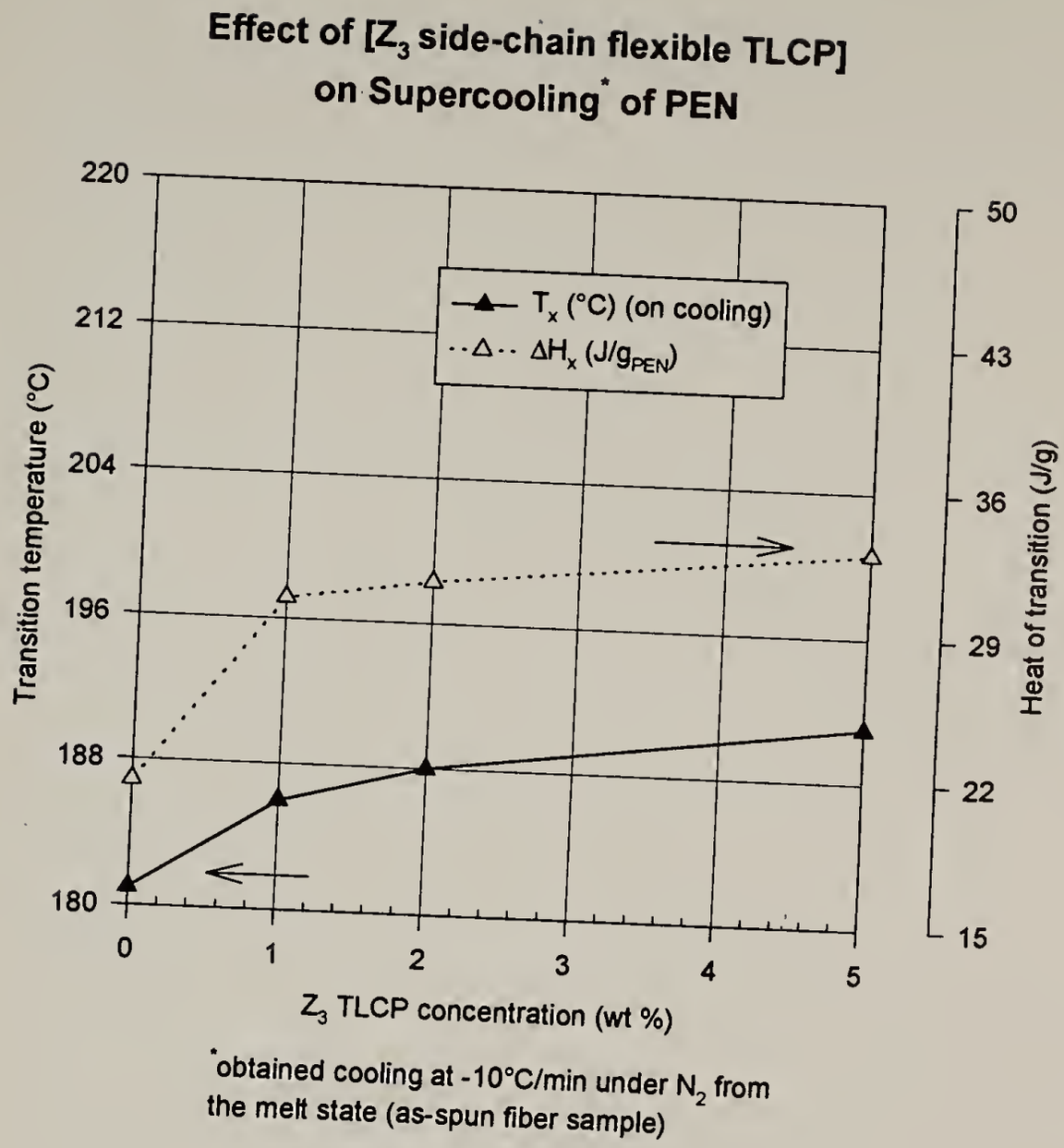

Figure 5.25. Supercooling effects of Z_3 side-chain flexible random copolyester in PEN.

CHAPTER 6

POST-TREATMENT EQUIPMENT AND TECHNIQUES

6.1 Introduction

Thus far, this thesis has discussed pure and TLCP-blended fibers of PEN. Specially designed to have greater flexibility than Vectra®, the TLCPs used in these studies prove amenable to post-treatment when embedded in a PEN matrix. Just as there are a seemingly endless number of compositions for blend compatibilization studies, there are similarly numerous ways to arrive at the same final draw ratio λ through different post-treatment schedules. It is plain, however, that without post-treatment any composition of TLCP-blended PEN fiber displays stiffness values insignificantly different from that of fibers of neat PEN. Re-stated, without post-treatment all fibers have essentially the same mechanical properties regardless of TLCP content.

The quantity λ captures only net elongational draw information. It does not capture the kinetic aspects of drawing which arise when addressing the general question, "Do different approaches to attaining the same λ matter for both practical and theoretically-based reasons?"

The draw ratio of a fiber can take on the same value under different circumstances. For example, consider a laboratory drawing process in which as-spun fiber feeds in at the rate of 1 m/min over a heated region and exits at the rate of 3 m/min. The final draw ratio is 3:1. Consider another process, more likely encountered industrially, by which fiber feeds in at 1000 m/min and exits at 3000 m/min. While the final draw ratio for both processes is exactly three, the industrial process transforms 1000 times more fiber than the laboratory process per minute. The characteristic time for relaxation processes occurring during this transformation must take place

more quickly for the industrial process or become frozen in. In the limit of very high-speed spinning operations approaching 10,000 m/min, the melt-spun product essentially exits as a high-performance fiber with further post-treatment steps being unnecessary or impossible. Clearly, rate effects can become important as a practical issue. Preliminary studies of PEN fiber show that fiber cold-drawn at different rates has different mechanical properties as shown in Figure 6.1. Finding the best combination of post-treatment temperatures and through-put rates is a seemingly large search problem for the researcher. In this case, it is desirable to have a means of determining optimal processing conditions more quickly and systematically.

Separately, a more fundamental issue concerns the physical structure of the fiber as it draws and its implications on processing reproducibility and final properties. For example, § 1.2 discussed fiber necking as a type of yielding phenomenon which may spontaneously develop during the cold-drawing of crystallizable polymers. In fact, the physical nature and position of the neck can play a significant role in determining steady-state processing conditions: the neck appears as a singularity in an otherwise continuous, one-dimensional fiberline. Understanding how a necked fiberline reaches steady-state conditions involves re-casting the physical parameters of such a system into conservation of mass arguments as depicted in Figure 6.2. The system formally reaches steady-state conditions within a control volume when the mass within the control volume becomes constant. Let the parameter α denote the fraction of the fiberline length L which is necked. The neck is modeled as the localized zone in the fiberline over which drawing takes place. For example, if $\alpha = 0.5$, this means that the neck occurs in the middle of the line. The following relationships show that that the mass flow rate, (dm/dt), within this volume varies essentially as a function of the time-varying linear density of fiber, $\rho_2(t)$ after it draws down:

$$\frac{dm}{dt} = v_1\rho_1 - v_2\rho_2(t) \tag{8}$$

$$\frac{m(t)}{m(t=0)} = \alpha\left(\frac{v_1}{v_2}\right) + (1-\alpha) + \left[\alpha\left(1-\frac{v_1}{v_2}\right)\right]\exp(-t/\tau) \tag{9}$$

where $\tau = \alpha L/v_2$. Figure 6.3 is a plot showing the approach to steady-state conditions as a function of the imposed draw ratio.

The results of this trivial model indicate that the general approach to steady-state within the fiberline's "black box" is not entirely obvious, even for a highly-simplified drawn system. Coupling this with the large search problem for more practical matters leads one to ask whether instrumentation exists to address either issue. There is currently none available to yield all of the types of information desired. The rest of this chapter, however, discusses the investigation of several of the techniques and prototype development of one of the techniques based on the one-dimensional transverse wave equation.

6.2 Measuring Monofilament Diameter

The expression for draw ratio involves calculating the ratio of the squares of fiber diameter. As a result, monitoring changes in fiber diameter effectively allows monitoring of the draw ratio. The monofilaments from which bundled fibers are made are typically 10-100 μm in diameter. There are a number of techniques to handle the task of determining diameters in real-time and relating the quantities to draw ratio. Most of the techniques are, however, expensive to implement.

6.2.1 Automated Microscopy

Static fiber diameter data is routinely obtained through optical microscopy. Fiber diameter measurements for tensile tests are done manually at high magnification. As an extension of this method, the most straightforward way to view the fiberline at a fixed point while it draws-down is using a microscope attached to a CCD camera that feeds into a frame buffer. A computer program can study the contents of the frame buffer and directly determine the diameter and uniformity of the fiberline easily in real-time. While the idea is straightforward, this actual approach is both costly and detailed, principally due to the programming complexity required to tie together data from a dedicated microscope and camera. Also, the physical environment close to the actual drawing zone is hostile (up to 250°C) -- leading to other instrument complications. Of course, one could position two microscopes, the first well before the heating unit and the second after. This approach, however, results in lost information about the draw and nearly doubles the cost of the system.

A final note about this technique is that the vibration of a moving sample can provide error in diameter measurement, a difficulty presumably surmountable by combining optical microscopy with strobe lighting.

6.2.2 Laser Diameter Gauges

Another option for measuring the diameter of a fiber is a laser diameter gauge. Here, in a common design, a polygonal mirror and lenses are used to guide a collimated laser beam to uniformly scan a maximum length A over a time τ. If the width of the fiber blocks the beam for a time δ, then the diameter of the fiber is $A\delta/\tau$. For example, if a fiber of unknown diameter causes the sensor to detect that $\delta = \frac{1}{2}\tau$ then the diameter of the fiber is ½A. Figure 6.4 shows a schematic

of such a design made by LaserMike Corporation (this device requires additional hardware to translate and display the diameter data through a serial port). For our applications this measurement technique requires a pair of detectors, in order to enable diameter measurement both before and after the heater. While these units are suitable for a wide variety of *well-defined* applications (such as error detection outside given diameter limits), an inherent limitation concerns the width of their calibratable ranges. None of the laser scanning gauges can detect fiber diameters within the entire range of post-treatment (from 20 to 120 μm). While these gauges were tested during demonstration sessions only, it is also likely that vibration of the fiberline will introduce significant errors in diameter measurement.

6.2.3 Diffraction Method

If a laser beam is directed upon a fiber, a diffraction pattern will result on a screen placed at some distance behind the fiber. By measuring the spacings between nodal points in conjunction with the spacing between the fiber and the screen, it is possible to accurately estimate the fiber's diameter [Koedam, 1966] [Perry et al., 1974]. In experiments on a 66 μm PET fiber, this method was over 95% accurate using a polarized He-Ne laser. Over the general range of diameters anticipated during post-treatment, diffraction experiments showed that the measured error diminishes with increasing diameters from 7% to 3%.

One way to measure the diffraction pattern is to view it using a CCD camera and load the image into a frame buffer, which holds a digital representation of the diffraction pattern. This pattern can be studied using software that can determine the diameter of the fiber.

A less costly way to determine the radius is to place a linear CCD array directly under the diffraction pattern. The output of the CCD can pass serially (via shifting) to an A/D converter,

resulting in an inexpensive and robust measurement system. An array of photodiodes can substitute for the CCD if the intensity of the beam is sufficiently high. Tests of multi-channel arrays made by UDT Sensors which have a spectral responsivity of 0.38 amperes/Watt (A/W) at 632.8 nm revealed that diffraction from a 3 mW He-Ne laser at 85 mm was sufficient to trigger a low response. While the cost of either system is low, both require a good degree of electrical engineering to build. Such instruments would, however, make very useful additions to a fiber laboratory.

6.2.4 Wave Method

The "wave method" is a technique that allows the determination of the draw ratio by measuring the linear density of the monofilament [Chipalkatti et al., 1987]. In short, a fiber placed under tensile force F is struck at one end to initiate a mechanical transverse wavefront which starts to propagate down the length of the fiber. Two inexpensive hybrid interrupters, separated by a fixed distance d could detect the leading edge of the wavefront. By measuring the time for the wave to cross d and by knowing the composition (bulk density) of the fiber, one can determine D, the fiber's diameter. Figure 6.5 schematically illustrates the practical application of time-of-flight: (1) The striker first hits the fiber and creates a wave; (2) the wave propagates in both directions; (3) the wave passes the starting detector; and (4), the wave passes the stop detector. The difference in time between the triggering of the stop and start detectors divided by the detector separation distance provides the wave speed. A detailed discussion of how the speed of the wave (or the wave's time-of-flight) is related to fiber diameter is found in the Appendix.

6.3 The Prototype Time-of-Flight Instrument

This project involved the design and construction of an inexpensive instrument to assist in the characterization of fiber [Lo and Farris, 1995]. In particular, automation was an important goal, where one can (a) load a spool of fiber, (b) set a plate temperature and draw ratio range, and then (c) get a data set of tension and (d) time-of-flight (in fiber both before and after the point where the drawing is done), all as a function of time. The form of the delivered output should load readily into a spreadsheet program and allow conventional analysis techniques. Finally, it was important to give the instrument an intuitive interface where it is easy to understand and "user friendly."

The system was built in four layers. First is the mechanical layer, which consists of pieces of supporting metal, pulleys, micrometers (for fiber alignment), and the actual fiber samples under consideration. Second is the electro-mechanical/electric layer, which consists of motors, strikers, and the heater. Third are the sensors and non-programmable electronics, which condition the signals and report on the behavior of various mechanical parts. Finally is the control system, which issues commands to motors and heaters, provides a window- and mouse-oriented interface for the user, and tabulates the data which is collected. Figure 6.6 provides a schematic illustration of the instrument and Figure 6.7 shows a photograph of the completed instrument.

6.3.1 Mechanical Construction

It is imperative that the mechanical construction of the instrument be of very high quality. Accurate detection of a wave requires precise positioning (to 2 μm) of the detectors above the string. The system must be isolated so that leaning on a table or walking on the floor does not

produce erratic results. Therefore, investigations of the mechanical design and construction required great care.

6.3.1.1 Base (Rheovibron)

The most desirable base on which to build an instrument of this type is an isolated optical bench. The cost of such a bench is, however, prohibitively high, and its generality is unnecessary. A reasonable "one-dimensional" solution is to use a Rheovibron base, a massive single piece of steel with a carefully cut channel running down its middle for mounting of accessories. Accessories become mountable by clamping them (using set screws) to machined aluminum plates which exactly matches the channel. Most of the mechanical systems and all of the sensors attached to the base in this fashion. Two abutted Rheovibrons were placed onto thick rubber padding placed on a benchtop to form the foundation of the instrument. A rigid plate fitted to the Rheovibron channel effectively joined them together, making the entire instrument about 2 m long.

6.3.1.2 Pulleys (Wheels)

Monofilament fiber feeds through the machine, and small pulley wheels with precision ball-bearings serve to guide the fiberline. While the open-race precision bearings used (high-precision ABEC-11 rating) were of the lowest frictional coefficient possible ($\mu = 0.10$) for metal bearings, their apparent eccentricity was sufficient to cause significant fiber motion to falsely trigger the wave detectors. Therefore, in stages where the fiber was being positioned, this was corrected by using small riser rods made of Teflon®.

6.3.1.3 Fiber Guides

Teflon® risers as fiber guides were used to stabilize the height of the fiber before the fixed wave-detection sensors. The critical component of each guide is a micrometer, where one side mounts to the Rheovibron, and the other holds a machined piece of aluminum with a Teflon® riser insert. The fiber undergoes a very small angular displacement over the Teflon® insert, such that the friction that it produces is negligible. Each detector is associated with one fiber guide.

6.3.1.4 Point Crossing (Wave) Detector Holder

Carriers machined for laser-diode and photodetector interruptor pairs are "U-shaped" channels. Figure 6.8 shows a photograph of two detector pairs. Each carrier holds its two components at a fixed separation (2 inches) and mounts to the Rheovibron. The laser diode has firm contact with its carrier which also acts as a heat-sink and draws away heat generated during diode operation.

6.3.2 Electro-Mechanical/Electric

Electro-mechanical devices manipulate the fiber. The motors advance the fiber (providing lateral movement), while the striker generates transverse waves. The heater is responsible for bringing the fiber to the correct temperature range for post-processing.

6.3.2.1 Heater

Figure 6.9 shows the heater unit. The fiber loads into the heater from the underside. Two fiberglass-insulated heating elements packaged in flexible silicone rubber were adhered to the inner sides of the heater, each providing 1.6 W/cm^2 to heat the air between these inner faces. A piece of transparent Pyrex glass rests on top of the heater and allows easy viewing of the passing fiberline below. The heater connects to a control unit which will be discussed separately in §6.4.

6.3.2.2 Motors

Brushless DC motors were selected to drive the fiber line. It took some amount of searching to find motors geared (30:1) to run as low as the 60 rpm range—most are geared to run far faster. The motor interfaced to a proprietary controller discussed in §6.4. Motors and controllers were from Bodine Corporation.

6.3.2.3 Strikers

Finding a proper striker for the fiber took significant effort. Initially, striker units were 12 VDC solenoid valves rated for 30 psi which released a controlled amount of pressurized air flowing from a gas cylinder. Though the response time of the valve was only 20 to 30 milliseconds, the overall approach met with very limited success for two reasons. First, the pressures required to displace very taut fibers became dangerously high. Second, the general dependence of required air pressure on fiber tension (to produce a succession of uniform displacements) became too complicated to incorporate as part of an operating method.

Next, a loud speaker was used with a striker glued to it. A mid-sized speaker can reproduce sounds up to 10 kHz, so it seemed reasonable to expect an impact on the order 100 microseconds. Unfortunately, the speaker was difficult to drive and the choice of a proper electrical excitation was unclear. Finally a striker arm was glued to a simple relay. When excited, the relay's electro-magnet would move the striker arm which would give a sharp blow to displace the fiber. Figure 6.10 shows the striker and its accompanying micropositioner.

Time-of-flight measurements using this approach were extremely uniform (less than 2% standard deviation) using the relay as a striker.

6.3.3 Sensors

The sensor system must be able to report on the tension of the fiber line as well as the wave time-of-flight between detector pairs.

6.3.3.1 Crossing Detector

Commercial solid-state opto-electronic switches made by Honeywell based on infrared light-emitting diodes as the source failed to trigger a signal when laboratory fibers were used for interruption.

Thus, a custom hybrid switch, or interruptor, was designed. The most important difference is the use of a laser diode (LD) instead of a light-emitting diode (LED) as the source. In short, a 3mW Mitsubishi laser diode (ML4402-01) emits 780 nm light from a point source which can be detected by a high-sensitivity Hewlett Packard (HP) photo-diode (HFBR-2523) coupled with a 1000 μm core low-loss optical fiber also made by HP (Versatile series). When the taut

polymer fiber crosses the gap between the laser diode and the detector, the amount of transmitted light drops and the detector's digital output creates a pulse. A set-reset flip-flop can detect and store (note) this momentary change in output. The flip-flop can be made from a very inexpensive transistor-transistor logic (TTL) chip with two NotAND (NAND) gates on it. (Once the flip-flop is "set," the wave has been detected. The computer resets it later when one wishes to make another measurement. A flip-flop can be considered analogously as a mousetrap: when the trap is armed, it is called "reset." When triggered, it is called "set." Repeatedly triggering a mousetrap has no effect after the first triggering.) The electronics are discussed later in §6.3.5. This detector ultimately worked very well except that it is affected by the amount of ambient light in the room. As a result, experiments were performed in an unlit room usually used as a photographic darkroom.

Figure 6.11 shows an alternate, perhaps more elegant, detector design. In short, if there is no fiber, light cannot reach the detector—it is blocked by a beamstop. If, however, a fiber crosses the beam, diffraction results. Two lenses can focus and steer this diffracted light onto the detector. While the test system corresponding to this design also worked well, this system was ultimately not chosen because it would have required machining a new detector carrier.

6.3.3.2 Tension

Tension was measured using a 5 pound full-scale ("Minibeam") load cell made by Interface, Inc. Its non-linearity is rated at ±3% and hysteretic effect rated at 2% of the output. A custom mount holds it in place and a pulley wheel attaches as a fitting for the load. The fiber winds once around this wheel, so the resulting measurement is twice the tension. Figure 6.12 shows a close-up photograph of this configuration. A standard signal-conditioning module from

Analog Devices [AD 2B30/2B31 J] was used to generate an analog signal between zero and five volts, providing a gain of about 2000 from the load cell signal.

6.3.4 Control

This system required a control mechanism to make it work in harmony. The main purpose of a control system is to run the experiment, save data, and provide a meaningful interface to a human user. The control was built in several levels.

Shown in Figure 6.13, a piece of hardware known as a microcontroller (μC) provides the lowest level of control. The μC can set/read digital wires and measure time intervals to the microsecond level. As such, the μC is both an input and output device. As an output device, it can for example, set wires to (a) fire striker #1 and (b) later reset the signal conditioners which are attached to the wave detectors, etc. The μC was also loaded with a program that could read signals. By "polling" a signal and using its internal clock, the μC serves as an input device which can determine how long a signal was asserted. This is precisely how the time-of-flight of each particular wave is determined.

Communicating with the μC is clearly troublesome. The μC is a low-level device which worries about bit and byte details. Compared with the development tools and debugging devices available on PC software, the μC has a volatile and highly limited (128 Kb RAM) development environment. Also, the μC has only 64Kb to store data. Therefore, the μC communicates to a second computer, which in this case is a PC. The μC is connected to the PC using a serial cable. The μC operates using custom-written BASIC functions at a "high level." These functions made it easier to measure times-of-flight and to manage other tasks like controlling the strikers.

The last level of control allows the user to construct an experiment. This level was written in BASIC as well, using a novel object-oriented Microsoft program called Visual BASIC. Using this language, a mouse- and window-based interface was also designed. The interface works with the lower levels of BASIC which in turn speak to the μC which in turn work with the circuit boards. For example, Figure 6.14 shows the PC in conjunction with the feed motor loaded with a standard fiber spool. The window on the PC has several "soft" slidebars which allow the user to set targeted motor speeds. Because the VisualBASIC interface is intuitive to the user, program execution is necessarily event-driven. Figure 6.15 gives an example of the actual higher-level code that runs when one opens the initial communication port (interfacing) with the μC module by clicking on a "soft" button.

This system architecture is also capable of controlling the heater, but Omega Scientific makes a convenient stand-alone controller (CN8500) and resistive thermistor device (RTD) intended for heater control.

6.3.4.1 Microcontroller

The μC is a programmable controller made by Blue Earth Research (Micro-485). This module contains an Intel 8051 family microprocessor. The μC also contains a small BASIC interpreter, making it easy to program. The μC also has digital input and output pins. The output pins are used to reset logic and trigger strikers. The input pins are used to look for times associated with the waves. There is also an analog input, which feeds to an internal analog to digital (A/D) converter to turn the load-cell output voltage signal into a force value used in further computations.

The program that runs on the μC is downloaded and started by means of a separate BASIC program that runs on a PC.

6.3.4.2 Personal Computer

The PC used to run this experiment was a Gateway 486 DX2-100 PC. This PC initially served as a terminal emulator to talk to the μC. After the μC program worked, more software was written in Microsoft Visual BASIC to enable proper user control of the instrument. Visual BASIC proved itself highly suitable as software for event-driven programs such as those found in a controller software. The resulting system is very easy to use.

As the Visual BASIC program runs, it writes the data that the μC collects to a file. This file appears in a format easily read with a common spread-sheet program (Excel). The spreadsheet was used to examine data that the instrument generates.

6.3.5 Custom Electronic Circuits

Designing and making custom circuits to support devices used in this instrument took time as well. These circuits were wired onto Vector® boards and then placed inside a card cage. Specially color-coded wires and connectors provided an array variety of voltages: ±15VDC for operational amplifiers, +5VDC for TTL logic, electronic ground, motor ground, and motor power. The system required two types of grounding to separate digital electronic ground from a noisier ground for motors and relays. The color code and connector wiring are given in Figure 6.16. It is wired such that a device requiring power can plug into any of the connectors on a specially- wired power harness (without danger of mis-wiring a device).

6.3.5.1 Laser-Diode Current Sources

Laser diodes are small devices (the "can" is shown in Figure 6.17) which are easily destroyed through over-heating. Because the resulting current passing through the device varies widely as an exponential function of source voltage, there was no option other than to build a constant-current source to induce lasing at 40 mA. The use of a constant current source is necessary for nearly all types of laboratory lasers. The schematic is shown in Figure 6.18. Four of such boards were necessary, one for each diode.

6.3.5.2 Crossing-Detector Signal Conditioner

A (digital) conditioning board consisting of NAND gates can make a set-reset flip-flop. This flip-flop looks at the output of the crossing detector. If it detects any fiber-crossing, this sets the output of the crossing detector until later reset by the μC. Each detector has one of these conditioners. Each pair of detectors has their conditioner's output feeding to a XOR (Exclusive OR) gate. If the two one-bit digital inputs of the XOR are identical, the output value is 0 (low); if its inputs are different, its output value is 1 (high). This signal is high for the exact duration of time that it takes for the wave to traverse the physical distance between the detectors. (To understand this, consider the wave tripping the first detector. This detector will issue detector output transitions which will immediately set the flip-flop in its conditioner. The XOR gate will note that its inputs differ, so it will output a high signal—this signifies that the wave has started to pass. When the wave finally reaches the second detector, the second conditioner will mark the wave's passing, and the XOR will no longer observe a difference in its inputs; hence, it will now report a low signal, indicating that the wave has passed.)

The output of the XOR feeds to the microcontroller. The μC has the ability to count for how many microseconds a particular signal is enabled (i.e., for how long the signal is high), and therefore how long it takes for the wave to travel between the detectors. The speed of this electronic logic is fast compared to the motion of the wave such that extreme accuracy results. This clocking mechanism was tested using a signal generator and universal timer (Tektronix DC5009) which allowed the generation of signals for a very well-defined short period of time (from several hundred to several thousand microseconds). All of the specified times and the recorded times were exactly the same in all cases.

6.3.5.3 Striker Launcher

A board was also designed to fire the striker by means of computer control. Figure 6.19 gives its electronic schematic. In short, the digital signal directs current through the base of a transistor in order to drive it to the heavily saturated region. The transistor then acts like a switch and turns on the relay. The diode that lies across the relay serves to protect the transistor against the back-EMF produced by an inductive load like a solenoid. Running the circuit without the diode will destroy the transistor within minutes.

6.3.6 An Example of Operation

A consequence of the solution of the wave equation is that $F=\rho v^2$ where F is the tension in the fiberline, ρ is the linear density of the fiber within a detection region, and v is the velocity of a wave traveling within the detection region. Plotting v^2 versus F gives, in theory, a line with a slope of ρ^{-1}. A typical calibration plot done on nylon 6 monofilament sample is shown in Figure 6.20,

showing measured points of ν and F. The fit to a line is excellent. The resulting slope was compared to careful estimates made on pre-cut lengths of fiber weighed on a precision balance. These results are accurate to a few percent.

6.4 Summary and Future Design Improvements

This prototype machine indicates that there is great promise in building instruments to process fibers. Were there a task to re-design this machine, a number of things should be done differently. The first would be to implement redundant diameter detection using wave detection (but with the diffraction-based wave sensor) as well as diffraction with a linear CCD to measure diameter. While this approach would have been more expensive—due to the need for collimated lasers—it would be more fruitful to have internal real-time self-consistency checks instead of having to insert test samples of known diameter. Secondly, the use of bearings (wheels) should be avoided altogether. Bending the fiber at slight angles using Teflon® guides works better, as the eccentricities of the wheels produce annoying vibrations.

Finally, it would be interesting to study the fiber in the heater as it is being drawn by placing a microscope in its proximity. From the current body of knowledge on fiber drawing, it is clear that the actual evolution of structural changes which occur during draw remains largely uninvestigated. This information could reveal a wealth of interesting facts about drawing and more importantly, their relevance to final mechanical properties. Instead of using traditional optical microscopy involving uniform light transmission, using a flashing strobe light to capture the fiber drawing transformation at several hundred times per second would provide a more vital record of this important process.

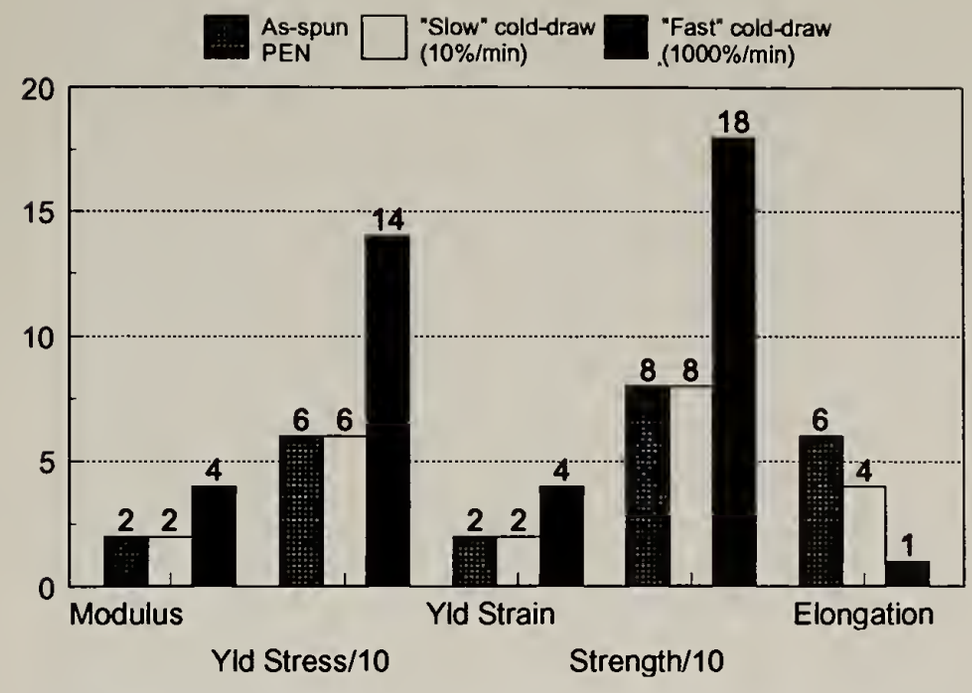

Tested samples (g.l. = 50 cm) were drawn at 130°C at ^{1} ~3.

Figure 6.1. Rate effects of cold-drawing on mechanical properties of PEN.

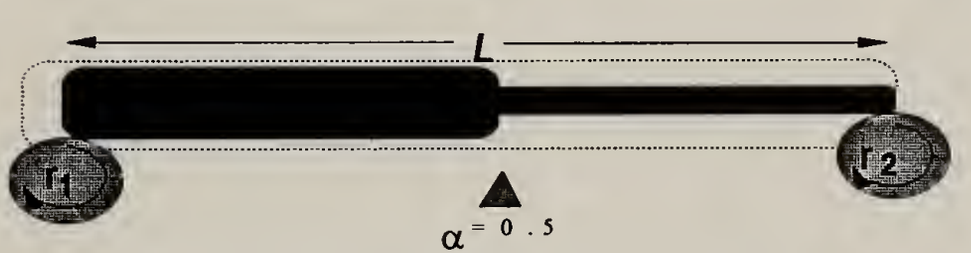

Figure 6.2. The physical parameters of a simplified post-treatment set-up.

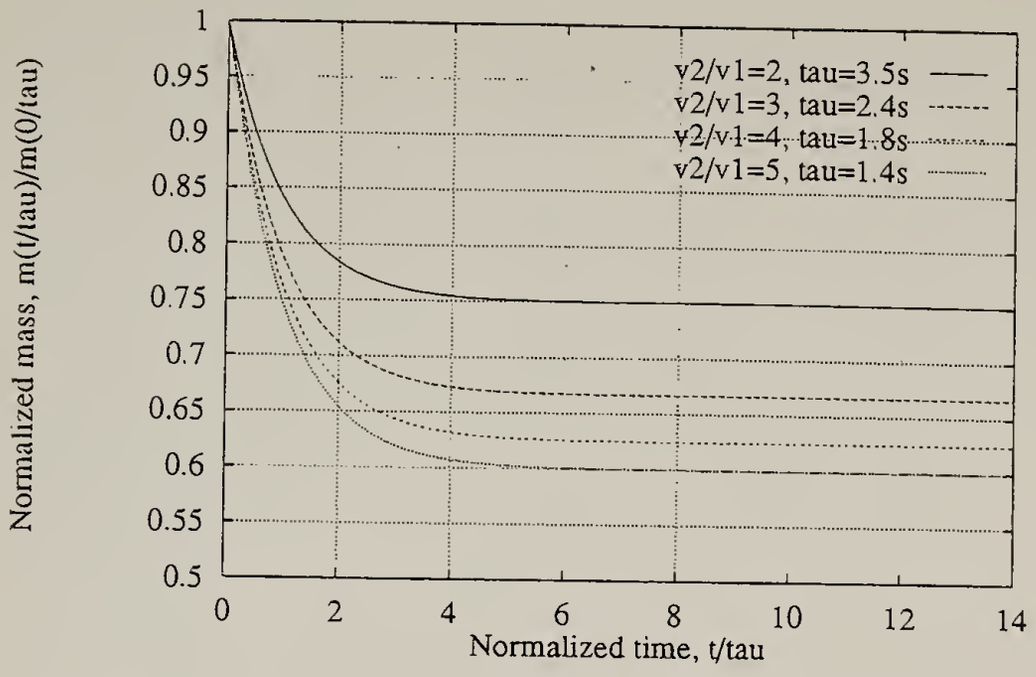

Figure 6.3. The effect of draw ratio on the mass flux within a drawing volume.

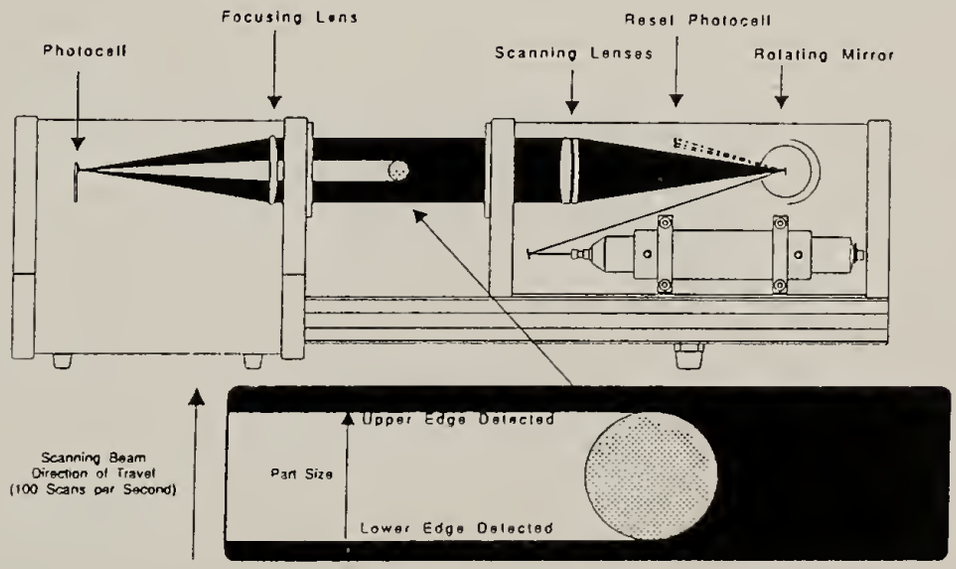

Figure 6.4. A schematic operational diagram of a LaserMike diameter gauge.

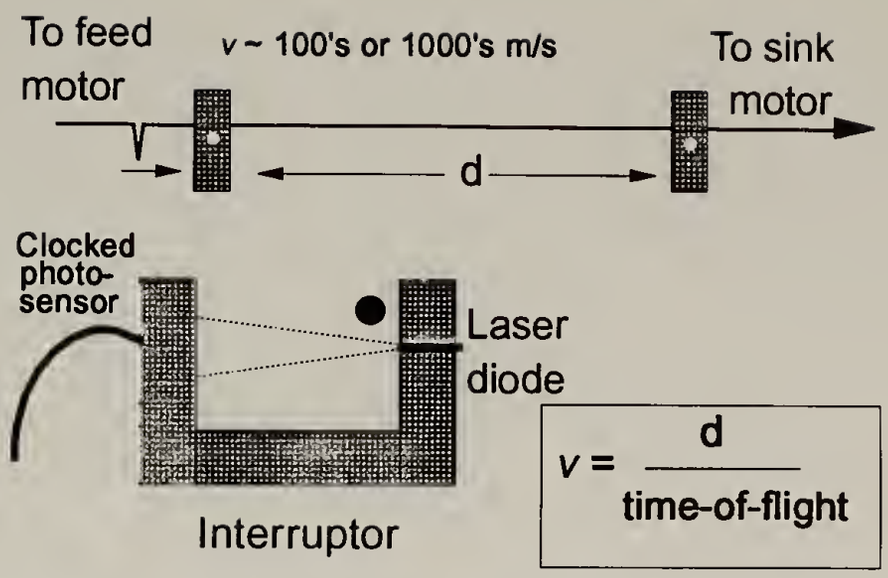

Figure 6.5. The practical applications of time-of-flight for fiber studies.

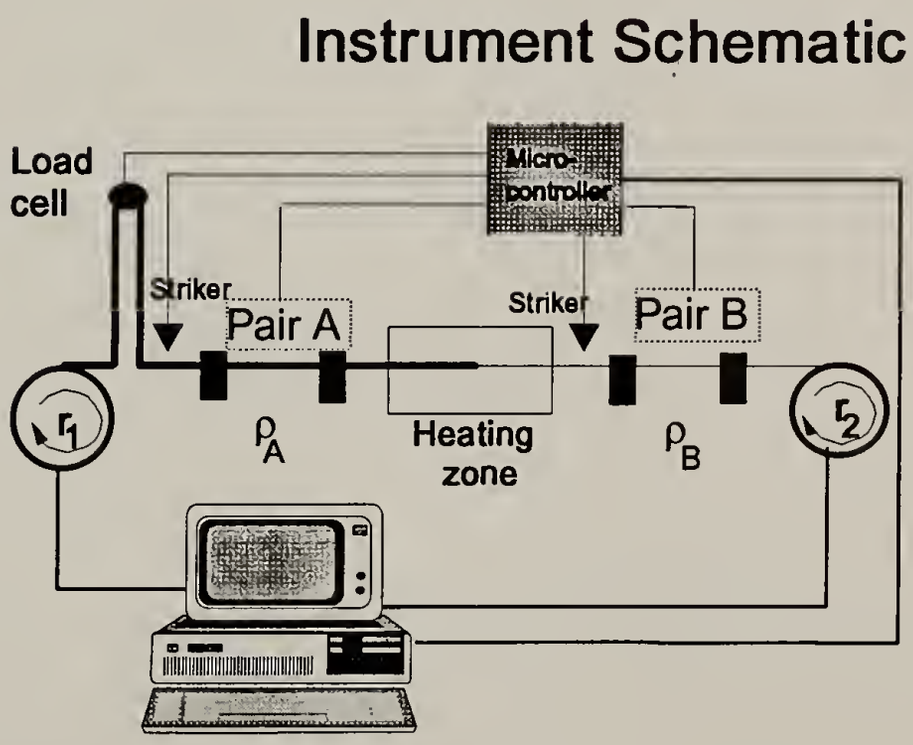

Figure 6.6. A schematic illustration of the instrument.

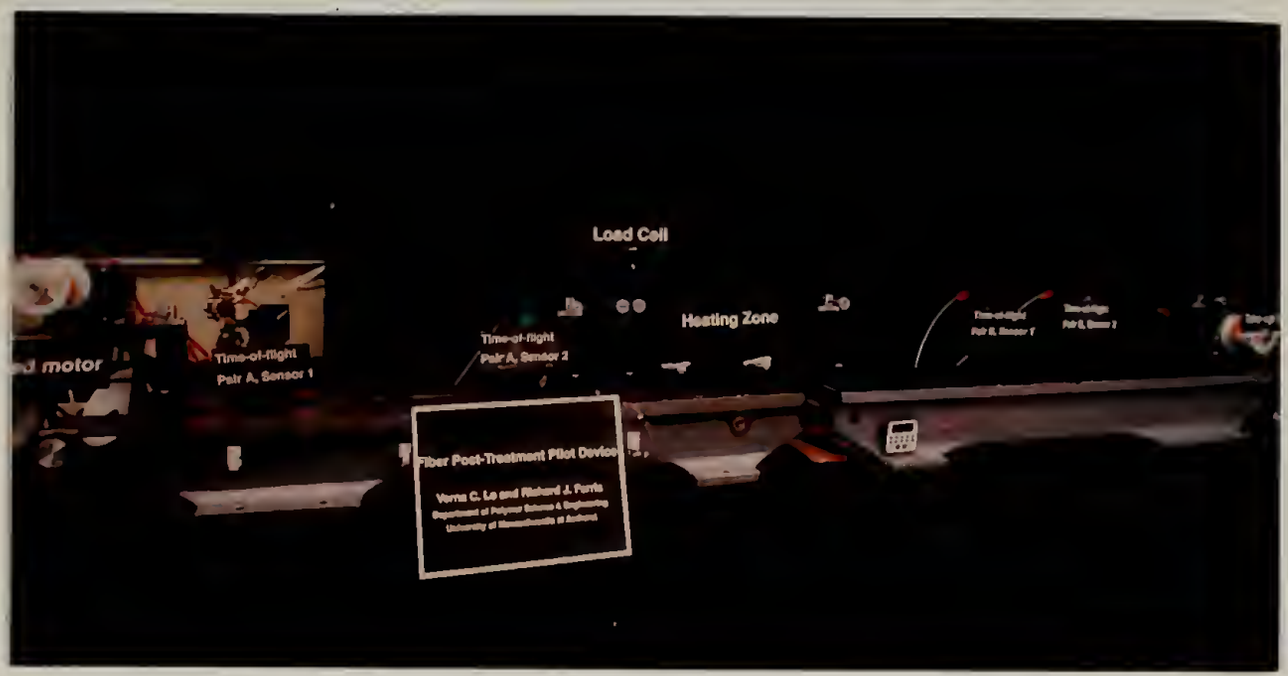

Figure 6.7. A photograph of the completed instrument.

Figure 6.8. A photograph of two custom-fabricated laser diode interruptors.

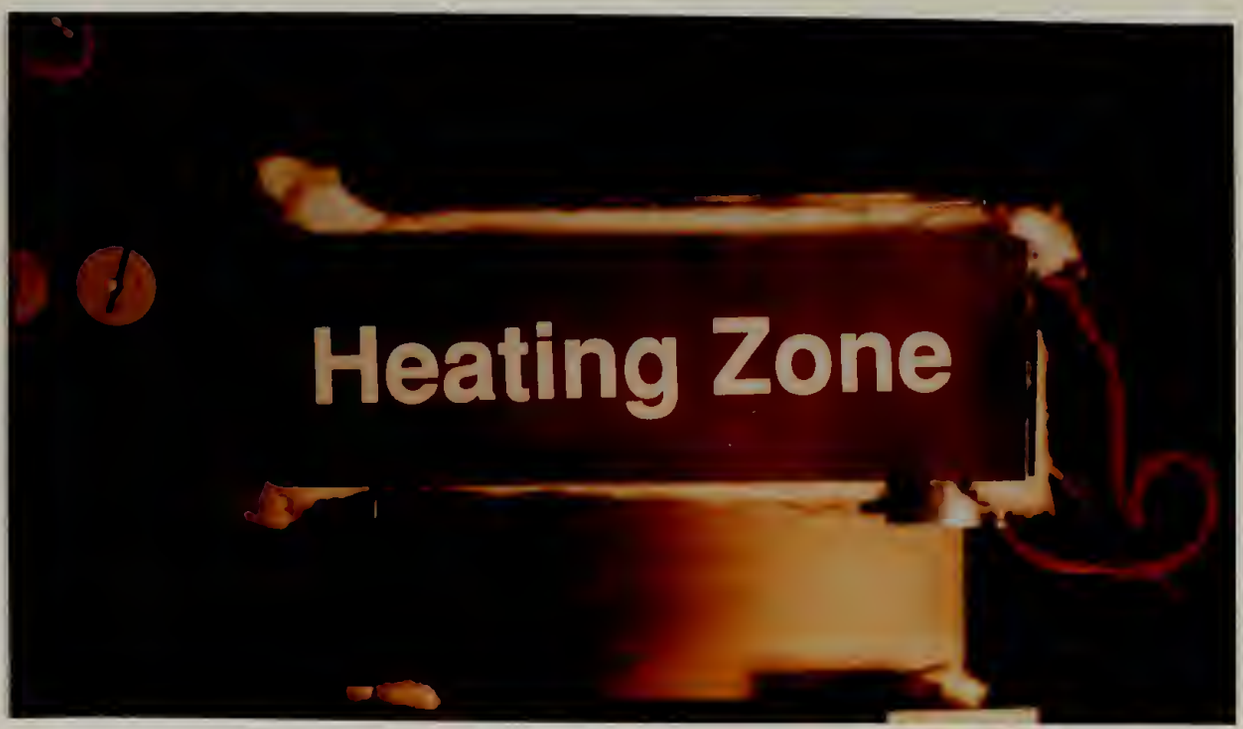

Figure 6.9. The heater unit in which drawing takes place.

Figure 6.10. The striker and its micropositioner.

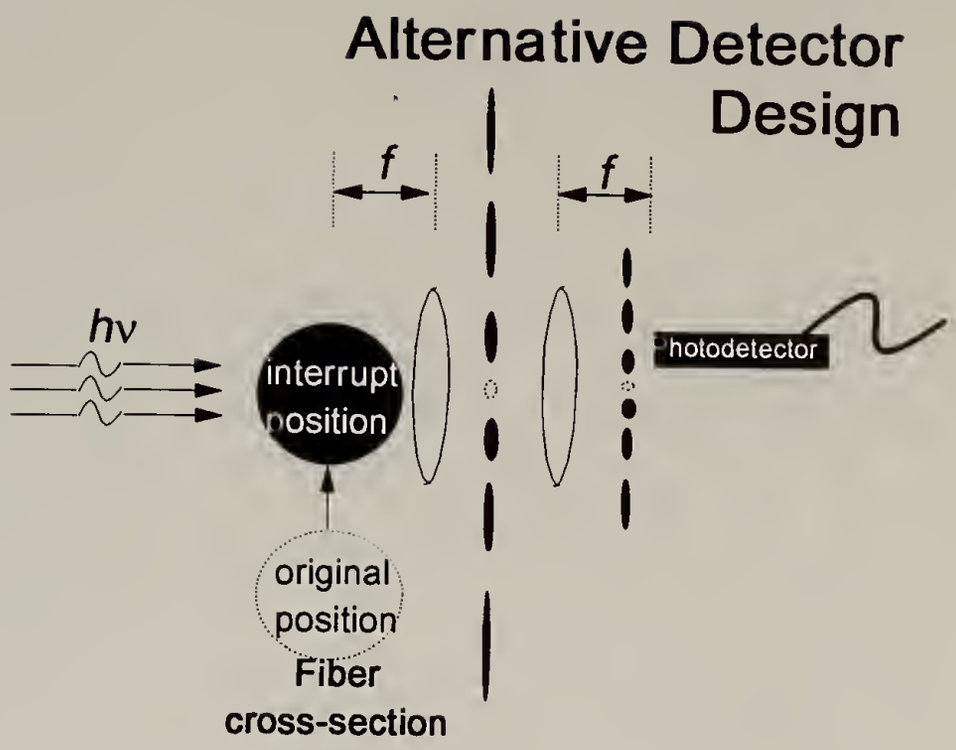

Figure 6.11. Diagram of an alternate detector design.

Figure 6.12. A close-up photograph of the load-cell configuration.

Figure 6.13. A microcontroller (made by Blue Earth Research Corporation) for the lowest tier of instrument control.

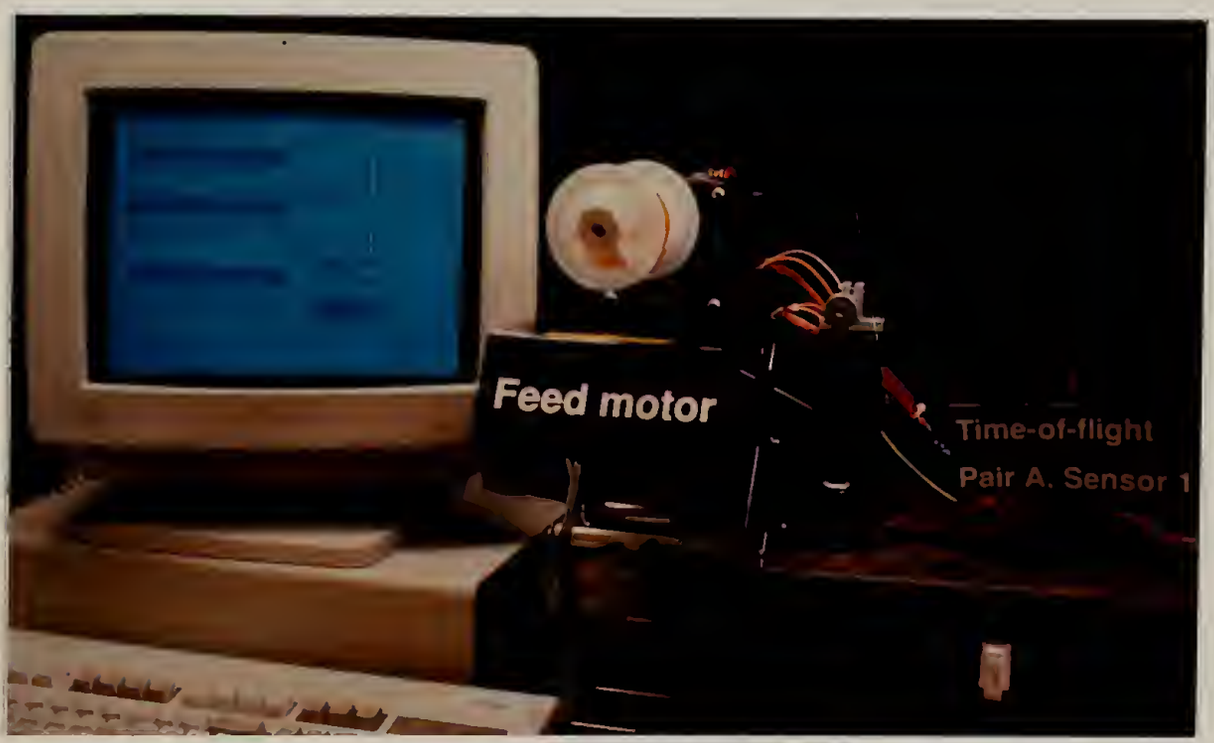

Figure 6.14. The PC and the feed motor (already loaded with a standard spool).

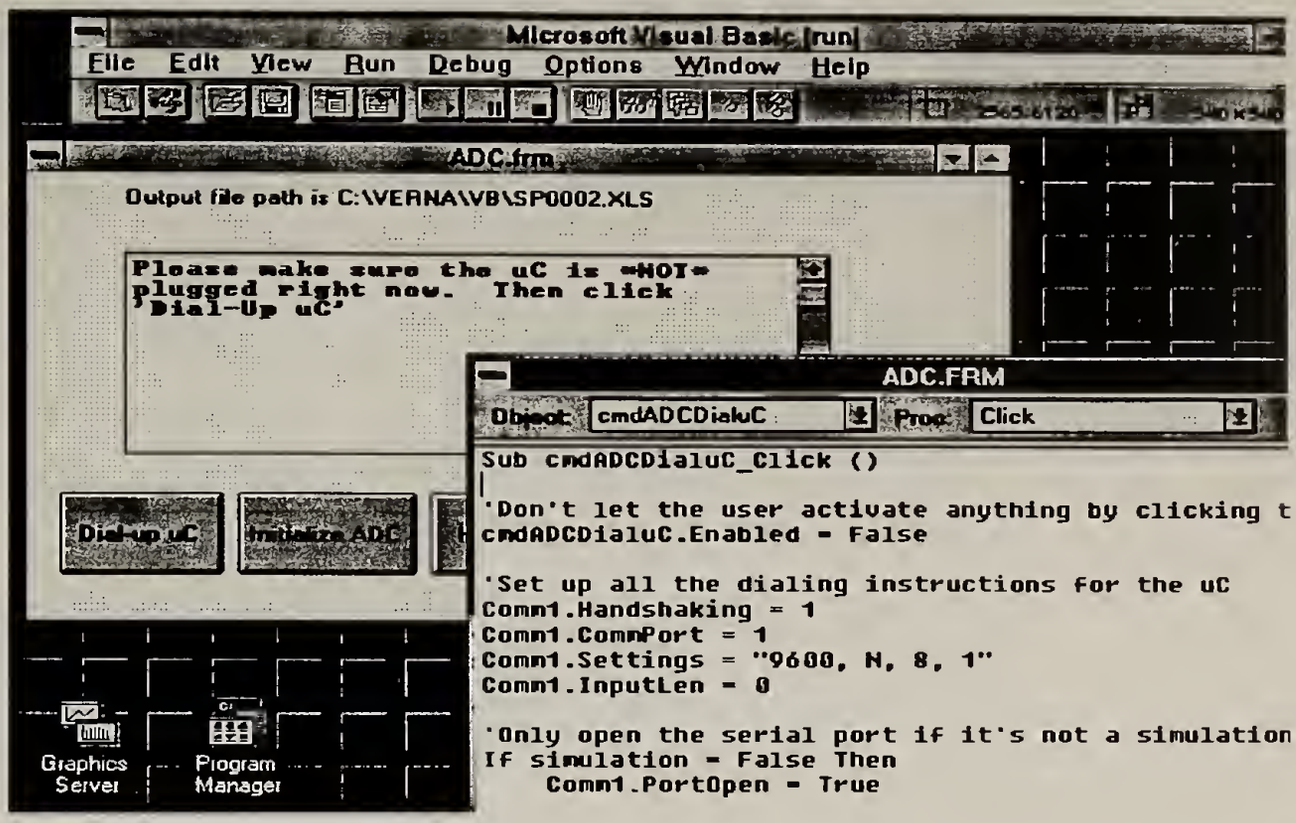

Figure 6.15. The software interface of code generated in Visual BASIC when one opens the initial communication port. The port is opened by the "clicking" on the soft button.

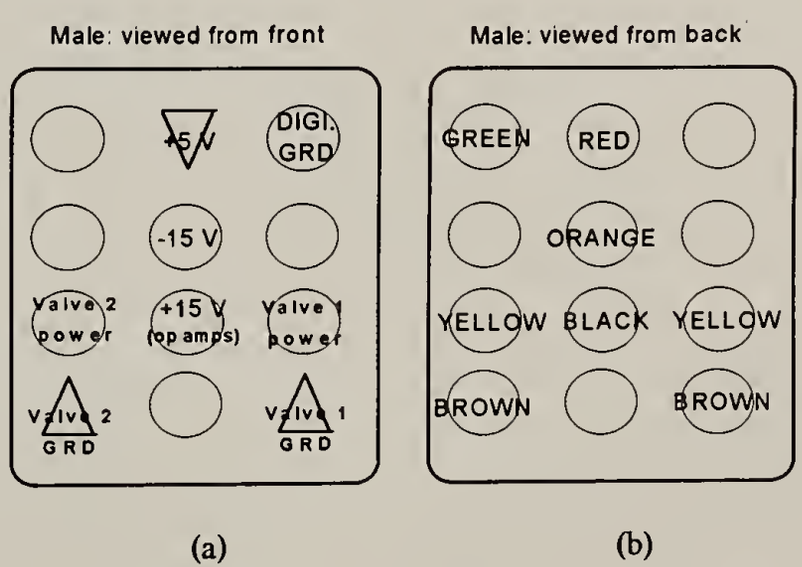

Figure 6.16. Wiring diagrams for (male) power connectors. (a) Line voltages as viewed from front of connector; (b) Wiring color code as viewed from rear of connector.

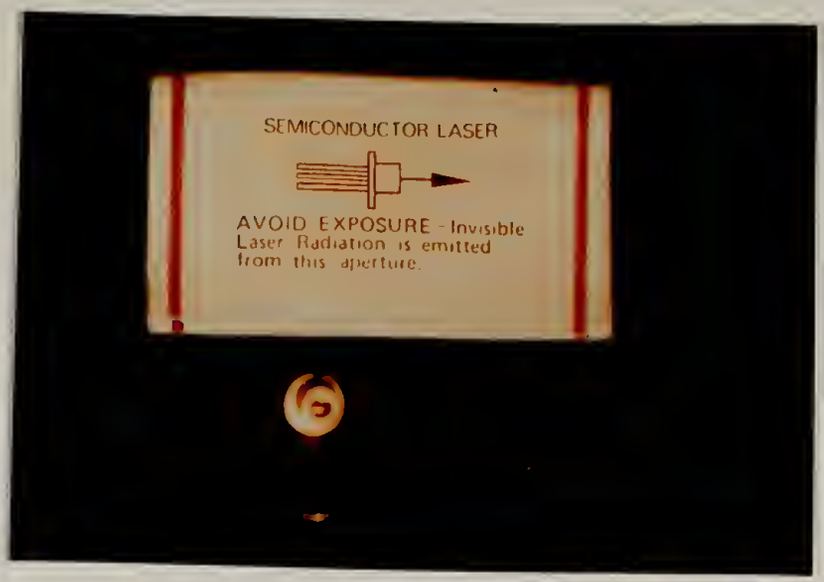

Figure 6.17. A Mitsubishi laser diode "can."

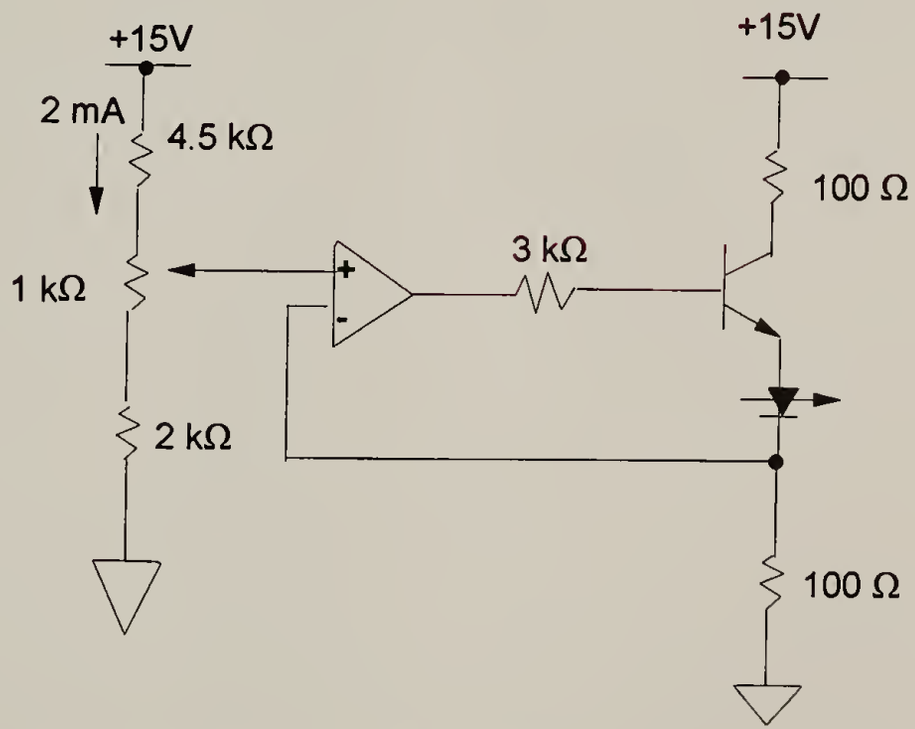

Figure 6.18. Constant current source electronic schematic.

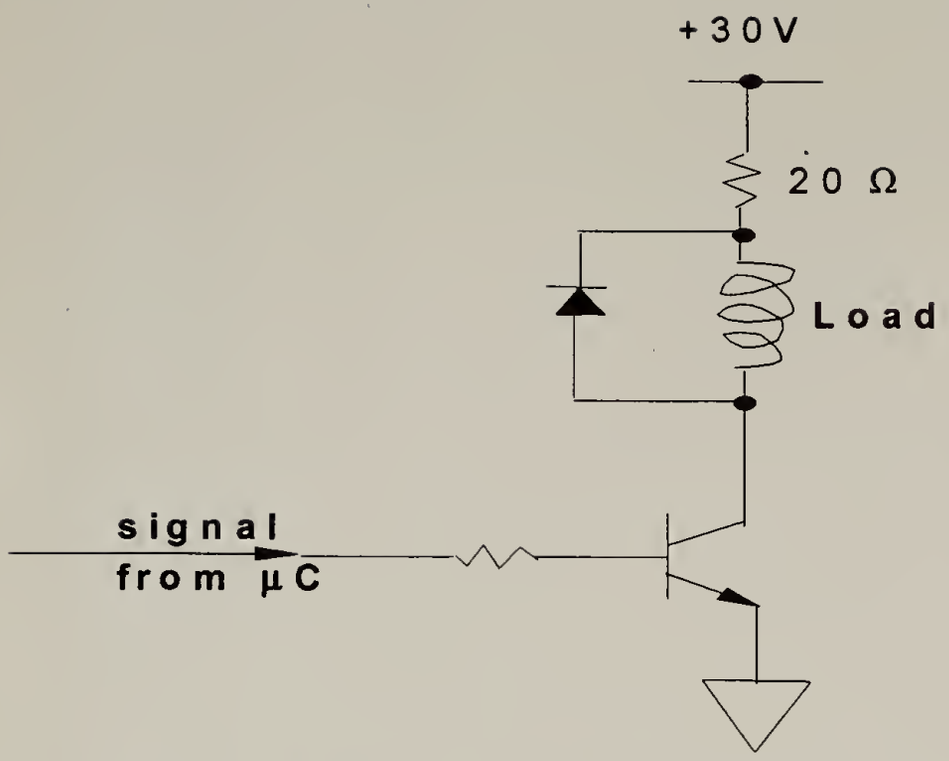

Figure 6.19. Electronic schematic of the board used to fire strikers.

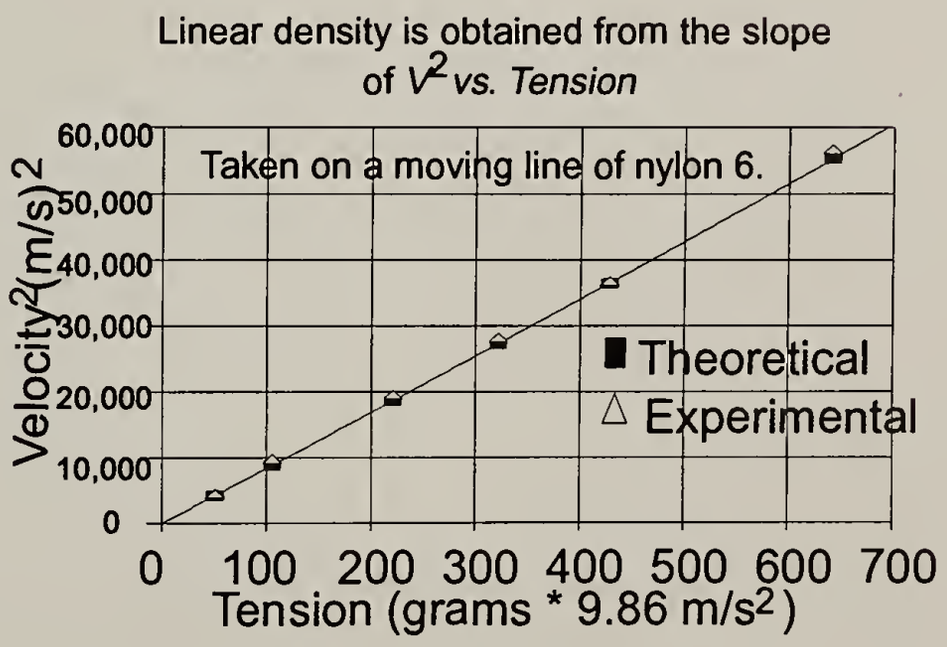

Figure 6.20. A typical calibration curve using nylon 6 monofilament.

CHAPTER 7

CONCLUSIONS AND SUGGESTIONS FOR FUTURE WORK

7.1 Summary of Studies

This thesis centered on fiber studies of poly(ethylene 2,6-naphthalate) and its blends with several novel semi-flexible thermotropic liquid crystalline copolyesters synthesized expressly for this purpose. This area of applied research remains fertile, in terms of both academic and commercial interest.

7.1.1 Pure PEN Studies

The first portion of the work focused on the structure-property relationships of the pure PEN matrix as it forms and draws as a fiber. Determining the melt-extrusion parameters of pure PEN revealed that PEN has a narrow processing window. The processing window shrinks as the molecular weight of the PEN increases. (It is suggested for those wishing to spin and draw PEN fiber to first review the procedure outlined in Chapter 2).

The fibers were tested for mechanical performance in terms of Young's modulus ultimate strength and ultimate strain at different levels of draw. These types of structure-property relationships on drawn PEN fiber have not been reported previously. The modulus and strength of PEN both increase with the draw ratio. It was also found that the level of elongation obtained during the cold-drawing segment sharply affects both the structure and mechanical properties of PEN.

Properties of pure PEN fibers made in the above fashion were compared to those obtained in an industrial pilot process for PEN fibers. The findings were that laboratory-made PEN fibers result in mechanical properties comparable to those for the pilot process. The difference is that the laboratory procedure contains favorably fewer steps and uses less aggressive conditions to form and treat the fiber.

7.1.2 Pure TLCP Studies

Each of the ten TLCPs was classified according to their chemical structure. They varied in their molecular weights and mesogen contents. All gave rise to nematic mesophase textures within a certain temperature range. Only the alternating copolymers cleared at temperatures below that of significant weight loss through degradation. None of the TLCPs exhibited a discernible T_g in DSC studies.

7.1.3 Studies of PEN Blended with TLCPs

The largest portion of the work concerned the systematic evaluation of mechanical and thermal effects of each of three general types of TLCPs within the PEN matrix. There was typically less than 10 grams total of each TLCP available for study. Due to the limited availability of the pure TLCPs, their roles in mechanical and thermal property enhancement for the PEN matrix were assessed in dilute concentration in blends. The total range of TLCP concentrations used for blended fiber studies was 0.25% to 20% by weight. Fibers were spun using the same laboratory-scale melt-extruder used for pure PEN fiber. The total exposure of the materials to high temperature was minimized. Both the temperature of the extruder barrel and the residence time of the

polymer within the barrel were kept low in order to avoid polymer degradation and to minimize transesterification.

Like PEN, the blends also exhibited a narrow processing window. The TLCPs, however, served as a processing aid for PEN by lowering the apparent processing viscosity. TLCPs containing naphthalene allowed spinning to occur at slightly lower temperatures than for pure PEN.

7.1.3.1 Mechanical Properties

Drawn fibers were tested for mechanical performance in terms of Young's modulus, ultimate strength and ultimate strain. Compared to values for the neat matrix and values from rule-of-mixtures prediction, the results for Young's modulus showed that mechanical property improvements were seen at many levels of TLCP inclusion. The stiffnesses at 1% inclusion were nearly the same for all blends expect those involving side-chain flexible random copolymer (Z_3). For most of the copolymer blends, the stiffness enhancement was 130% that of neat PEN spun and drawn in the same manner.

The main-chain random copolyesters (Z_1 and Z_2) gave rise to the highest levels of stiffness improvements. A type of side-chain random copolyester used in studies with PET did not give rise to as marked improvements in PEN.

7.1.3.2 Thermal Properties

The TLCPs were also effective as plasticizing and nucleating agents for PEN. All copolymers except Z_3 were able plasticize the PEN matrix by lowering the apparent T_g (on heating).

Neither Z_3 nor its analog in PET blends showed discernible ability to alter the T_g of its polyester matrix.

None of the TLCPs had a significant effect on the melting point of PEN at any concentration level. All of the TLCPs did display the general ability to raise ΔH_m of PEN with increasing concentration (on heating). Similarly, all of the TLCPs could raise the re-crystallization temperature (T_x) of PEN (on cooling). In most cases, increases in the heats of fusion scale in the same manner as T_x with concentration.

It was seen that an alternating thermotropic copolyester (Y_1) in its isotropic state could also nucleate crystallization of PEN.

7.1.3.3 Mechanical-Thermal Property Relationships

The data collected during the cooling segment of DSC for as-spun fibers shed some light onto structure-property relationships for the polyblends. While the heats of fusion (on cooling) do not scale directly with TLCP content, certain correlations are striking.

The highest value of ΔH_x corresponds to the lowest value of Young's modulus seen for final hot-drawn fibers of that blend in all cases examined. Thus, the amount of re-crystallized material (from the melt) is related to how the fiber performs mechanically after it undergoes additional crystallization steps which occur during fiber drawing. This is not an unusual effect: the crystallized structure established in the as-spun precursors of PET fibers can affect their maximum draw ratios and the extent to which property improvements can be achieved [Zhou et al., 1995] [Brody, 1983].

While there is evidence for establishing the lower bound (for what results in the poorest mechanical properties), there was not an obvious structure-property correlation for compositions

that resulted in the highest mechanical properties. The likely result is that there is an optimal level of crystallinity which when established in the as-spun state, lead to optimal mechanical properties.

The Young's modulus at 1% were approximately the same for most of the polyblends. In fact, for any particular TLCP polyblend system, the modulus values at 1% were in most cases the maximum stiffness attained. For both X and Y classes of TLCPs, the sharpest increase in ΔH_x occurs between 0% to 1% addition. That is, the change in the percentage of PEN re-crystallized from the melt is largest for 1% levels of inclusions of these polymers.

7.1.4 Instrumentation Studies

Several methods to determine the draw ratio of a fiberline during post-treatment were also investigated. These included diffraction, direct imaging, shadow imaging, time-of-flight, and combinations of these methods. To this extent, a pilot device based on time-of-flight techniques was constructed with accompanying software. The instrument, when properly calibrated, allows the user to detect the time it takes a wave to travel a fixed distance along the fiber. The speed of the wave can be related to the linear density of the fiber which in turn can be related to the draw ratio.

7.2 Suggestions for Future Work

There are three studies suggested to better understand the role the role of TLCPs spun into fibers with a polyester matrix such as PEN. They are listed in order of precedence.

7.2.1 Isotropic TLCPs

The role of the nematic state for inducing matrix modification bears further study. Thermal studies seem to suggest that an isotropic TLCP at very low levels of inclusion can modify the crystallization behavior of the PEN matrix in much the same manner as a nematic TLCP.

In order to investigate this effect, a low clearing temperature TLCP similar to Y_1 should be used in additional thermal studies with PET. The idea is then to quench samples of blend both above and below the clearing temperature in order to compare their effects on nucleation and supercooling of the matrix. PET rather than PEN is suggested as a matrix because its melting point is more widely separated from the clearing point of the TLCP. Also, there is a large body of data on the crystallization kinetics of PET whereas less is known about PEN in general.

The ability of the TLCP to nucleate crystallinity in a polyester matrix lies at the heart of structure-property relationships for the polyblends. Information which can clarify the reason that TLCPs are effective nucleating agents is essential.

7.2.2 Transesterification Studies

There is a strong chance that transesterification reactions (as known as ester interchange) inevitably occur within all of the polyblends of LC copolyester with PEN unless such blends are handled very carefully. In particular, the thermal cycling of samples during DSC scans result in their exposure to high temperatures for up to 90 minutes. During this time, ester interchange reactions are likely promoted within the samples.

Transesterification can result in randomizing a blocky copolymer [Jo et al., 1995] or making an otherwise random copolymer more blocky [Pucciariello and Carfagna, 1994]. Such

reactions are common and not necessarily undesirable for blending studies such as those presented in this thesis. It is seen that ester interchange can result in increased compatibility and adhesion of an nematic copolyester with its matrix [Su and Wei, 1995] [Choi et al., 1996]. If, however, trans-esterification occurs to a great extent then the products of the reaction necessarily result in a mixture that may no longer be considered binary (which is the the assumption of the polyblends of TLCPs with PEN where the number of components, n, equals 2.). If this becomes the case, then the examination of all properties, both thermal and mechanical, should be analyzed within a framework of higher order (n>2) or using a more sophisticated model to account for the role of chemical intermediaries.

In any case, it would be interesting to see how sequence distributions actually change during processing. For these purposes, the use of a simple polyblend system such as PEN with TR-4 mesogen is suggested. A ^{13}C-NMR study would be useful to track how the sequence distributions of naphthalate, oxybutylene, and 4-oxybenzoyl units evolve as a function of exposure of the blend to high temperatures such as those encountered during processing.

The evolution of sequence distribution can then be correlated with mechanical and thermal properties. For drawn fiber studies, such information would help make a definitive statement about the actual role of TLCP chemical architecture in final mechanical property values.

7.2.3 Post-Treatment Studies

The results suggest that PEN mechanical properties are strongly affected by the level of elongation attained in cold-drawing. The stiffness for PEN fibers was seen to increase more than 400% between the range of $4.4 < \lambda < 6.9$ in cold-drawing. These changes are tied to evidence of an abruptly emerging crystal structure during cold-drawing. Also, the results for PEN from these

studies and from literature show that the rate of draw and temperature of cold-drawing affects the final mechanical properties of PEN as well [Huijts and De Vries, 1993].

Based on the data gathered thus far for PEN, a good way to achieve the high Young's modulus is to draw the PEN fiber quickly at high temperature. For cold-drawing, the recommended temperature should be well-above T_g and at least high enough such that a necking phenomenon is no longer visible. A systematic study of drawing conditions is suggested in order to identify optimal conditions. The parameters are temperature, throughput rates, and final draw ratio.

Once the post-treatment studies of pure PEN are complete, a comparable study for TLCP polyblends would be interesting. Optimal mechanical properties of the blends would help to identify the optimal as-spun precursor crystallinity properties as suggested by existing structure-property results.

APPENDIX

APPLICABILITY OF TIME-OF-FLIGHT TO DIAMETER MEASUREMENT

The following describes how to relate the speed of a transverse wavefront, v, which advances within the medium of a one-dimensional string, to the average diameter, D, of said string within the same region over which the wave speed is detected. The assumption is that the only restoring force to the transverse disturbance is the tension, F, in the string.

Let a string of length L having linear density ρ_L be constrained under a tension F and held at zero displacement at its ends such that $y(0,t) = y(L,t) = 0$. For every given transverse disturbance $y(x',t') = u$ to the string, its response to the disturbance may be described by:

$$F\frac{\partial^2 y}{\partial x^2} = \rho_L \frac{\partial^2 y}{\partial t^2} \qquad (10)$$

Frequently equation (10) is written in the more generalized form:

$$\frac{\partial^2 y}{\partial x^2} = \frac{1}{v^2}\frac{\partial^2 y}{dt^2} \qquad (11)$$

Here, the coefficient is the inverse square of the wave speed. The general solution of (11) is

$$y(x,t) = f(x - vt) + g(x + vt) \qquad (12)$$

which indicates that two wavefront (both equal in amplitude) will immediately propagate from the point of disturbance, x', in opposite directions at the same wave speed, v. Thus, knowledge of the wave speed can provide information about physical properties of the string. Substituting the identity that the linear density, ρ_L, is equivalent to the bulk density of the string, ρ, multiplied by the cross-sectional area of the string allows a direct relationship between the diameter of the string and the wave speed:

$$D = \frac{2}{v}\sqrt{\frac{F}{\pi\rho}} \qquad (13)$$

The reader is referred to the text by Graf [1975] for further background.

BIBLIOGRAPHY

Allen, S. R., *Mechanical and Morphological Correlations in Poly-(p-phenylenebenzobisthiazole) Fibers*, PhD Thesis, University of Massachusetts Amherst, (1983).

Backson, S.C.E., Kenwright, A.M., and Richards, R.W., *Polymer*, **36**(10), 1991-1998, (1995).

Baird D.G. and Sun, T., *Liquid Crystalline Polymers*, Ch. 29, eds. Weiss, R.A. and Ober, C.K., American Chemical Society, Washington D.C., (1990).

Bassett, B.R. and Yee, A.F., *Polym. Composites*, **11**(1), 10-18, (1990).

Bechtel, S.E., Cao, J.Z., and Forest, M.G., **37**(2), 237-287, (1993).

Bekhet, N.E., Barton, D.C., and Craggs, G., *Process. Advanc. Mater.*, **3**(4), 199-207, (1993).

Bonis, L.J., "PET-LCP Alloys," lecture presented at *Soc. Plastic Eng. ANTEC*, Boston, MA (1995).

Brody, H., *J. Macromol. Sci. Phys.*, **B22**(1), 19, (1983).

Buchner, S., Wiswe, D., and Zachmann, H.G., *Polymer*, **30**, 480-488, (1989).

Cakmak, M., Wang, Y.D., and Simhambhatla, M., *Polym. Engin. and Sci.*, **30**(12), (1990).

Calundann, G., Jaffe, M., Jones, R.S., and Yoon, H., *Fibre Reinforcements for Composite Materials*, ed. Bunsell, A.R., Elsevier, Amsterdam, (1988).

Carraher Jr., C.E., *Polym. News*, **18**(11), 332-334, (1994).

Chang, J-H. and Farris, R.J., *Polym. J.*, **27**(8), 780-789, (1995).

Chang, J-H., Jo, B-W., and Jin, J-I., *Polym. Eng. and Sci.*, **35**(20), 1602-1614, (1995).

Chapleau, N., Carreau, P.J., Peleteiro, C., Lavoie, P-A., and Malik, T.M., *Polym. Eng. and Sci.*, **32**(24), 1876-1885, (1992).

Cheng, S.Z.D. and Wunderlich, B., *Macromolecules*, **21**, 789-797, (1988).

Cheng, S.Z.D., Janimak, J.J., Zhang, A., Guan, J., and Chu, A.L., *Polym. Bulletin*, **20**, 449-453, (1988).

Chipalkatti, M., Farris, R., and Hutchinson, J., *Rev. Sci. Instrum.*, **58**(1), 112-116, (1987).

Choi, J-K., Farris, R.J., and Kantor, S.W., unpublished results on TLCP synthesis, (1996).

De Gennes, P.G. and Prost, J., *The Physics of Liquid Crystals*, Oxford University Press, New York, (1993).

De' Nève, T., Kléman, M., and Navards, P., *Liq. Cryst.*, **18**(1), 67-71, (1994).

Deak, D., *ACS Abstracts (Chicago 1995)*, American Chemical Society, Washington D.C., (1996).

Dealy, J.M., *J. Rheol.*, **28**(3), 181-195, (1984).

Dicke, H.R. and Lenz, R.W., *J. Polym. Sci., Polym. Part A: Polym. Chem.*, **21**, 2581, (1983).

Donald, A.M. and Windle A.H., *Liquid Crystalline Polymers*, Ch. 3, Cambridge University Press, Cambridge, (1992).

Dutta, D., Fruitwala, H., Kohli, A., and Weiss, R.A., *Polym. Eng. and Sci.*, **30**(17), 1004-1017, (1990).

Economy, J. and Goranov, K., *Advances in Polymer Science Vol. 117*, Springer-Verlag, Berlin, (1994).

Egorov, E.A. and Zhizhenkov, V.V., *Intern. J. Polymeric Mater.*, **22**, 41-47, (1993).

El-Amouri, I. and Skoulis, A., *Macromol. Chem. Phys.*, **196**(7), 2081-2097, (1995).

Federico, O., *In-Situ Composites of a Thermotropic Liquid Crystalline Polymer and Polycarbonate: Processing, Morphology, and Properties*, PhD dissertation, University of Massachusetts Amherst, (1989).

Feyder, G., *Proc. 6th Eur. Capacitor and Resistor Techn. Symp.*, 21-31, (1992).

Friedel, G., *Ann. Physique*, **18**, 273, (1922).

Germroth, T., "PEN - A New Commercial Polymer," plenary lecture at *Graduate Res. Polym. Conf.*, Blacksburg, VA, (1996).

Ghanem, A.M. and Porter, R.S., *J. Polym. Sci. Part B: Polym. Phys.*, **27**, 2587-2603, (1989).

Godshall, J. and Petrohilos, H., *SPIE Opt. Ind. Insp.*, **665**, 346-351, (1987).

Graf, K., *Wave Motion in Elastic Solids*, Ch. 1, Clarendon Press, Oxford, (1975).

Greener, J., Eastman Kodak Corporation, personal communication, (1994).

Grulke, E., *Polymer Process Engineering*, Ch. 1, Prentice Hall, Englewood Cliffs, (1994).

Halpin, J.C., *Primer on Composite Materials*, Technomic Pub. Co., Lancaster, PA, (1984).

Halpin, J.C. and Kardos, J.L., *Polym. Eng. and Sci.*, **16**, 344, (1976).

Hamana, I., Fuziwara, Y., and Kuwakawa, S. (assignors to Teijin Ltd., Japan), United States Patent 4,000,239, 1976.

Han, C.D., Chang, S., and Kim, S.S., *Macromolecules*, **27**, 7699-7712, (1994a).

Han, C.D., Chang, S., and Kim, S.S., *Mol. Cryst. Liq. Cryst*, **254**, 335-368, (1994b).

Han, C.D. and Kim, S.S., *Macromolecules*, **28**, 2089-2092, (1995).

Handlos, A.A. and Baird, D.G., *J. Mater. Sci. - Rev. Macromol. Chem. Phys.*, **C35**(2), 183-238, (1995).

Heino, M., *Acta Polytechnica Scandinavica, Chemical Technology and Metallurgy Series*, Ch. 220, 1-49, (1994).

Ho, B.C., Chen, J.C., Chen W.C., Chang Y.H., Yang S.Y., Chen J. J., Tseng, T.W., *Polym. J.*, **3**, 310-313, (1995).

Huijts, R.A. and De Vries, A.J., *Intern. J. Polymeric Mater.*, **22**, 231-236, (1993).

Huijts, R.A. and Peters, S.M., *Polymer*, **35**(14), 3119-3121, (1994).

Hwang, W.F., Wiff, D.R., Benner, C.L., Helminiak, T.E., *J. Macromol. Sci. Phys.*, **B22**, 231, (1983).

Ignatious, F., Lu, C., Kantor, S.W., and Lenz, R.W., *Macromolecules*, **27**(26), 7785-7793, (1994).

Jaffe, M., Chen, P., Choe, E-W. Chung, T-S., and Makhija, S., *High Performance Polymers*, Ch. 7., ed. Hergenrother, P.M., Springer-Verlag, Berlin, (1994).

Jager, J., Juijn, J.A., Van den Heuvel, J.M., Huijts, R.A., *J. Appl. Polym. Sci.*, **57**, 1429-1440, (1995).

Jang, S.H. and Kim, B.S., *Polym. Eng. and Sci.*, **35**(6), 538-545, (1995).

Jo, B-W., Chang, J-H., and Jin, J-I., *Polym. Eng. and Sci.*, **35**(20), 1615-1620, (1995).

Joslin, S.L., *The Thermal and Mechanical Behavior of Poly(Ethylene Terephthalate) Fibers Incorporating Novel Thermotropic Liquid Crystalline Polymers*, PhD dissertation, University of Massachusetts Amherst, (1994).

Joslin, S.L., Geisa, R., and Farris, R.J., *Polymer*, **35**, 4303, (1994).

Kantor, S.W., University of Massachusetts, personal communication, (1995).

Katayama, K. and Yoon M.G., *High-Speed Fiber Spinning*, ed. Ziabicki, A. and Kawai, H., John Wiley & Sons, New York, (1985).

Kawaguchi, T., *High-Speed Fiber Spinning*, ed. Ziabicki, A. and Kawai, H., John Wiley & Sons, New York, 1985.

King, C.M., *J. Appl. Polym. Sci.: Appl. Poly. Sympos. 47*, 171-184, (1990).

Kiss, G., *Polym. Eng. and Sci.*, **27**(6), 410-422, (1987).

Koedam, M. *Philips Tech. Rev.*, **27**(7), 208-210, (1966).

Kyotani, M., Kato, A., and Nakayama, K., *Polymer*, **33**(22), 4756-4762, (1992).

Lee, K-S. and Lee, W-K., *Mol. Cryst. Liq. Cryst.*, **254**, 37-48, (1994).

Lee, W.C., Dibenedetto, A.T., Gromek, J.M., Nobile, M.R., and Acierno, D., *Polym. Eng. and Sci.*, **33**(3), 156-165, (1993).

Lenz, R.W. and Go, S.J., *J. Polym. Sci., Part A: Polym. Chem.*, **11**, 2927, (1973).

Leslie, F.M., *Quart. J. Mech. Appl. Math.*, **19**, 357, (1966).

Li, X-G., Zhou, Z-L., Wu, Z-G., and Sun, T., *J. Appl. Polym. Sci.*, **51**, 1913-1921, (1994).

Lin, Q., Jho, J. and Yee, A.F., *Polym. Eng. and Sci.*, **33**(13), 789-798, (1993).

Lin, Q. and Yee, A.F., *Polymer*, **35**(16), 3463-3469, (1994).

Liu, S-F., Lee, Y-D., *Macromol. Chem. Phys.*, **196**, 629-643, (1995).

Lo, V.C. and Farris, R.J., *SPIE Optomechan. and Precis. Instrum. Design*, **2542**, 47-57, (1995).

Lo, V.C., Choi, J-K, and Farris, R.J., unpublished results on PEN and blend fibers (1996).

Macosko, C., "Compatibilization of Polymer Blends," plenary lecture at *Soc. Plastic Eng. ANTEC Meeting*, Boston, MA 1995.

Majnusz, J., Catala, J.M., and Lenz, R.W., *Eur. Polym. J.*, **19**, 1043, (1983).

Mehta, S. and Deopura, B.L., *Polym. Eng. and Sci.*, **33**(14), 931-935, (1993).

Mencik, Z., *Chem. Prumysl.*, **17**(2), 78, 1967.

Miller, E., *Engineered Materials Handbook: Volume 1 Composites*, ed. Dostal, C.A., ASM International, Metals Park, OH, 1988.

Minkova, L.I., Paci., M., Pracella, M., and Magagnini, P., *Polym. Eng. and Sci.*, **32**(1), 57, (1992).

Murakami, S., Nishikawa, Y., Tsuji, M., Kawaguchi, A., Kohjiya, S., and Cakmak, M., *Polymer*, **36**(2), 391-397, (1995).

Nakamae, K., Nishino, T., Tada, K., Kanamoto, T., and Ito, M., *Polymer*, **34**(15), 3322-3324, (1993).

Narayan-Sarathy, S, *Synthesis and Characterization of Thermotropic Liquid Crystalline Polyesters for Use in Molecular Composites*, PhD dissertation, University of Massachusetts Amherst, (1995).

Narayan-Sarathy, S., Wedler, W., Lenz, R.W., and Kantor, S.W., *Polymer*, **36**(12), 2467-2471, (1995).

Ouchi, I., Hosoi, M., and Tomie, T., *Japan. J. Appl. Phys. Part 1*, **31**(8), 2505-2507, (1992).

Pakhomov, P.M., Shablygin, and M.V., Chegolya, A.S., *Intern. J. Polymeric Mater.*, **22**, 201-208, (1993).

Perry, A, Ineichen, B., and Eliasson, B., **9**, 1376-1378, (1974).

Pucciariello, R. and Carfagna, C., *Colloid. and Polym. Sci.* **272**, 1501-1507, (1994).

Richter, B., *Wire*, **42**(6), 529-532, (1992).

Roviello, A. and Sirigu, A., *J. Polym. Sci., Polym. Lett.*, **13**, 455, (1975).

Rueda, D.R., Viksne, A., Malers, L., Calleja, F.J.B, and Zachmann, H.G., *Macromol. Chem. Phys.*, **195**, 3869-3876, (1994).

Sarlin, J. and Tormala, P., *J. Polym. Sci. Part B: Polym. Phys.*, **29**, 395, (1991).

Shaw, J.P. and Gilbert, M., *Plast., Rubber, and Composites Process. and Applic.*, **22**(1), 9-27, (1994).

Shi, F., *Inter. J. Polymeric Mater.*, **23**, 207-214, (1994).

Shima, T., Yamashiro, S., Yoshimura, M., Kuratsuji, T., Kato, Y., Maeda, K. (assignors to Teijin Ltd., Japan), United States Patent 3,616,832, 1971.

Shin, B.Y. and Chung, J., *Polym. Eng. and Sci.*, **30**(1), 13-29, (1990).

Spies, C., and Zachmann, H.G., *Polymer*, **35**(18), 3816-3826, (1994).

Stewart, M.E., Cox, A.J., and Naylor, D.M., *Proc. of Soc. of Plastics Engineers ANTEC Symp.*, 1222-1226, Boston, MA, (1993).

Su, K-F. and Wei, K-H., *J. Appl. Poly,. Sci.*, **56**, 79-89, (1995).

Sukhadia, A.M., Done, D., and Baird, D.G., *Polym. Eng. and Sci.*, **30**(9), 519, (1990).

Tendolkar, A., Narayan-Sarathy, S., Kantor, S.W., and Lenz, R.W., *Polymer*, **36**(12), 2463-2466, (1995).

Turek, D.E., Simon, G.P., and Tiu, C., *Polym. Eng. and Sci.*, **35**(1), 52-62, (1995).

Ward, I.M., *Physica Scripta*, **T55**, 224-227, (1994).

Yen, S.P.S., Lowry, L. Cygan. P.J., and Jow, T.R., *Proc. 13th Capacitor and Resistor Tech. Symp.*, 7-13, (1993).

Yoon, K.H., Lee, S.C., and Park, O.O., *Polym. J.*, **26**(7), 816-821, (1994).

Zachmann, H.G. and Thiel, S., *Proceedings of the Third International Workshop on Non-Crystalline Solids*, World Scientific, Singapore, (1992).

Zachmann, H.G., Spies, C., and Thiel, S., *Physica Scripta*, **T49A**, 247-252, (1993).

Zaitsev, M.G., and Varyukhin, S.Y., *Intern. J. Polymeric Mater.*, **22**, 33-40, (1993).

Zhou, Q., Wu, G., Tucker, P.A., and Cuculo, J.A., *J. Polym. Sci. Part B: Polym. Phys*, **33**, 909-917, (1995).

Ziabicki, A., *High-Speed Fiber Spinning*, ed. Ziabicki, A. and Kawai, H., John Wiley & Sons, New York, 1985.

Zimmerman, J., *Comprehensive Polymer Science: Vol. 7 Specialty Polymers and Polymer Processing*; ed. Allen, G., Pergamon Press, New York, 1992.